The Hong Kong Polytechnic University

Department of Building Services Engineering

A Study of Helmholtz Resonators on Broadband Noise Control and Their Potential Application on Ventilation

Wang Xu

A thesis submitted in partial fulfillment of the requirements for the Degree of Doctor of Philosophy

August, 2012

Certificate of Originality

I hereby declare that this thesis is my own work and that, to the best of my knowledge and belief, it reproduces no material previously published or written, nor material that has been accepted for the award of any other degree or diploma, except where due acknowledgement has been made in the text. I also declare that the intellectual content of this thesis is the product of my own work, even though I may have received assistance from others on style, presentation and language expression.

_____(Signed)

Wang Xu (Name of student)

Department of Building Services Engineering

The Hong Kong Polytechnic University

Hong Kong, China

August, 2012

Dedication

To my parents

Wang Ya-sheng and Zhang Shi-fang
who always support me with warm care

To my wife

Wang Xiao-nan
who always accompany me patiently with her love

Abstract

Noise abatement and ventilation control are two important aspects in improving the indoor environmental comfort in buildings. The aims of this thesis were to achieve a better understanding of the broadband noise control and ventilation effects of Helmholtz resonators.

Helmholtz resonator (or simply called resonator), a noise control device that has a resonance peak, is useful when noise centralized in a narrow frequency band. In this thesis, both the lumped- and distributed-parameter models of the Helmholtz resonator were considered. The latter model considering the multi-dimensional wave propagation inside its neck and cavity gave a better prediction of its resonance frequency.

To obtain a boarder noise attenuation band, combing several resonators is a possible way. This thesis reported a theoretical study of sound propagation in a one-dimensional duct with identical side-branch resonators mounted periodically. Bloch wave theory and the transfer matrix method were used to investigate wave propagation in these spatially periodic resonators. Three types of stop-bands were discussed, and their bandwidths were predicted. The results predicted by the theory

fit well with the computer simulation using a three-dimensional finite element method and the experimental results. This study indicated that the wave coupling in this periodic system resulted in the distribution of the frequency band into the stop- and the pass-bands. The long-term significance is that periodic resonators may more effectively control noise in ducts by broadening the bandwidth they attenuate.

This thesis also considered the disorder in the periodic duct-resonator system. Two cases were investigated: the disorder in periodic distance and the disorder in the geometries of Helmholtz resonators. The latter case was then compared to the traditional case of an array of differently tuned resonators without periodic mount. It was found that the analysis of the disorder in the geometries of resonators with periodic distance being kept unchanged provides a useful way for the design of such a system to achieve a relatively wide noise attenuation band and to track some narrow noise peaks within it.

Apart from their extensive application on noise control, Helmholtz resonators were found to have the effect on ventilation. This thesis presented the results of a theoretical investigation of the airflow through the neck into the cavity of a side-branched Helmholtz resonator. It was found that the motion of the airflow in the opening may result in an air jet formed in the resonator that provided the fresh air

from the ventilation duct. This air jet was composed of the “escaped” air masses, and the “escaped” air masses resulted from the behavior of the airflow in the region of opening-enclosure interface that can be regarded a sink-jet model. This ventilation method can be considered as “AC” ventilation with the electrical analogy, which is far less understood than the traditional ventilation method.

It is hoped that the present study can provide a stepping stone for investigation of both the acoustic and ventilation performance of Helmholtz resonators, and seeking their potential application in improving the indoor environmental comfort in buildings.

Publications Arising from the Thesis

Published papers

X. Wang and C.M. Mak. Wave propagation in a duct with a periodic Helmholtz resonators array. *Journal of the Acoustical Society of America* **131**, 1172-1182 (2012).

X. Wang and C.M. Mak. Acoustic performance of a duct loaded with identical resonators. *Journal of the Acoustical Society of America* **131**, EL316-EL322 (2012).

Conference paper

X. Wang and C.M. Mak. The theoretical investigation of Helmholtz resonators array for broad-band noise control in ventilation systems. *Proceeding of Inter-noise* 2012, New York, USA.

Paper under review

X. Wang and C.M. Mak. Disorder in a periodic Helmholtz resonators array. Submitted to *Journal of the Acoustical Society of America* (2012).

Paper in preparation

X. Wang and C.M. Mak. Ventilation performance of Helmholtz resonators. In preparation.

Acknowledgements

I would like to express deepest appreciation to my chief supervisor, Prof. Mak Cheuk-ming for his thoughtful insight and warm encouragement to me. The study will not be successful without his invaluable guidance and support.

I would also like to take this opportunity to acknowledge my Co-supervisor, Prof. Niu Jian-lei, for his valuable advice and help during my study.

Furthermore, I would like to thank the technicians in the Department of Building Service Engineering of The Hong Kong Polytechnic University for their kind support in preparing experimental setups.

All works including numerical work and experimental work reported in this PhD thesis were entirely conducted in The Hong Kong Polytechnic University.

Nomenclature

A	Cross sectional area of the opening
c_0	Sound speed (mean value)
$\mathbf{c}_n$	Vector represents the wave component in the duct segment of the nth periodic element
D	Periodic distance
E	Ensemble average
f	Periodic function
f_0	Resonance frequency
f_n	Resonance frequency of nth Helmholtz resonator
J_0	Bessel function of first kind and order zero
J_1	Bessel function of first kind and order one
k	Wave number
$k_{r,n}$	Radial wave number of mode n
$k_{z,n}$	Axial wave number of mode n
K	Damping force coefficient
l_1	Neck length of the circular concentric Helmholtz resonator
l_2	Cavity length of the circular concentric Helmholtz resonator
$l_1^{'}$	Effective neck length of the circular concentric Helmholtz resonator
l_e	Effective length of flow through opening

L_{begin}	Length of the duct before the first resonator
L_{end}	Length of the duct after the last resonator
M	Characteristic function of the random "periodic" distance
p	Probability density function
P	Sound pressure
P_1	Sound pressure in the neck of the Helmholtz resonator
P_2	Sound pressure in the cavity of the Helmholtz resonator
$\mathbf{P}$	Matrix composed of the corresponding eigenvectors of $E[\mathbf{A}]$
q	Airflow rate
Q	Strength of the sink/jet
r_1	Neck radius of the circular concentric Helmholtz resonator
r_2	Cavity radius of the circular concentric Helmholtz resonator
r_n	Reflection coefficient of nth Helmholtz resonator
S_1	Neck cross sectional area of the circular concentric Helmholtz resonator
S_2	Cavity cross sectional area of the circular concentric Helmholtz resonator
S_d	Duct cross sectional area
t_{ij}	Entry in the ith row and the jth column of $\mathbf{T}$
t_n	Transmission coefficient of nth Helmholtz resonator
T	Time-dependent term: $\exp(j\omega t)$
TL	Transmission loss

$\overline{TL}$	Averaged transmission loss
$\mathbf{T}$	Periodic transfer matrix
U	Centerline velocity of jet
v_s	Flow velocity along a streamline
V	Volume of the enclosure
V_1	Particle velocity in z-direction in the neck of the Helmholtz resonator
V_2	Particle velocity in z-direction in the cavity of the Helmholtz resonator
	Cavity volume of circular concentric Helmholtz resonator
$\mathbf{v}$	The eigenvector of the periodic transfer matrix
	Flow velocity vector
W	Width of the opening in z-direction
χ_n	The nth root of the function $J_0'(\chi_n) = 0$
Z_r	Acoustic impedance of the Helmholtz resonator
Z_d	Acoustic impedance of the duct
$Z_r^{'}$	Acoustic characteristic impedance of the Helmholtz resonator
$Z_d^{'}$	Acoustic characteristic impedance of the duct
α	Reflection coefficient of the end termination of the duct
	Entrainment coefficient
β	Contraction ratio
γ	Isentropic index
γ_t	Fraction of the momentum flux
$\mathbf{\Gamma}$	Diagonal matrix containing the eigenvalues of $E[\mathbf{A}]$

δ	Represents $\exp(-2jkD)$
δ_n	Ratio of the positive- and negative-going characteristic wave types in the duct segment of the nth periodic cell
$\Delta_{1,2}$	Stop-band boundaries
Δ_{BW}	Relative bandwidth
κ	Ratio of the cavity's volume to the duct's volume in a periodic cell
λ	Eigenvalue of the transfer matrix
μ	Propagation constant
	Ratio of area at vena contract and the opening area
μ_r	Attenuation constant
μ_i	Phase constant
ρ_0	Air density (mean value)
ρ'	Instantaneous air density perturbation
σ	Standard deviation
ϕ	Velocity potential
ψ	Streamline function
ω_0	Resonance circular frequency
ω_m	Circular frequencies of Bragg reflection

Table of Contents

List of Figures

Chapter 1

Introduction

1.1 Helmholtz Resonator

Helmholtz resonators (or simply called resonators hereafter) are devices created in the 1850s by Hermann von Helmholtz.[1] A classical Helmholtz resonator consists of a cavity and a hollow neck. It is useful to control noise centralized in a narrow frequency band. Many studies were conducted to accurately predict its resonance frequency. Initially, Rayleigh assumed Helmholtz resonator as a lumped-parameter system,[2,3] in which the air in the neck acts as a mass piston and the air inside its cavity acts as a spring. To calculate its resonance frequency, the effective length of neck is introduced, which is derived by regarding the sound energy radiation from the neck as an additional "radiation mass" to the piston and leads to adding end corrections to the real length of the neck. In Rayleigh's work, the interior and exterior end corrections are the same; despite the interior space and exterior space may be quite different. The work about a piston with different terminations was carried out by Ingard,[4,5] and a more accurate end correction was then derived.[5] Different form previous works on the lumped-parameter model of Helmholtz resonator, Tang and Sirignano [6] derived a general model that considers

one-dimensional wave propagation inside both the neck and cavity. This work was subsequently improved upon by Panton and Miller[7] by adding interior and exterior end corrections that include the influence of the resonator shape. However, all these models only work well when the Helmholtz resonator is with such an extremely thin geometry that only plane wave propagated inside. This model was then expanded by Monkewitz and colleagues[8] and Selamet and colleagues.[9, 10] Their studies investigated two- and three-dimensional wave propagations in Helmholtz resonators. The distributed-parameter model is shown to fit the experimental results better than a lumped one.[10] In addition to the previous researchers who focused on the symmetrical Helmholtz resonator, Chanaud[11] discussed the influence of asymmetrically placed orifice work and deriving an explicit interior end correction formula with an experimental verification[12].

Since a single resonator has a narrow resonance peak, combining several resonators is a possible way to obtain a broader band of noise attenuation. An array of differently tuned resonators was used in some previous works to attenuate broadband noise.[13,14] The duct with multiple similar resonators that includes a duct with the boundary of a perforated or micro-perforated plate backed by air cavities was discussed.[15,16] It is found that when resonators of similar resonance frequency are in close proximity, they can interact and lead to a decrease in the overall performance

compared to that of a single resonator.[17] To avoid this interaction, the resonators at some distance between each other were considered in most of the works.[15,16]

1.2 Periodic Structure

A periodic structure is composed of a number of identical structural components that are joined together end-to-end and/or side-by-side to form a whole complex.[18] Periodic structures can be classified into three categories: (1) the periodic medium, (2) the periodically inhomogeneous medium, and (3) the periodically bounded medium.[19] The study of Rayleigh[20] on wave propagation in a stretched string with periodic density is an example of the first class of periodic structures, i.e. the periodic medium. Related work can be found on structure-borne sound, in particular, on sound propagation in one-, two-, and three-dimensional periodic structures, such as beams,[21,22] plates,[23,24] and shells[25,26] in various combinations and support conditions, or even with multiple layers[27]. An example of the second class is a fluid having a periodic variation in ambient density or sound speed.[20] The work involving periodically inhomogeneous media is about the quantum theory of electrical conductivity.[28] The third class of periodic structures is a system composed of a homogeneous medium with a periodically vary boundary. Related work can be found on air-borne sound, in particular, on sound propagation in a duct with periodically

varying cross section,[29] a duct loaded periodically with quarter-wavelength tubes,[19] or a duct with periodic arrays of obstacles inside.[30] A duct loaded with identical resonators investigated by Sugimoto and Horioka[31] is found to be a new class of ultrasonic metamaterial[32].

A periodic structure is sometimes imperfect; it may contain defects or perturbations. A single disorder of an infinite periodic structure, which can be regarded as two semi-infinite periodic structures connecting through the disordered element[33], was studied. It was found that defects in the perfect periodicity may lead to narrow frequency transmission bands (i.e. defect states) within the original stop-band gaps.[34,35]

Sometimes the "defect" means the adiabatic variations of the geometries of some periodic elements in the whole system.[36] The perturbations in the geometries of the "periodic" element are random and have some statistical properties. Wave propagation through a medium with random impurity modulation will cause the phenomenon of Anderson localization,[37] which was originally discovered in the field of solid state physics and then introduced to the acoustic context.[38] It has been found that even in the absence of any dissipation, the propagation of vibration in a structure which is not perfectly periodic is impeded by the irregularities, resulting in

an exponential decay in vibration level away from the driving point.[38] In the presence of irregularities, the individual modes making up each pass-band change from being extended throughout the whole system in the periodic case to being localized in local areas. This can be interpreted as follows: if the nature modes of each periodic element of the structure are significantly different, the modes will be localized around the individual periodic element.[39] When the random irregularity of the geometries of the "periodic" elements is small compared to its mean value, as a perturbation, this kind of system is sometimes called a near-periodic system.[40] The study of vibration localization due to random disorder in near-periodic structures has been the subject of much recent research.[41,42]

Sometimes the "defect" means the non-adiabatic variations of the geometries of the periodic element, which means that substantial geometric variations occur from one cell to another.[36] The non-adiabatic local perturbation of the geometries affects the global characteristics of the whole system, which is then called quasi-periodic structure.[43] The quasi-periodic system can be described by the "quasi-Bloch" theory.[44] The distinguishing behavior of sound propagation in a quasi-periodic system lies between the corresponding behavior in a periodic and a random disorder system. It has been found that the spectrum of a quasi-periodic structure is a discrete dense set with discontinuous spectral intensities, which clearly lie between a periodic

and a random disorder system.[45]

1.3 Ventilation

Ventilation is a process of providing sufficient quantities of outside fresh air into a building and diluting the concentration of pollution to achieve a higher indoor air quality.[46] Methods for ventilating a building may be divided into mechanical and natural types.[47] Natural ventilation refers to the ventilation that is driven by pressure difference due to the wind effect or/and temperature difference;[48] while the mechanical ventilation refers to the use of mechanical fans for supplying and/or extracting air.[49] According to its characteristic, the airflow in ventilation can be divided into two types: laminar flow and turbulent flow. Laminar flow is a completely steady flow that at any fixed point, the velocity and pressure do not vary with time, which means the airflow is traveling in well-ordered layers (or lamina).[50] Generally, laminar flow exists in a situation with small ventilation opening, slow airflow speed and high flow viscosity. In fluid mechanics, this type of flow can be analyzed by simple steady-state methods, which is based on the equation for pressure drop across the opening. Such methods are recommended in current codes of practice.[51] Turbulent flow is an unsteady flow with its velocity and pressure fluctuating irregularly, covering a wide range of amplitudes and frequencies.[50] In the

description of the turbulent flow, the flow quantities are usually divided into two parts: a mean part and a fluctuating part. If the mean part is independent of time, the turbulent flow is statistically stationary, which is also called steady turbulent flow in spite of the instantaneous quantities of the flow are varying with time.[49] In practice most ventilation flows through openings can be considered to be stationary, and the mean quantities are of main interest. If the mean quantities cannot be found, the turbulent flow is non-stationary, or called unsteady turbulent flow. In the literature on ventilation, the unsteady flows have received relatively little attention and are least well understood.[49] In natural ventilation, it is difficult to analyze the unsteady flow through multiple openings of the building under the complex governing equations combined with complicated boundary conditions. For mechanical ventilation, most of mechanical ventilation systems operate with steady airflow.

The acoustic and the ventilation performances of Helmholtz resonators are the two major aspects concerned in the thesis, both of which aim at the improving the indoor environmental comfort in buildings. When considering the ventilation of an enclosure through a single opening, where the enclosure with single opening can also be regarded as a Helmholtz resonator, the flow in the neck of resonator driven by the external pressure variation can be described by a non-linear oscillator equation.[52,53,54] In both Ref. 53 and 54, the fundamental derivation of the non-linear

oscillator equation was discussed, different linearization processes were presented, and the corresponding experiment validations were carried out.

1.4 Objective and Scope of Research

This thesis aims at the improving the indoor environmental comfort in buildings by investigating the acoustic and the ventilation performances of Helmholtz resonators. The first objective of this thesis is to investigate the wave propagation in the duct with identical resonators mounted periodically. Compared with those studies[21-27] on wave propagation in periodic solid structures, air-borne sound propagation in periodic systems, especially in periodic side-branched resonators array attracts less attention. Different from the previous works on resonators array,[31,32] this thesis mainly considers the influence of the number of resonators on the noise reduction behavior of a finite periodic duct-resonator system, as well as the influence of the disorder in it. Meanwhile, the present study is different from the previous work of Seo and Kim[15] by achieving a broad noise attenuation band using identical resonators that mounted periodically. Furthermore, although those previous works on a duct with the boundary of a perforated or micro-perforated plate backed by air cavities can be regarded as identical resonators mounted periodically,[16,17] the distance between two nearby resonators considered in this thesis is much larger in

order to investigate the unusual attenuation of sound transmission in the periodic structure at low to medium frequencies.

The second objective of this thesis is to investigate the ventilation effect of Helmholtz resonators. Although in building ventilation, the airflow in the single opening of an enclosure (can be regarded as the neck of a Helmholtz resonator) driven by the external pressure variation can be described by the non-linear oscillator equation,[52-54] this does not provide any information about the actual ventilation performance of a single-opening enclosure since that may only describe the backward-forward motion of the "air piston" in the opening. The actual ventilation performance, if any, can be described by the air exchange between the external and the internal air of the enclosure through the opening. This thesis further looks into the air exchange mechanism of Helmholtz resonators.

The current chapter covers a review of the existing knowledge on Helmholtz resonator and ventilation methods. In chapter 2, a single Helmholtz resonator is investigated, in both the lumped- and distributed parameter model. Chapter 3 considers the case with multiple resonators and provides a theoretical study of sound propagation in a one-dimensional duct with identical side-branch resonators mounted periodically. Their noise reduction effect is investigated and compared with

the numerical simulation using finite element method and the experiment results. “Defects” of the periodicity in this duct-resonator system is discussed in Chapter 4, in which both the case of disorders in periodic distance between any two nearby resonators and in the geometries of Helmholtz resonators are considered. In Chapter 5, the ventilation effect of a Helmholtz resonator is discussed. It is a mechanical ventilation method different from the traditional way using mechanical fans for supplying and/or extracting air. The final chapter, Chapter 6 provides a conclusion to all the findings in the thesis, as well as suggestions for future work.

Chapter 2

Single Helmholtz Resonator

In this chapter, the theoretical analysis of a single Helmholtz resonator is presented. Firstly, the lumped-parameter model is introduced; then, the distributed-parameter model is discussed; finally, these two models are compared with the numerical simulation based on the finite element method. It should be noted that both the lumped-parameter and distributed-parameter model described in this chapter come from the existing literature. Interested readers can find a detailed discussion of these two models in Ref. 5 and 10. However, for the sake of completeness, the description of these two models is incorporated into the thesis here, and the distributed-parameter model is rewritten here in terms of matrices.

2.1 The Lumped-parameter Model

In Chapter 2, 3 and 4, only circular concentric Helmholtz resonators in the lossless case are considered. As shown in Fig. 2-1, a resonator, with neck/cavity radius r_1/r_2, cross sectional area S_1/S_2 and length l_1/l_2 respectively, is mounted on a duct with cross sectional area S_d as a side branch. The volume of the cavity is

$V_2 = \pi r_2^2 l_2$. According to Ingard[5], the acoustic impedance of the resonator Z_r is given as

$$Z_r = j\frac{\rho_0 l_1^{'}}{S_1 \omega}(\omega^2 - \omega_0^2) \tag{2.1}$$

where ρ_0 is the air density, $l_1^{'}$ is the length of the neck with end correction, and ω_0 is the resonance circular frequency (i.e. $\omega_0 = c_0\sqrt{S_1 / l_1^{'} V_2}$, c_0 the speed of sound in the air).

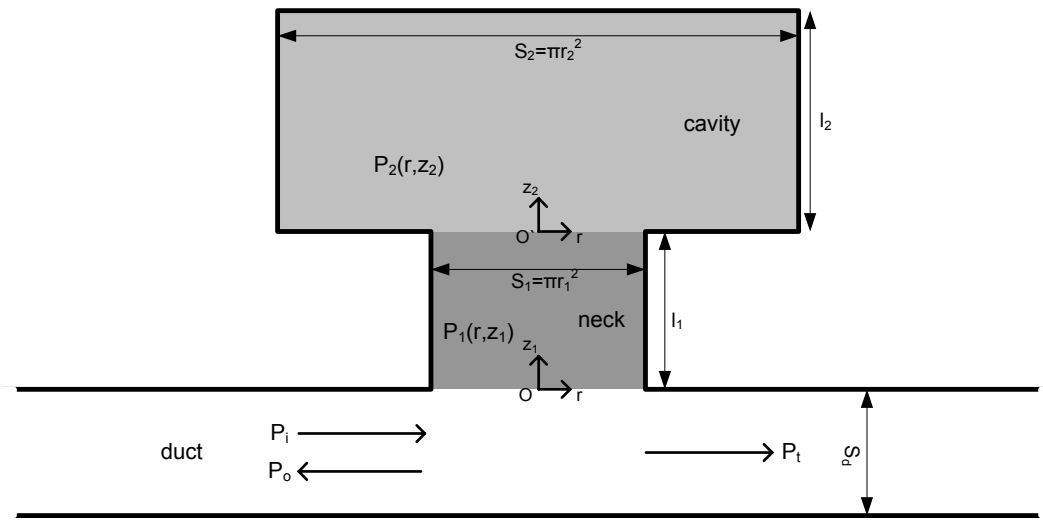

Figure 2-1. A simple model of a side-branched Helmholtz resonator

2.2 The Distributed-parameter Model

When considering the multi-dimensional wave propagation in this circular concentric resonator as shown in Fig. 2-1, the sound pressure in the neck (P_1) and

cavity (P_2) can be expressed as[10,55]

$$P_q(r,z_q) = A_0^{(q)} e^{-jkz_q} + \sum_{n=1}^{+\infty} A_n^{(q)} J_0(k_{r,n}^{(q)} r) e^{-jk_{z,n}^{(q)} z_q}$$

$$+ B_0^{(q)} e^{jkz_q} + \sum_{n=1}^{+\infty} B_n^{(q)} J_0(k_{r,n}^{(q)} r) e^{jk_{z,n}^{(q)} z_q}, \qquad q = 1,2 \tag{2.2}$$

in a cylindrical coordinate as the combination of inward-going planar waves (the first term), radial waves (the second term), outward-going planar waves (the third term), and radial waves (the fourth term), where the subscript or superscript q=1 indicates that it is a parameter considered in the neck of the resonator; the subscript or superscript q=2 indicates that it is a parameter considered in the cavity of the resonator. Herein $A_0^{(q)}$, $A_n^{(q)}$, $B_0^{(q)}$, and $B_n^{(q)}$ are the complex constants related to the magnitude of the corresponding wave mode. J_0 is the Bessel function of first kind and order zero.[56] k, $k_{r,n}^{(q)}$, and $k_{z,n}^{(q)}$ represent the wave number, the radial wave number of mode n, and the axial wave number of mode n (respectively), with the relation $k^2 = (k_{r,n}^{(q)})^2 + (k_{z,n}^{(q)})^2 \quad (q = 1,2)$. In terms of the momentum equation, the particle velocity in z-direction can be obtained as

$$V_q(r,z_q) = \frac{A_0^{(q)}}{\rho_0 c_0} e^{-jkz_q} + \frac{1}{\rho_0 \omega} \sum_{n=1}^{+\infty} A_n^{(q)} k_{z,n}^{(q)} J_0(k_{r,n}^{(q)} r) e^{-jk_{z,n}^{(q)} z_q}$$

$$- \frac{B_0^{(q)}}{\rho_0 c_0} e^{jkz_q} - \frac{1}{\rho_0 \omega} \sum_{n=1}^{+\infty} B_n^{(q)} k_{z,n}^{(q)} J_0(k_{r,n}^{(q)} r) e^{jk_{z,n}^{(q)} z_q}, \qquad q = 1,2 \tag{2.3}$$

The wall of the resonator is assumed to be rigid without any absorption materials, so the boundary conditions

$$\left.\frac{\partial P_1(r,z_1)}{\partial r}\right|_{r=r_1}=0\,,\quad \left.\frac{\partial P_2(r,z_2)}{\partial r}\right|_{r=r_2}=0\,,\quad \left.\frac{\partial P_2(r,z_2)}{\partial z_2}\right|_{z_2=l_2}=0 \tag{2.4}$$

give

$$k_{r,n}^{(1)}=\chi_n/r_1,\qquad k_{r,n}^{(2)}=\chi_n/r_2 \tag{2.5}$$

and

$$B_0^{(2)}e^{jkl_2}=A_0^{(2)}e^{-jkl_2}\,,\qquad B_n^{(2)}e^{jk_{z,n}^{(2)}l_2}=A_n^{(2)}e^{-jk_{z,n}^{(2)}l_2} \tag{2.6}$$

where χ_n is the nth root of the function[56] $J_0'(\chi_n)=0$.

At the neck-cavity interface of the resonator, the continuity conditions of sound pressure and particle velocity

$$P_1(r,z_1)\big|_{z_1=l_1}=P_2(r,z_2)\big|_{z_2=0}\,,\qquad 0\le r\le r_1 \tag{2.7}$$

$$V_1(r,z_1)\big|_{z_1=l_1}=V_2(r,z_2)\big|_{z_2=0}\,,\qquad 0\le r\le r_1 \tag{2.8}$$

give

$$\frac{1}{2}r_1^{\,2}(A_0^{(1)}e^{-jkl_1}+B_0^{(1)}e^{jkl_1})=\frac{1}{2}r_1^{\,2}(A_0^{(2)}+B_0^{(2)})+\sum_{n=1}^{+\infty}(A_n^{(2)}+B_n^{(2)})\frac{r_1r_2}{\chi_n}J_1(\frac{r_1}{r_2}\chi_n) \tag{2.9}$$

$$\frac{1}{2}r_1^{\,2}[J_0(\chi_m)]^2(A_m^{(1)}e^{-jk_{z,m}^{(1)}l_1}+B_m^{(1)}e^{jk_{z,m}^{(1)}l_1})$$

$$=\sum_{n=1}^{+\infty}(A_n^{(2)}+B_n^{(2)})\frac{r_1}{(\frac{x_n}{r_2})^2-(\frac{x_m}{r_1})^2}\frac{\chi_n}{r_2}J_0(\chi_m)J_1(\frac{r_1}{r_2}\chi_n) \tag{2.10}$$

and

$$r_1^{\,2}(A_0^{(1)}e^{-jkl_1}-B_0^{(1)}e^{jkl_1})=r_2^{\,2}(A_0^{(2)}-B_0^{(2)}) \tag{2.11}$$

$$\frac{1}{2}r_2^{\,2}k_{z,m}^{(2)}[J_0(\chi_m)]^2(A_m^{(2)}-B_m^{(2)})-k(A_0^{(1)}e^{-jkl_1}-B_0^{(1)}e^{jkl_1})\frac{r_1r_2}{\chi_m}J_1(\frac{r_1}{r_2}\chi_m)$$

$$= \sum_{n=1}^{+\infty} k_{z,n}^{(1)} (A_n^{(1)} e^{-jk_{z,n}^{(1)} l_1} - B_n^{(1)} e^{jk_{z,n}^{(1)} l_1}) \frac{r_1}{(\frac{\chi_m}{r_2})^2 - (\frac{\chi_n}{r_1})^2} \frac{\chi_m}{r_2} J_0(\chi_n) J_1(\frac{r_1}{r_2}\chi_m) \tag{2.12}$$

where J_1 is the Bessel function of first kind and order one,[56] and $m = 1,2,\ldots,+\infty$ in both Eqs. (2.10) and (2.12).

The frequency range concerned in the present study is well below the cut-on frequency of the resonator neck and the duct. It means that the nonplanar waves excited at the discontinuity junction (the duct-neck interface) will decay exponentially. Therefore, only planar waves are assumed to exist in the duct-neck interface. This is an approximation, which helps us to develop a direct relation of the sound pressure in the duct and neck by ignoring the multi-dimension effect in this complex interface. However, this assumption will be the limitation of the distributed parameter model, which will be shown in the Section 2.2 and discussed in Section 2.3. This indicates that the frequency concerned in this thesis should be low enough that not only below the cut-on frequencies of the duct and neck but also make the evanescence waves excited at the duct-neck interface decay rapidly enough to be ignored. Usually, the distributed model works well on the resonator with long and thin neck. Due to this assumption, $A_n^{(1)}$ is set to zero. At the meantime, nonplanar waves can also be excited at the neck-cavity interface due to the sudden area discontinuity. This multi-dimension effect can no longer be ignored since it can be

considered as sounds radiate into a bigger space (cavity) and the frequency may not below the cut-on frequency of the cavity. However, the nonplanar waves excited at the neck-cavity interface traveling in the neck in negative-z direction will decay over the length of the neck (i.e., $k_{z,n}^{(1)}$ should be imaginary). In this case, P_1 is assumed to be one-dimensional in the duct-neck interface and two-dimensional in the neck-cavity interface. So P_1 is no longer a variation of r in the vicinity of $z_1 = 0$. At the duct-neck interface, the continuity conditions of sound pressure and volume velocity can be expressed as

$$P_i + P_o = P_1\big|_{z_1=0} = P_t \tag{2.13}$$

$$\frac{P_i - P_o}{\rho_0 c_0} S_d = V_1\big|_{z_1=0} S_1 + \frac{P_t}{\rho_0 c_0} S_d \tag{2.14}$$

which give

$$S_d P_i = (S_d + 0.5S_1)A_0^{(1)} + (S_d - 0.5S_1)B_0^{(1)} \tag{2.15}$$

Combining Eqs. (2.6), (2.9)-(2.12), and (2.15) yields an equation set that determines the complex coefficients $A_0^{(1)}$, $B_0^{(1)}$, $B_n^{(1)}$, $A_0^{(2)}$, $B_0^{(2)}$, $A_n^{(2)}$, and $B_n^{(2)}$. Since higher-order harmonic components have a diminishing effect on the solution,[10,57] we can use a finite number of terms instead of an infinite summation of all modes and still ensure that the solution is reasonably accurate. Assuming that P_1 / P_2 is made of harmonic components up to order *N*/*M* respectively, the equation set can then be rewritten in terms of matrices, as

$$\mathbf{U}\mathbf{x} = \mathbf{y} \quad \text{or} \quad \mathbf{x} = \mathbf{U}^{-1}\mathbf{y}, \tag{2.16}$$

where $\mathbf{x}$ and $\mathbf{y}$ are both $(4+N+2M)$-dimensional vectors, which are given by

$$\mathbf{x} = \begin{bmatrix} A_0^{(1)} & B_0^{(1)} & B_1^{(1)} & \cdots & B_N^{(1)} & A_0^{(2)} & B_0^{(2)} & A_1^{(2)} & B_1^{(2)} & \cdots & A_M^{(2)} & B_M^{(2)} \end{bmatrix}^T \tag{2.17}$$

$$\mathbf{y} = \begin{bmatrix} S_d P_i & \mathbf{0}_{1\times(3+N+2M)} \end{bmatrix}^T \tag{2.18}$$

And $\mathbf{U}$ is a square matrix of dimension $(4+N+2M)\times(4+N+2M)$, which can be written as $\mathbf{U} = \begin{bmatrix} \mathbf{U}_1 & \mathbf{U}_2 & \mathbf{U}_3 & \mathbf{U}_4 \end{bmatrix}^T$. Herein the $3\times(4+N+2M)$-dimensional matrix $\mathbf{U}_1$ is given by

$$\mathbf{U}_1 = \begin{bmatrix} S_d + 0.5S_1 & S_d - 0.5S_1 & \mathbf{0}_{1\times N} & & \mathbf{0}_{1\times(2+2M)} & \\ r_1^2 e^{-jkl_1} & -r_1^2 e^{jkl_1} & \mathbf{0}_{1\times N} & -r_2^2 & r_2^2 & \mathbf{0}_{1\times 2M} \\ r_1^2 e^{-jkl_1} & r_1^2 e^{jkl_1} & \mathbf{0}_{1\times N} & -r_1^2 & -r_1^2 & \mathbf{C}_{1\times 2M} \end{bmatrix} \tag{2.19}$$

where $\mathbf{0}$ denotes a zero matrix, with the subscript such as $1\times N$ indicating its dimension, and

$$\mathbf{C}_{1\times 2M} = -2r_1 r_2 \begin{bmatrix} \frac{1}{\chi_1} J_1(\frac{r_1}{r_2}\chi_1) & \frac{1}{\chi_1} J_1(\frac{r_1}{r_2}\chi_1) & \cdots & \frac{1}{\chi_M} J_1(\frac{r_1}{r_2}\chi_M) & \frac{1}{\chi_M} J_1(\frac{r_1}{r_2}\chi_M) \end{bmatrix} \tag{2.20}$$

$\mathbf{U}_2$ is a $(M+1)\times(4+N+2M)$ matrix, as $\mathbf{U}_2 = \begin{bmatrix} \mathbf{0}_{(M+1)\times(N+2)} & \mathbf{D}_{(M+1)\times(2+2M)} \end{bmatrix}$, where

$$\mathbf{D}_{(M+1)\times(2+2M)} = \begin{bmatrix} e^{-jkl_2} & -e^{jkl_2} & & & \cdots & & 0 \\ & & e^{-jk_{z,1}^{(2)}l_2} & -e^{jk_{z,1}^{(2)}l_2} & & & \\ \vdots & & & & \ddots & \ddots & \vdots \\ 0 & & \cdots & & & e^{-jk_{z,M}^{(2)}l_2} & -e^{jk_{z,M}^{(2)}l_2} \end{bmatrix} \tag{2.21}$$

The $N\times(4+N+2M)$-dimensional matrix $\mathbf{U}_3$ is given by

$\mathbf{U}_3 = \begin{bmatrix}\mathbf{0}_{N\times 2} & \mathbf{E}_{N\times N} & \mathbf{0}_{N\times 2} & \mathbf{F}_{N\times 2M}\end{bmatrix}$, in which

$$\mathbf{E}_{N\times N} = \frac{1}{2} r_1^2 \begin{bmatrix} [J_0(\chi_1)]^2 e^{jk_{z,1}^{(1)} l_1} & & \\ & \ddots & \\ & & [J_0(\chi_N)]^2 e^{jk_{z,N}^{(1)} l_1} \end{bmatrix}$$

(2.22)

$$\mathbf{F}_{N\times 2M} = \frac{r_1}{r_2} \begin{bmatrix} \Psi_{1,1} & \cdots & \Psi_{M,1} \\ \vdots & \ddots & \vdots \\ \Psi_{1,N} & \cdots & \Psi_{M,N} \end{bmatrix} \times \begin{bmatrix} 1 & 1 & & & \\ & & \ddots & \ddots & \\ & & & 1 & 1 \end{bmatrix} \tag{2.23}$$

where

$$\Psi_{m,n} = \frac{\chi_m}{(\frac{\chi_m}{r_2})^2 - (\frac{\chi_n}{r_1})^2} J_0(\chi_n) J_1(\frac{r_1}{r_2}\chi_m) \quad \text{for} \quad n = 1,2,...N \quad \text{and} \quad m = 1,2,...,M \ .$$

$\mathbf{U}_4$ is a $M \times (4 + N + 2M)$ matrix, as $\mathbf{U}_4 = \begin{bmatrix}\mathbf{I}_{M\times 2} & \mathbf{J}_{M\times N} & \mathbf{0}_{N\times 2} & \mathbf{K}_{M\times 2M}\end{bmatrix}$, in which

$$\mathbf{I}_{M\times 2} = -k r_1 r_2 \begin{bmatrix} \dfrac{J_1(\frac{r_1}{r_2}\chi_1)}{\chi_1} \\ \vdots \\ \dfrac{J_1(\frac{r_1}{r_2}\chi_M)}{\chi_M} \end{bmatrix} \times \begin{bmatrix} e^{-jkl_1} & -e^{jkl_1} \end{bmatrix} \tag{2.24}$$

$$\mathbf{J}_{\mathbf{M\times N}} = \frac{r_1}{r_2} \begin{bmatrix} k_{z,1}^{(1)} \Psi_{1,1} e^{jk_{z,1}^{(1)} l_1} & \cdots & k_{z,N}^{(1)} \Psi_{1,N} e^{jk_{z,1}^{(1)} l_1} \\ \vdots & & \vdots \\ k_{z,1}^{(1)} \Psi_{M,1} e^{jk_{z,1}^{(1)} l_1} & \cdots & k_{z,N}^{(1)} \Psi_{M,N} e^{jk_{z,1}^{(1)} l_1} \end{bmatrix} \tag{2.25}$$

$$\mathbf{K}_{M\times 2M} = \frac{1}{2} r_2^2 \begin{bmatrix} [J_0(\chi_1)]^2 k_{z,1}^{(2)} & & \\ & \ddots & \\ & & [J_0(\chi_M)]^2 k_{z,M}^{(2)} \end{bmatrix} \times \begin{bmatrix} 1 & -1 & & & \\ & & \ddots & \ddots & \\ & & & 1 & -1 \end{bmatrix}$$

(2.26)

So the acoustic impedance of the Helmholtz resonator in the neck opening, can be derived by $Z_r = P_1/(V_1 S_1)\big|_{z_1=0}$, where P_1 and V_1 are described in Eqs. (2.2) and (2.3). An example of the MATLAB codes of the distributed-parameter model of Helmholtz resonator is attached in the appendix.

2.3 Numerical Simulation

To compare the theoretical prediction of Helmholtz resonator using lumped- and distributed-parameter models, the three-dimensional finite element method (FEM) using the commercial software COMSOL Multiphysics® version 2009 is used in the thesis as a validation tool, which also offers an extensive interface to MATLAB and its toolboxes for a large variety of programming and postprocessing works. In this chapter, the following parameters are set in both theoretical calculation and numerical simulation: $c_0 = 344$ m/s, $\rho_0 = 1.21$ kg/m^3. To ensure accuracy, a fine mesh spacing of less than $0.01\,\mathrm{m}$ was used and the model was divided into more than 3600 elements for both two cases in Fig. 2-2. The geometries of the duct and resonator in Fig. 2-2(a) are: $r_1 = 2$ cm, $r_2 = 8$ cm, $l_1 = 5$ cm, $l_2 = 12$ cm; and those in Fig. 2-2(b) are: $r_1 = 2$ cm, $r_2 = 5$ cm, $l_1 = 5$ cm, $l_2 = 7$ cm.

2.4 Results and Discussion

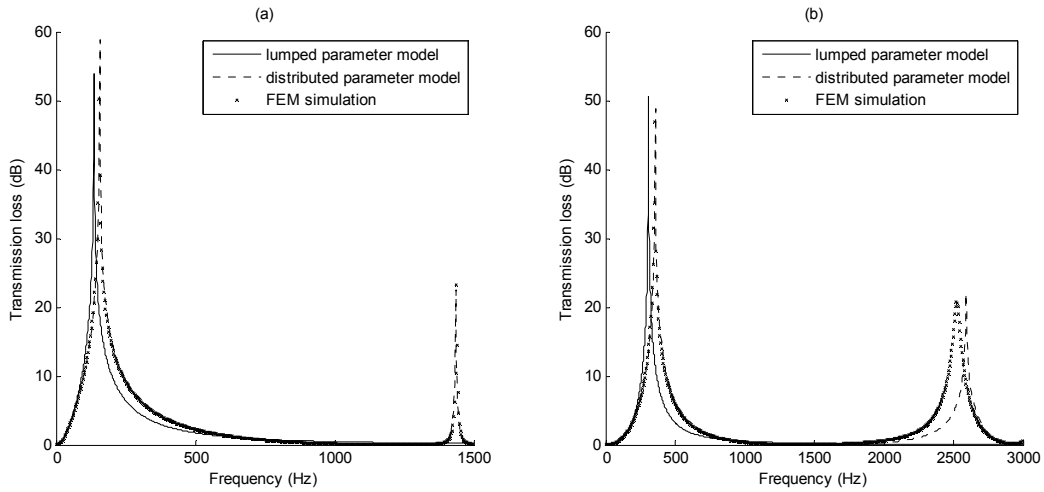

Figure 2-2. Transmission loss comparison between the lumped-parameter model, the distributed-parameter model, and FEM simulation of Helmholtz resonator.

The comparison of HR transmission loss (*TL*) derived by the distributed-parameter model, the lumped-parameter model, and FEM simulation is shown in Fig. 2-2(a) and Fig. 2-2(b). It can be seen that the traditional lumped-parameter model does not agree well with the FEM simulation in both Figs. 2-2(a) and 2-2(b) particularly at the fundamental resonance frequency at around 160 Hz in Fig. 2-2(a) and 340 Hz in Fig. 2-2(b). Strictly speaking, this indicates that the lumped-parameter model has a bigger relative error with the FEM simulation than the distributed model. This deviation between the lumped distributed model and the FEM simulation is large

enough to lead to the misprediction of the fundamental resonance peak due to its narrow bandwidth, which is similar to that observed in Ref. 10. Compared with lumped-parameter model, the model of a distributed-parameter Helmholtz resonator agrees very well with the FEM simulation at most frequencies, including the fundamental resonance frequency at around 160 Hz in Fig. 2-2(a) and 340 Hz in Fig. 2-2(b), and the second resonance frequency at around 1450 Hz in Fig. 2-2(a). This may indicate that the multidimensional effects in the neck-cavity interface considered in the distributed model have a more accurate description on the frequency characteristic of the Helmholtz resonator than the interior end correction in the lumped model in this case. However, it can also be observed in Fig. 2-2(b) that the discrepancy between the distributed-parameter and the FEM simulation increases as the frequency increases, especially, at around the second resonance peak of around 2500 Hz. It may be due to the assumption of the distributed model that the planar wave propagated in the neck-duct interface becomes invalid as the frequency increases to above 2000 Hz. It should be noted that this assumption (only planner wave exists in the duct-neck interface) comes from the mathematical difficulties on solving the non-planner waves in this complex interface. The discrepancy on the 2nd resonance peak shows the frequency limitation of this distributed-parameter model due to this assumption. In general, the comparison in both Fig. 2-2(a) and (b) show clearly that the model of distributed-parameter HR has a more accurate description

of the frequency characteristic of an HR in most frequencies provided that the planar wave propagation in the neck-duct interface can be ensured.

Chapter 3

Periodic Helmholtz Resonators Array

3.1 Wave Propagation in a Semi-infinite Duct Loaded Periodically with Resonators

3.1.1 Theoretical Outline

This section considers a semi-infinite duct loaded periodically with resonators, as shown in Fig. 3-1. Compared with the length of duct segment between two nearby resonators *D*, the diameter of the neck of the resonator is assumed to be negligible since the length *D* usually much larger than the diameter of the neck (as shown in the remainder part of the chapter). In other words, *D* also can be regarded as the periodic distance.

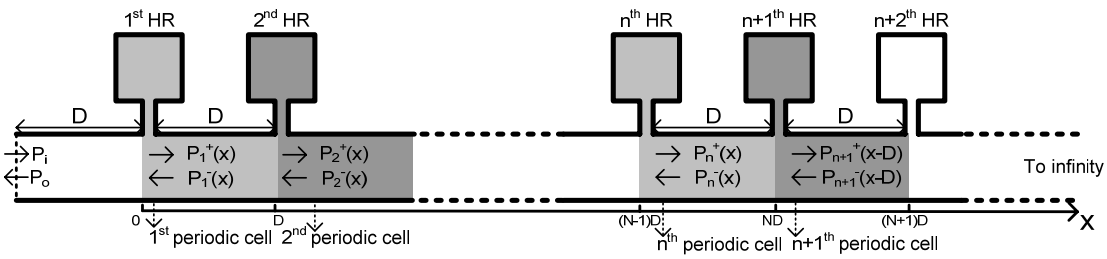

Figure 3-1. Semi-infinite duct loaded periodically with resonators.

As shown in Fig. 3-1, a typical periodic cell consists of the duct segment and a resonator attached to the left side. As assumed in Chapter 2, only planar waves exist in the duct and the vicinity of the opening of the resonator. In the region of the nth periodic element, $(n-1)D \le x \le nD$, the sound traveling in positive- and negative-x directions can be described with sound pressure $P_n^+(x) = C_n^+ e^{-jk(x-(n-1)D)}$ and $P_n^-(x) = C_n^- e^{jk(x-(n-1)D)}$, where C_n^+ and C_n^- are complex constants related to the magnitude of positive- and negative-going planar waves in the nth duct segment respectively. In the region of the next cell, $nD \le x \le (n+1)D$, the acoustic field has a similar form, with sound pressure $P_{n+1}^+(x) = C_{n+1}^+ e^{-jk(x-nD)}$ and $P_{n+1}^-(x) = C_{n+1}^- e^{jk(x-nD)}$. Combining the continuity of sound pressure and volume velocity at the point $x = nD$ yields the relation between the nth cell and n^{th}+1 cell in the form of matrix, called the periodic transfer matrix[36] **T**, as

$$\begin{bmatrix} C_{n+1}^+ \\ C_{n+1}^- \end{bmatrix} = \mathbf{T} \begin{bmatrix} C_n^+ \\ C_n^- \end{bmatrix} \tag{3.1}$$

where the 2×2-dimensional matrix **T** is given by

$$\mathbf{T} = \begin{bmatrix} (1 - \frac{1}{2}\frac{S_1}{S_d}\frac{\rho_0 c_0}{Z_r^{'}})e^{-jkD} & -\frac{1}{2}\frac{S_1}{S_d}\frac{\rho_0 c_0}{Z_r^{'}} e^{jkD} \\ \frac{1}{2}\frac{S_1}{S_d}\frac{\rho_0 c_0}{Z_r^{'}} e^{-jkD} & (1 + \frac{1}{2}\frac{S_1}{S_d}\frac{\rho_0 c_0}{Z_r^{'}})e^{jkD} \end{bmatrix} \tag{3.2}$$

The entry in the ith row and the jth column of **T** is denoted as t_{ij}, and $Z_r^{'}$ is the acoustic characteristic impedance of the resonator, which can be derived by using the lumped-parameter model in Section 2.1 or the distributed-parameter model in

Section 2.2, as $Z_r^{'} = Z_r / S_1$.

Dynamic periodic systems are unlike static periodic systems, which can be described in terms of a periodic function $f(x)$, with the relation $f(x+L) = f(x)$, where L is the periodicity of the function. Instead, dynamic periodic systems (such as the sound field distribution in the periodic structure considered in this section) can be described by the function $f(x+L) = e^{\mu} f(x)$. This is called the Bloch wave theory.[28] Therefore, Eq. (3.1) can be rewritten in another form, as

$$\begin{bmatrix} C_{n+1}^{+} & C_{n+1}^{-} \end{bmatrix}^T = e^{\mu} \begin{bmatrix} C_n^{+} & C_n^{-} \end{bmatrix}^T \tag{3.3}$$

Combining Eqs. (3.1) and (3.3), the analysis of a periodic resonator system boils down to an eigenvalue problem that involves finding the eigenvalue $\lambda = e^{\mu}$ and the corresponding eigenvector $\mathbf{v} = \begin{bmatrix} v^{+} & v^{-} \end{bmatrix}^T$ for the transfer matrix **T**.

3.1.2 Nature of the Characteristic Wave Type

μ in Eq. (3.3) is called the propagation constant,[22] which is a complex value composed of a real part μ_r, called the attenuation constant, and an imaginary part μ_i, called the phase constant ($\mu = \mu_r + j\mu_i$). In principle there are ranges of frequencies in which the solution contains the real part μ_r. This result indicates that the energy gets attenuated when waves travel through each periodic cell, and those frequency ranges are called the stop-bands. In other frequency ranges, the solution

only contains the imaginary part μ_i, which indicates that there is only a phase delay when a wave travels through each cell. These frequency ranges that the waves are allowed to propagate through are called the pass-bands.

Combining Eqs. (3.1) and (3.3) yields the characteristic polynomial[58] of **T**. Note that—for a passive system—the determinant of the matrix **T** is unity[36] and

$$e^{2\mu} - (t_{11} + t_{22})e^{\mu} + t_{11}t_{22} - t_{12}t_{21} = e^{2\mu} - (t_{11} + t_{22})e^{\mu} + 1 = 0 \tag{3.4}$$

Consequently, we can write

$$\cos(j\mu) = \frac{1}{2}(t_{11} + t_{22}) = \frac{1}{2}(e^{jkD} + e^{-jkD}) + \frac{1}{4}\frac{S_1}{S_d}\frac{\rho_0 c_0}{Z_r^{'}}(e^{jkD} - e^{-jkD}) \tag{3.5}$$

Eq. (3.5) indicates that μ is a function of the frequency and other geometric parameters, such as periodic distance (*D*) and resonator acoustic characteristic impedance ($Z_r^{'}$). In general, the eigenvalue $\lambda = e^{\mu}$ describes the propagation property of a characteristic wave type, and the characteristic wave type is defined by its corresponding eigenvalue $\begin{bmatrix} v^+ & v^- \end{bmatrix}^T$, which represents the specific linear combination of positive- and negative-going planar waves. There are two solutions of μ in Eq. (3.5) that occur in opposite pairs: $\mu = \pm(\mu_r + j\mu_i)$ in the stop-bands, and $\mu = \pm j\mu_i$ in the pass-bands. Assumed that $\mu_r > 0$ and $0 \le \mu_i < 2\pi$, $\mu_1 = -(\mu_r + j\mu_i)$ describes the propagation property of the "positive-going" characteristic wave type (or simply positive wave type), defined by the corresponding eigenvector $\mathbf{v}_1 = \begin{bmatrix} v_1^+ & v_1^- \end{bmatrix}^T$. Similarly, $\mu_2 = \mu_r + j\mu_i$ describes the

propagation property of the "negative-going" characteristic wave type (or simply negative wave type), defined by the corresponding eigenvector $\mathbf{v}_2 = \begin{bmatrix} v_2^+ & v_2^- \end{bmatrix}^T$. It can be imagined that these two wave type are of the same characteristic wave type but traveling in opposite directions, and there are relations between two corresponding eigenvectors ($\mathbf{v}_1 = \begin{bmatrix} v_1^+ & v_1^- \end{bmatrix}^T$ and $\mathbf{v}_2 = \begin{bmatrix} v_2^+ & v_2^- \end{bmatrix}^T$) , as $\left|v_1^+\right| = \left|v_2^-\right|$, and $\left|v_1^-\right| = \left|v_2^+\right|$.

When planar waves travel in the semi-infinite duct with periodic resonators considered in this section, only the positive-going characteristic wave type $\mathbf{v}_1$ exists in duct segments of all periodic cells, as

$$\begin{bmatrix} C_n^+ \\ C_n^- \end{bmatrix} = a_n \mathbf{v}_1 = a_n \begin{bmatrix} v_1^+ \\ v_1^- \end{bmatrix}, \qquad n = 1,2,...,\infty \tag{3.6}$$

where a_n is a complex constant. By introducing Eq. (3.1), Eq. (3.6) can be expressed as

$$\begin{bmatrix} C_n^+ \\ C_n^- \end{bmatrix} = \mathbf{T} \begin{bmatrix} C_{n-1}^+ \\ C_{n-1}^- \end{bmatrix} = \mathbf{T}^2 \begin{bmatrix} C_{n-2}^+ \\ C_{n-2}^- \end{bmatrix} = \ldots = \mathbf{T}^{n-1} \begin{bmatrix} C_1^+ \\ C_1^- \end{bmatrix} = a_1 \mathbf{T}^{n-1} \mathbf{v}_1 = a_1 \lambda_1^{\,n-1} \mathbf{v}_1 \tag{3.7}$$

which gives $a_n = a_1 \lambda_1^{\,n-1}$. Eq. (3.7) indicates that the positive- and negative-going planar waves in duct segments of all periodic cells have the same amplitude ratio $\left|v_1^+ / v_1^-\right|$ and decay at the same rate $\left|a_{n+1} / a_n\right|$ $(= e^{-\mu_r})$ when they pass through each periodic cell along the positive-*x* direction. In other words, they propagate as a whole in the positive-*x* direction, denoted as the positive-going characteristic wave type.

Let $\mu_1 = -jqD$ ($\lambda_1 = e^{-jqD}$), the sound pressure in the duct segment of nth periodic cell can be expressed as

$$P_n(x) = C_n^+ e^{-jk(x-(n-1)D)} + C_n^- e^{jk(x-(n-1)D)}$$

$$= [a_1 v_1^+ e^{-jk(x-(n-1)D)} + a_1 v_1^- e^{jk(x-(n-1)D)}] e^{-jq(n-1)D} \tag{3.8}$$

Let us set $x_n = x-(n-1)D$ ($0 \le x_n \le D$), which is a local variable. The exponential component of Eq. (3.8) (i.e. $e^{-jq(n-1)D}$) represents net changes of the characteristic wave type from cell to cell in a positive-x direction. The terms in square bracket ($a_1 v_1^+ e^{-jkx_n} + a_1 v_1^- e^{jkx_n}$) represent components of the characteristic wave type, and its behavior in a periodic cell. Besides, Eq. (3.8) indicates that the positive-going characteristic wave type $\mathbf{v}_1$ contains the negative-going planer wave component v_1^-. Moreover, Eq. (3.8) can be expressed as

$$P_n(x) = [a_1 v_1^+ e^{-j(k-q)x_n} + a_1 v_1^- e^{j(k+q)x_n}] e^{-jqx} = \Phi_1(x_n) e^{-jqx} \tag{3.9}$$

It can be noted that the x in the exponential term e^{-jqx} is a global variable; Eq. (3.9) describes the sound pressure distribution in the whole duct. This is another expression of the positive-going characteristic wave type. It can be seen that q is the wave number of the wave type.

Fig. 3-2 shows the distribution of the attenuation constant μ_r, in terms of $20\log_{10}(e^{\mu_r})$, and the phase constant μ_i. Resonators, with neck radius r_1=1.7 cm, length l_1=4.55 cm and cavity radius r_2=4.7 cm, length l_2=4 cm, mounted on a

duct of cross sectional area S_d=13.2 cm^2 is selected here, with periodic distance D=40 cm. The positive-going characteristic wave type is seen to propagate without attenuation over the two broad bands of 0-240 Hz and 630-870 Hz with a phase change per cell μ_i. A strong stop-band is found in the frequency range of 240-630 Hz, with a phase inversion between two nearby periodic cells (i.e. $\mu_i = \pi$). A sharp peak is observed at around 420 Hz, which is due to the resonance of the Helmholtz resonators. It should be noted that there is a sharp gap at around 425 Hz in the stop-band, which belongs to the phase inverse of a single resonator at its resonance frequency f_0. Basically, the frequency positions of the peak and gap of the stop-band are related to the f_0 of the single resonator, the bandwidth of which is controlled by the periodic distant *D*, as well as the geometries of both duct and resonators. The distribution of the frequency band into the stop- and pass-bands is due to wave coupling, which is similar to the waves that Yun and Mak[27] observed propagating in a periodic structure. Different kinds of the stop-bands including their peaks and gaps will be discussed in detail further in Section 3.1.4.

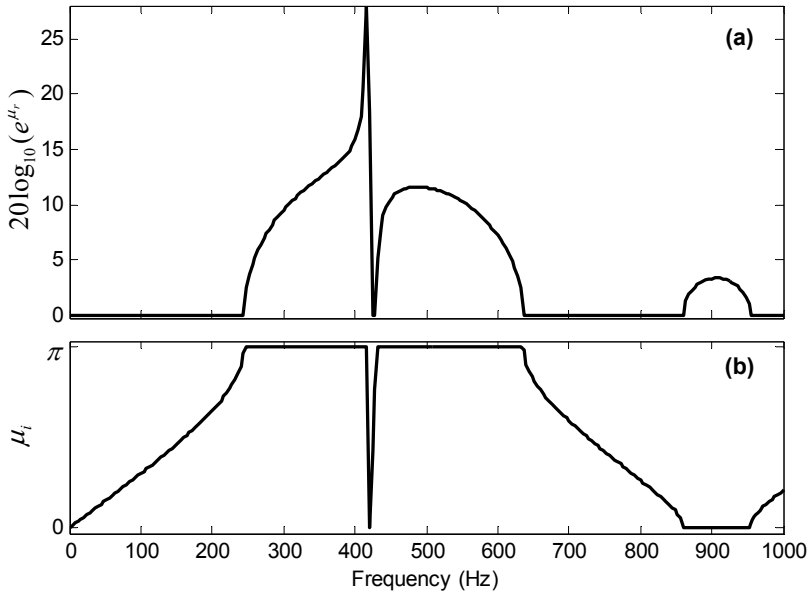

Figure 3-2. Frequency variation of the real and imaginary parts of the propagation constant for the positive-going characteristic wave type in the semi-infinite duct with periodic resonators.

Fig. 3-3 shows the ratio of negative- and positive-going planar wave components in the positive-going characteristic wave type in terms of $\left|v_1^- / v_1^+\right|$, ignoring the phase difference between them. The dimensions of duct, resonators and periodic distance used here maintain the same as those used in Fig. 3-2, i.e. r_1=1.7 cm, l_1=4.55 cm r_2=4.7 cm, l_2=4 cm, S_d=13.2 cm^2 and D=40 cm. The stop- and the pass-bands are the same as shown in Fig. 3-2(a). It can be seen that even in the pass-bands of the positive-going characteristic wave type as shown in Fig 3-2(a), a small amount of negative-going planar wave component v_1^- exists, which means the "pass-band" is fully passed for the characteristic wave type, but not for the planar waves. In the situation of planar waves traveling though a single resonator, a full reflection only

occurs at the resonance frequency f_0 of the resonator. In contrast, a full reflection (i.e. $\left|v_1^- / v_1^+\right| = 1$) is observed here in the whole stop-band (240-630 Hz and 870-940 Hz) regardless of whether the characteristic wave type decays significantly or only slightly.

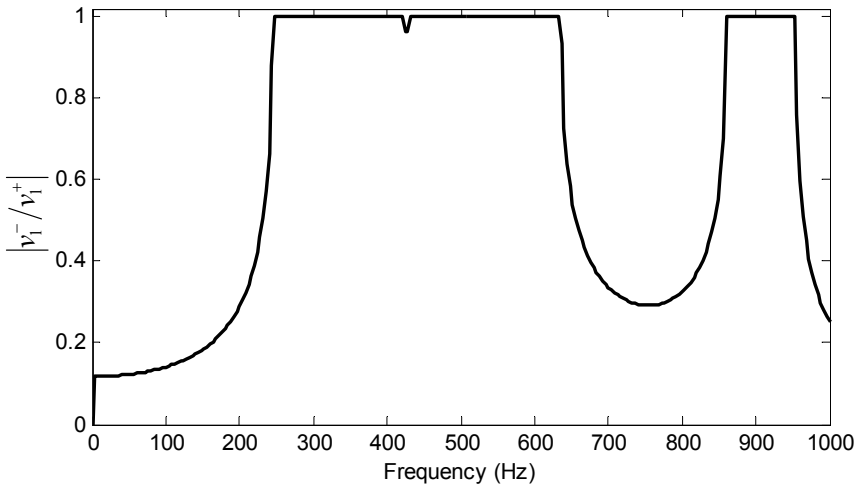

Figure 3-3. Frequency variation of the positive- and negative-going planar wave components of the positive-going characteristic wave types in the semi-infinite duct with periodic resonators.

3.1.3 Response of a Semi-infinite Duct Loaded Periodically with Resonators

This study also investigated a semi-infinite duct with periodic resonators responding to external excitation, which is a positive-going sound wave of pressure magnitude $P_i = 1$. The sound propagation can be described by the maximum sound pressure in the duct segments of the first five periodic cells. The maximum sound pressure in the

duct segment of the nth cell $P_{n,\max}$ can be calculated by finding the maximum[59] of

$$P_n(x) = P_n^+(x) + P_n^-(x) = C_n^+ e^{-jk(x-(n-1)D)} + C_n^- e^{jk(x-(n-1)D)} \qquad n = 1,2,\ldots,5 \tag{3.10}$$

The dimensions of the duct, resonators and periodic distance used in Fig. 3-4 maintain the same as those used in Fig. 3-2, i.e. r_1=1.7 cm, l_1=4.55 cm r_2=4.7 cm, l_2=4 cm, S_d=13.2 cm^2 and D=40 cm. Fig. 3-4 clearly shows the occurrence of the pass-bands and stop-bands that are associated with the corresponding propagation constant in Fig. 3-2(a). In the main stop-band of 240-630 Hz, the energy of the propagating waves drops at a rate of about 10 dB per periodic cell. It is also seen that the system has a strong attenuation peak at the natural frequency of a single resonator (i.e., around 415 Hz).

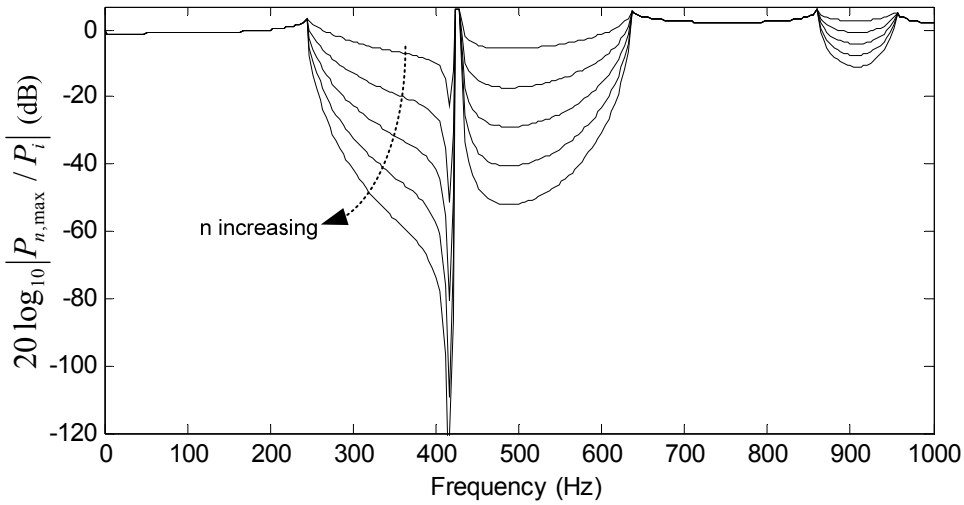

Figure 3-4. Frequency variation of the maximum sound pressure in duct segments of the first five periodic cells of the semi-infinite structure, *n*=1,2,…,5.

3.1.4 Bandwidth Discussion of the Characteristic Wave Type

In this section, the stop-band width of the characteristic wave type is investigated. Although Eq. (3.5) describes the frequency characteristics of the characteristic wave type, it does not give an explicit expression about the position of the stop-bands, as well as their bandwidth. Furthermore, although the distributed-parameter model provides a more accurate prediction for the resonance frequency, only the lumped-parameter model is used here to give readers a clear and direct impression of the tendency of bandwidth to vary with the geometries of the resonators. The theoretical prediction of the bandwidth has been proposed by Sugimoto and Horioka[31] for small resonators (compared to the geometries of the duct), and this section will expand their work to a wider applicable range by adding some modification. In general, three types of stop-bands result from either the resonance of the resonators or the Bragg reflection, or from both.[31] Using the definitions of Z_r (lumped-parameter model) and Z_d, as

$$Z_r = j\frac{\rho_0 l_1^{'}}{S_1\omega}(\omega^2 - \omega_0^2) \quad \text{and} \quad Z_d = \rho_0 c_0 / S_d \tag{3.11}$$

where Z_d is the acoustic impedance of the duct. Eq. (3.5) can be rewritten as

$$\cos(qD) = \cos(kD) + \frac{V_2 k}{2S_d\left[(\omega/\omega_0)^2 - 1\right]}\sin(kD) \tag{3.12}$$

When the right hand side of Eq. (3.12) is smaller than or equals to unity, the wave number of the characteristic wave type q is real; and the corresponding frequency range is the pass-band. At the meanwhile, when the right hand side of Eq. (3.12) is larger than unity, q is a complex number; and the corresponding frequency range is the stop-band. Therefore the position of the stop-band is determined by the stop-band boundary when the right hand side of Eq. (3.12) equals to unity.

The first kind of stop-band (referred to as stop-band I) results from the resonance of the resonators. The stop-band is near ω_0, as $\omega/\omega_0 = 1+\Delta$, where $|\Delta| < 1$ is assumed. To differentiate it from the other two types of stop-bands, $k_0 D \neq m\pi$ here, where $k_0 = \omega_0 / c_0$. When the modulus of Eq. (3.12) is equal to unity, the approximated stop-band boundary $\Delta_{1,2}$ can be obtained, as

$$\Delta_1 = \frac{V_c k_0}{4S_d}\cot[\frac{k_0 D}{2}(1+\Delta_1)] = \frac{\kappa k_0 D}{4}[\cot(\frac{k_0 D}{2}) - \frac{1}{\sin^2(k_0 D/2)}\frac{k_0 D}{2}\Delta_1 + ...] \qquad (3.13)$$

$$\Delta_2 = -\frac{V_c k_0}{4S_d}\tan[\frac{k_0 D}{2}(1+\Delta_1)] = -\frac{\kappa k_0 D}{4}[\tan(\frac{k_0 D}{2}) + \frac{1}{\cos^2(k_0 D/2)}\frac{k_0 D}{2}\Delta_2 + ...] \qquad (3.14)$$

where κ is the ratio of the cavity's volume to the duct's volume in a periodic cell ($\kappa = V_2 / S_d D$), which is generally assumed to be smaller than unity ($\kappa < 1$). The terms in the square bracket of Eq. (3.13)/(3.14) are the series expansion of the cotangent/tangent terms, respectively. The zero order corrections (the first terms in the square brackets) of Eqs. (3.13) and (3.14) give $\Delta_1 = \kappa k_0 D/4 \cdot \cot(k_0 D/2)$ and

$\Delta_2 = -\kappa k_0 D/4 \cdot \tan(k_0 D/2)$, with a relative bandwidth $\Delta_{BW} = \kappa k_0 D/2 \cdot \left|\tan(k_0 D/2) + \cot(k_0 D/2)\right|$. These are obtained from Sugimoto and Horioka's examination of the issue,[31] which also includes a general discussion of stop-band I. The bandwidth Δ_{BW} is of the order κ. Furthermore, Δ_{BW} reaches its minimum value when $k_0 D$ is an odd number multiplied by $\pi/2$, and becomes broader when it approaches multiples of π. However, this approximation has a significant deviation when $|\Delta| > 0.1$. A more accurate result can be obtained by considering the first order corrections (the second terms in the square brackets) of Eqs. (3.13) and (3.14), or even the higher order corrections.

The second kind of stop-band (referred to as stop-band II) is the result of the Bragg reflection, which occurs when the periodic distance becomes a multiple of a half-wavelength of sound waves ($kD = m\pi \quad m = 1,2,...$).[31] The stop-band is near $\omega_m = m\pi c_0 / D$, as $\omega/\omega_m = 1 + \Delta$. To differentiate it from the third case, $\omega_m \neq \omega_0$ here. In the frequency range of stop-band II, Eq. (3.12) can be approximated as

$$\cos(qD) = \cos(m\pi + \Delta m\pi) + \frac{V_2 m\pi(1+\Delta)}{2DS_d\left[(\omega_m(1+\Delta)/\omega_0)^2 - 1\right]}\sin(m\pi + \Delta m\pi)$$

$$= (-1)^m \left\{1 + \frac{(m\pi)^2}{2}E\right\} \tag{3.15}$$

where

$$E = \frac{\kappa(1+\Delta)}{((1+\Delta)\omega_m/\omega_0)^2 - 1}\Delta - \Delta^2 \tag{3.16}$$

E can be approximated as $G\Delta - \Delta^2$, where $G = \kappa/[(\omega_m/\omega_0)^2 - 1]$, which gives $\Delta_1 = 0$ and $\Delta_2 = \kappa/[(\omega_m/\omega_0)^2 - 1]$ with the relative bandwidth $\Delta_{BW} = \kappa/\left|(\omega_m/\omega_0)^2 - 1\right|$. This is derived by Sugimoto and Horioka.[31] For stop-bands II where $\omega_m < \omega_0$, there is $1 + \kappa/[(\omega_m/\omega_0)^2 - 1] \le \omega/\omega_m \le 1$; for others in higher frequency ranges where $\omega_m > \omega_0$, there is $1 \le \omega/\omega_m \le 1 + \kappa/[(\omega_m/\omega_0)^2 - 1]$. In general, ω_m is always one stop-band boundary and the stop-band appears on either side of ω_m only, which depends on the relative position of ω_m and ω_0. The relative bandwidth Δ_{BW} is of the order κ, which becomes broader as it approaches the resonance frequency ω_0. Similarly, the approximation made above has a significant deviation when $|\Delta| > 0.1$. A modified approximation can be obtained by rewriting Eq. (3.16) as

$$E = \frac{\kappa(1+\Delta)\Delta}{2\gamma^2\Delta + \gamma^2 - 1} - \Delta^2 \tag{3.17}$$

where $\gamma = \omega_m/\omega_0$. In addition to $\Delta_1 = 0$, there are two other roots, as

$$\Delta_{2,3} = \frac{\kappa + 1 - \gamma^2 \pm \sqrt{(\gamma^2 - 1 - \kappa)^2 + 8\kappa\gamma^2}}{4\gamma^2} \tag{3.18}$$

For the stop-bands II of $\gamma < 1$, Δ_2 is in the range of (-1, 0), which is the physically reasonable root. For the stop-bands II of $\gamma > 1$, the Δ_3 in the range of (0, 1) should be selected.

The third case (referred to as stop-band III) results from both the resonance of the

resonator and the Bragg reflection (i.e. $\omega_m = \omega_0$). In the frequency range of stop-band III, Eq. (3.16) can be approximated as $E = \kappa / 2 - \Delta^2$, with $\Delta_{1,2} = \pm\sqrt{\kappa / 2}$ and the relative bandwidth $\Delta_{BW} = \sqrt{2\kappa}$. This is obtained from Sugimoto and Horioka.[31] Compared with the previous two types, this stop-band is widened to be of the order $\sqrt{\kappa}$. As D is in this case limited to $m\pi / k_0$ ($k_0 D = m\pi$), the relative bandwidth Δ_{BW} is at its maximum value when $m = 1$. Similarly, the approximation has a significant deviation when $|\Delta| > 0.1$. Substituting $\omega_m / \omega_0 = 1$ into Eq. (3.16) gives

$$\Delta^3 + 2\Delta^2 - \kappa\Delta - \kappa = 0 \tag{3.19}$$

The equation above has three roots,[60] as

$$\Delta_1 = -\frac{2}{3} - \frac{2}{3}\sqrt{4 + 3\kappa}\cos(\frac{\theta}{3}) \tag{3.20}$$

$$\Delta_{2,3} = -\frac{2}{3} + \frac{\sqrt{4 + 3\kappa}}{3}[\cos(\frac{\theta}{3}) \pm \sqrt{3}\sin(\frac{\theta}{3})] \tag{3.21}$$

where $\theta = \arccos(K)$, $K = (16 - 9\kappa)/[2(4 + 3\kappa)^{1.5}]$. As $\Delta_1 < -1$ is physically impossible, the other two roots $\Delta_{2,3}$ are chosen. Compared to the results obtained by Sugimoto and Horioka,[31] Eq. (3.21) indicates that f_0 is not exactly in the middle of the stop-band.

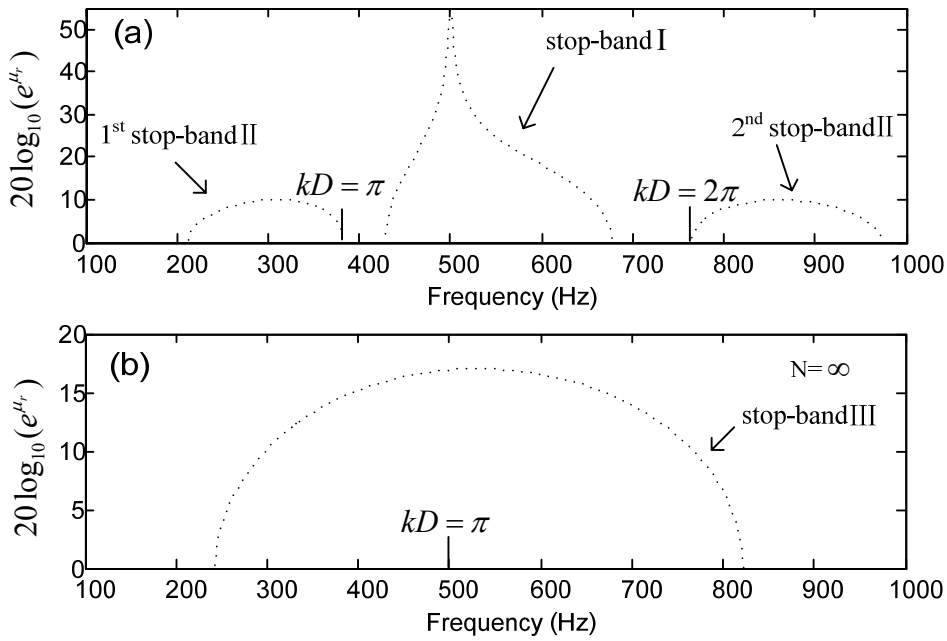

Figure 3-5. Three types of stop-bands.

Fig. 3-5 shows an example of three types of stop-bands. For Fig 3-5(a), the geometries of resonators and duct are: $r_1 = 2$ cm, $l_1 = 2.1$ cm, $V_2 = 136.75\pi$ cm^3, $S_d = 12$ cm^2, $D = 45$ cm; for Fig 3-5(b), $D = 34.4$ cm with others unchanged.

Stop-bands I and II are shown in Fig. 3-5(a). The Sugimoto and Horioka's approximation[31] gives stop-band I at around 280-1280 Hz ($\Delta_1 = -0.43$ and $\Delta_2 = 1.55$), and the first stop-band II at around -344-382 Hz (the prediction form Ref. 31 gives a physically meaningless lower frequency boundary in this case with big Helmholtz resonators). The modified approximation using Eqs. (3.13) and (3.14) gives stop-band I at around 430-590 Hz ($\Delta_1 = -0.14$ and $\Delta_2 = 0.18$, the consideration is up to the first order corrections) and the first stop-band II using Eq.

(3.18) at around 210-382 Hz. Comparing the predicted stop-band I at 425-680 Hz with the first stop-band II ($kD = \pi$) at 210-380 Hz using implicit equation, Eq. (3.5), it is clear that the modified approximation derived from Eqs. (3.13), (3.14) and (3.18) shows better agreement with the theoretical prediction than that of Sugimoto and Horioka.

Stop-band III is shown in Fig. 3-5(b). Sugimoto and Horioka's approximation gives stop-band III at 185-815 Hz, while the modified approximation derived from Eq. (3.21) gives stop-band III at around 240-850 Hz. Comparing the predicted stop-band III at 240-820 Hz using implicit equation, Eq. (3.5), the modified approximation has a relative error of 17%, which is less than the 24% relative error in Sugimoto and Horioka's approximation. The modified approximation makes only a slight improvement on the prediction, because the modified approximation on the cosine and sine terms of Eq. (3.15) has a relatively low accuracy as $|\Delta| > 0.5$.

3.2 Wave Propagation in a Finite-length Duct Loaded Periodically with *N* Resonators

3.2.1 Theoretical Outline

In the previous section, for a semi-infinite duct with periodic resonators, there is

only the positive-going characteristic wave type defined by the eigenvector $\mathbf{v}_1$. This section considers a more general situation: a finite-length duct with N periodic resonators. In this case, the influence of the end boundary condition should be considered. This means in addition to the positive-going characteristic wave type, the negative one defined by the eigenvector $\mathbf{v}_2$ needs to be considered, which can be regarded as the "reflected" characteristic wave type.

Fig. 3-6 shows a duct loaded periodically with N side-branch resonators at an identical distance D between two nearby resonators. At the beginning of the duct there is a loudspeaker that oscillates at the magnitude of sound pressure P_0 at the distance L_{begin} from the first resonator (the interested readers can also use a more realistic beginning boundary condition, a constant vibration velocity V_0, instead; and the right hand side of Eq. (3.25) becomes $\rho_0 c_0 V_0$). At the end of the duct there is a material with reflection coefficient ∂ at the distance L_{end} from the Nth resonator.

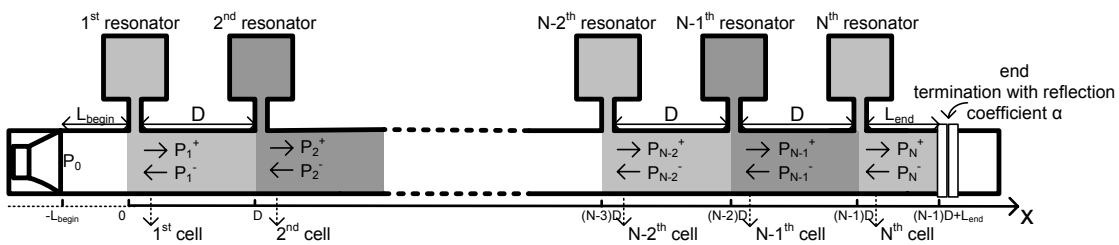

Figure 3-6. Finite periodic Helmholtz resonators array.

Similar to Section 3.1, the sound pressure in the duct segment of the nth periodic cell can be described as $P_n(x) = C_n^+ e^{-jk(x-(n-1)D)} + C_n^- e^{jk(x-(n-1)D)}$, in which the magnitude of positive- and negative-going planar waves can be obtained by adding the part of negative-going characteristic wave type $\mathbf{v}_2$ into Eq. (3.6), as

$$\begin{bmatrix} C_n^+ \\ C_n^- \end{bmatrix} = a_n \mathbf{v}_1 + b_n \mathbf{v}_2 = a_n \begin{bmatrix} v_1^+ \\ v_1^- \end{bmatrix} + b_n \begin{bmatrix} v_2^+ \\ v_2^- \end{bmatrix} \tag{3.22}$$

where b_n is also a complex constant. By introducing Eq. (3.1) , Eq. (3.22) also can be expressed as

$$\begin{aligned} \begin{bmatrix} C_n^+ \\ C_n^- \end{bmatrix} &= \mathbf{T} \begin{bmatrix} C_{n-1}^+ \\ C_{n-1}^- \end{bmatrix} = \mathbf{T}^2 \begin{bmatrix} C_{n-2}^+ \\ C_{n-2}^- \end{bmatrix} = \ldots = \mathbf{T}^{n-1} \begin{bmatrix} C_1^+ \\ C_1^- \end{bmatrix} \\ &= a_1 \mathbf{T}^{n-1} \mathbf{v}_1 + b_1 \mathbf{T}^{n-1} \mathbf{v}_2 = a_1 \lambda_1^{\ n-1} \mathbf{v}_1 + b_1 \lambda_2^{\ n-1} \mathbf{v}_2 \end{aligned} \tag{3.23}$$

Combining Eqs. (3.22) and (3.23) gives $a_n = a_1 \lambda_1^{\ n-1}$ and $b_n = b_1 \lambda_2^{\ n-1}$.

The pressure function in the Nth cell (as shown in Fig. 3-6) is also valid in the range $(N-1)D \le x \le (N-1)D + L_{end}$; and the sound pressure in $x = (N-1)D + L_{end}$ matches the end boundary condition, as

$$\begin{aligned} \left. \frac{P_N^-(x)}{P_N^+(x)} \right|_{x=(N-1)D+L_{end}} &= \left. \frac{C_N^- e^{jk(x-(N-1)D)}}{C_N^+ e^{-jk(x-(N-1)D)}} \right|_{x=(N-1)D+L_{end}} \\ &= \frac{a_1 \lambda_1^{\ N-1} v_1^- e^{jkL_{end}} + b_1 \lambda_2^{\ N-1} v_2^- e^{jkL_{end}}}{a_1 \lambda_1^{\ N-1} v_1^+ e^{-jkL_{end}} + b_1 \lambda_2^{\ N-1} v_2^+ e^{-jkL_{end}}} = \partial \end{aligned} \tag{3.24}$$

Similarly, the pressure function in the 0th cell (as shown in Fig. 3-6) is also valid in

the range $-L_{begin} \le x \le 0$; and the sound pressure in $x = -L_{begin}$ matches the beginning boundary condition, as

$$P_0^+(x) + P_0^-(x)\Big|_{x=-L_{begin}} = C_0^+ e^{-jk(x+D)} + C_0^- e^{jk(x+D)}\Big|_{x=-L_{begin}}$$

$$= (a_1\lambda_1^{-1}v_1^+ + b_1\lambda_2^{-1}v_2^+)e^{-jk(D-L_{begin})} + (a_1\lambda_1^{-1}v_1^- + b_1\lambda_2^{-1}v_2^-)e^{jk(D-L_{begin})} = P_0 \qquad (3.25)$$

So the complex constants a_1 and b_1 can be solved by combining the boundary conditions (Eqs. (3.24) and (3.25)), which means for a certain beginning- and end-boundary condition, the sound pressure in the duct segment of the nth periodic cell can be described by the specific combination of the positive- and negative-going characteristic wave types, as $a_1\lambda_1^{\text{n}-1}\mathbf{v_1} + b_1\lambda_2^{\text{n}-1}\mathbf{v_2}$.

General speaking, in the finite-length duct with N periodic resonators, the positive-going planar waves can be divided into two parts (i.e., $C_n^+ = a_n v_1^+ + b_n v_2^+$), the first part $a_n v_1^+$ decays at the rate a_{n+1}/a_n $(=\lambda_1)$ with the other part $b_n v_2^+$ increasing at the rate b_{n+1}/b_n $(=\lambda_2)$. Due to the relation $\lambda_1 = 1/\lambda_2$ discussed in previous section, these two parts actually decay at the same rate but in opposite directions: one $a_n v_1^+$ as a component of the positive-going characteristic wave type with the other $b_n v_2^+$ belonging to the negative-going characteristic wave type. Similarly, the negative-going planar waves can also be divided into two parts (i.e. $C_n^- = a_n v_1^- + b_n v_2^-$), with one $a_n v_1^-$ moving forward and the other $b_n v_2^-$ backward.

Similar to Eq. (3.9), the sound pressure field in the whole duct can be expressed as

$$P_n(x) = \Phi_1(x_n)e^{-jqx} + \Phi_2(x_n)e^{jqx} \tag{3.26}$$

where

$$\Phi_2 = b_1 v_2^+ e^{-j(k-q)x_n} + b_1 v_2^- e^{j(k+q)x_n} \tag{3.27}$$

represents the components of the negative-going characteristic wave type.

3.2.2 A Finite-length Duct-resonator System with Anechoic Termination

Although the positive- and negative-going characteristic wave types belong to the same characteristic wave type, they propagate in opposite directions along the duct. Their relative ratio in the duct segment of the nth periodic cell can be expressed as $\delta_n = |b_n / a_n|$, $(0 \le n \le N)$.

Under the condition of a semi-infinite duct with periodic resonators, there is no negative-going characteristic wave type (i.e. $\delta_n = 0$). In contrast, δ_n is a function of frequency in a finite-length duct with N periodic resonators. Fig. 3-7 shows the variation of δ_n under anechoic termination in a finite-length duct with 10 resonators (N=10). The dimensions of duct, resonators and periodic distance used here maintain the same as those used in Fig. 3-3, so the stop- and the pass-bands are the same as shown in Fig. 3-3(a). It should be noted that although Fig. 3-3 only shows the stop-

and the pass-bands of the positive-going characteristic wave type, it can be imagined that the negative one has the same frequency band distribution since they are of the same characteristic wave type. In the stop-bands (240-630 Hz and 870-940 Hz), there are few waves of the negative wave type in the duct segment of the first periodic cell ($\delta_n = 0$). In addition, it can be seen in the stop-bands that the amount of the negative wave type continues to increase in the subsequent periodic cells, and finally reaches the same amount as the positive one ($\delta_n = 1$) in the last periodic cell (the Nth cell). In other words, δ_n reaches its minimum value at the beginning (n=0) and its maximum value at the end (n=10). It is interesting to see that even though "anechoic termination" does not reflect any planar waves, it is an absolutely "rigid" termination for the characteristic wave type in the stop-bands, since it fully reflects the positive wave type in the Nth cell, as the dotted line in Fig. 3-7 shows.

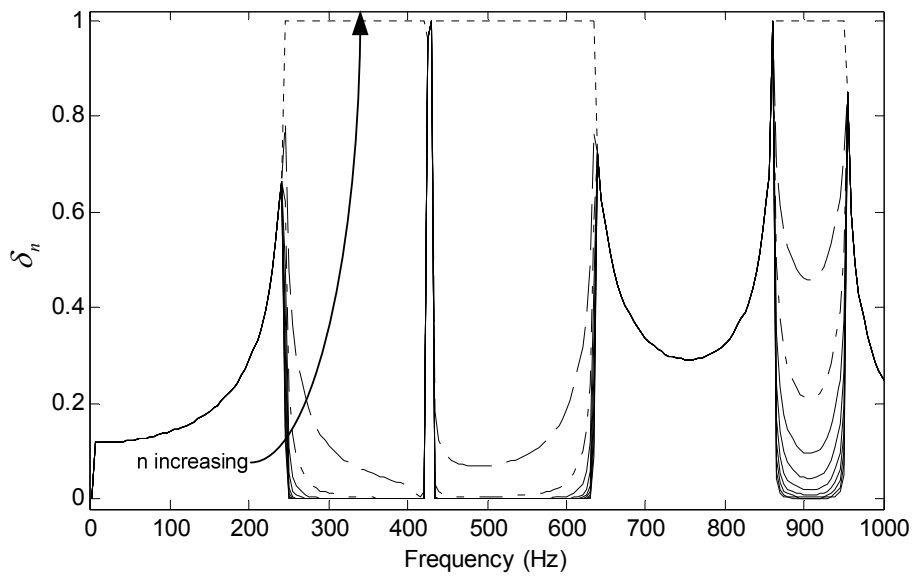

Figure 3-7. Frequency variation of the finite periodic structure under anechoic

termination, *n*=1,2,…,10.

In the pass-bands (0-240 Hz, 630-870 Hz, and above 940 Hz), it can be seen that all the lines overlap. This means that the relative ratio of the positive- and negative-going characteristic wave types (δ_n) has the same pattern in all periodic cells, as both the positive- and negative-going characteristic wave types propagate freely without any attenuation in the duct. In the pass-bands, the "anechoic termination" seems to be a partially reflective boundary for the characteristic wave type.

It should be noted that the amount of negative wave type quickly increases at the pass-band and stop-band junctures, at frequencies around 240, 430, 640, 870, and 940 Hz in all periodic cells. The system seems to respond strongly at these frequencies. It is more prominent in the gap of the stop-band, i.e., a sharp boundary at around 425Hz (as shown in Fig. 3-3(a)), because the characteristic wave type is fully reflected and the amount of negative wave type is nearly the same as that of the positive one. In general, unlike what it means to planar waves, anechoic termination cannot be regarded as "anechoic" to the characteristic wave type, and it can even be fully reflective at a particular frequency.

3.2.3 Estimating the Properties of the Characteristic Wave Type in an *N*-cell Duct-resonator Structure with Anechoic Termination

First of all, δ_N can be used to estimate the ratio of $\left|v_1^- / v_1^+\right|$ described in Section 3.1 by rewriting Eq. (3.24) under anechoic termination as

$$a_1\lambda_1^{N-1}v_1^- e^{jkL_{end}} + b_1\lambda_2^{N-1}v_2^- e^{jkL_{end}} = a_N v_1^- e^{jkL_{end}} + b_N v_2^- e^{jkL_{end}} = 0 \tag{3.28}$$

So there is

$$\left|\delta_N\right| = \left|\frac{b_N}{a_N}\right| = \left|\frac{v_1^-}{v_2^-}\right| = \left|\frac{v_1^-}{v_1^+}\right| \tag{3.29}$$

by using the relation $\left|v_1^+\right| = \left|v_2^-\right|$, which was discussed in Section 3.2. This can be verified by comparing Fig. 3-3 and the dotted line in Fig. 3-7.

Furthermore, the averaged transmission loss $\overline{TL}$ of this finite-length duct with N periodic resonators can be used to estimate the attenuation constant μ_r in terms of $20\log_{10}(e^{\mu_r})$. The averaged transmission loss $\overline{TL}$ can be expressed as

$$\begin{aligned}\overline{TL} &= \frac{20}{N}\log_{10}\left|\frac{P_0^+}{P_N^+}\right| = \frac{20}{N}\log_{10}\left|\frac{C_0^+}{C_N^+}\right| \\ &= \frac{20}{N}\log_{10}\left|\frac{a_1\lambda_1^{-1}v_1^+ + b_1\lambda_2^{-1}v_2^+}{a_1\lambda_1^{N-1}v_1^+ + b_1\lambda_2^{N-1}v_2^+}\right| = \frac{20}{N}\log_{10}\left|\mathrm{X}\right|\end{aligned} \tag{3.30}$$

Within the frequency range of stop-bands, there is

$$\lambda_1 = e^{-\mu_r - j\mu_i}, \lambda_2 = e^{\mu_r + j\mu_i}, \qquad \mu_r > 0 \quad \text{and} \quad 0 \le \mu_i < 2\pi \tag{3.31}$$

Because $|\lambda_1| < 1$, when $N \to \infty$, the first term in Eq. (3.28) approaches zero, so $b_1 = 0$. Therefore, Eq. (3.30) can be rewritten as

$$\overline{TL} = \frac{20}{N}\log_{10}\left|\frac{a_1\lambda_1^{-1}v_1^+}{a_1\lambda_1^{N-1}v_1^+}\right| = 20\log_{10}(e^{u_r}) \tag{3.32}$$

Within the frequency range of pass-bands, there is

$$\lambda_1 = e^{-j\mu_i}, \lambda_2 = e^{j\mu_i} \quad (0 \le \mu_i < 2\pi) \tag{3.33}$$

and the X in the Eq. (3.30) can be rewritten as

$$\mathrm{X} = \frac{e^{j\mu_i}a_1v_1^+ + e^{-j\mu_i}b_1v_2^+}{e^{-j(N-1)\mu_i}a_1v_1^+ + e^{j(N-1)\mu_i}b_1v_2^+} = \frac{a_0v_1^+ + b_0v_2^+}{e^{-jN\mu_i}a_0v_1^+ + e^{jN\mu_i}b_0v_2^+} \tag{3.34}$$

which can be regarded as the addition of the vectors $a_0v_1^+$ and $b_0v_2^+$ divided by the addition of themselves with an $N\mu_i$ degree rotation of $a_0v_1^+$ in the clockwise direction and an $N\mu_i$ degree rotation of $b_0v_2^+$ in the counter-clockwise direction. By substituting Eq. (3.34) into Eq. (3.30), $\overline{TL}$ fluctuates over the pass-band since the phase constant μ_i is the function of frequency. On the other hand, $\overline{TL}$ decreases at the rate of 1/*N* and the fluctuation of $\overline{TL}$ becomes smaller when the number of periodic cells (*N*) increases. Moreover, $\overline{TL}$ approaches zero (i.e., is close to $20\log_{10}(e^{\mu_r})$ with $\mu_r = 0$) within the pass-band in the semi-finite duct with periodic resonators when *N* approaches to infinity, as shown in Fig. 3-2(a).

Compared with the semi-infinite duct with periodic resonators discussed in Section 3.1, this section investigates two cases: two ducts with 3 and 10 resonators

respectively under anechoic termination, as shown in Fig. 3-8. It is noted that the case N=1 is also investigated, which is the common condition that a duct with a single side-branch resonator. In addition, the attenuation constant μ_r in terms of $20\log_{10}(e^{\mu_r})$ in Fig. 3-2(a) is re-plotted in Fig. 3-8, which has been verified above that equals to $\overline{TL}$ in the case N=∞. The dimensions of duct, resonators and periodic distance maintain the same as those used in Fig. 3-2, with the beginning and end conditions: $L_{begin} = 30$ cm, $L_{end} = 30$ cm, $P_0 = 1$ Pa and $\alpha = 0$. When the case N=1 is compared to other 3 cases (N=3, 10 and ∞), one can have a clear impression of the difference brought by structural periodicity. In the frequency range of 150-240 Hz and 640-860 Hz, different from a single resonator (N=1) providing slight attenuation of around 0.5-2 dB, planar waves propagate without any decay through the resonators array (N=∞). On the other hand, the combination of several identical resonators provides more averaged noise attenuation than the single resonator in the frequency range 240-380 Hz and 480-640 Hz of the main stop-band (N=∞). When the three cases of N=3, 10 and ∞ are compared, one can see that the averaged transmission loss $\overline{TL}$ approaches the attenuation constant μ_r in terms of $20\log_{10}(e^{\mu_r})$ (i.e. the case N=∞) in the stop-bands as N increases. Similarly, as N increases, $\overline{TL}$ approaches $20\log_{10}(e^{\mu_r})$ with the ripple pattern of $\overline{TL}$ decreasing in both cases of N=3 and 10 in the pass-bands. It should be noted that there is a undesirable dip in Fig. 3-8 at the Bragg reflection frequency (425 Hz). To eliminate

this dip, the resonance frequency of resonators should set accurately to this frequency; and this leads to a broad stop-band, i.e. stop-band III.

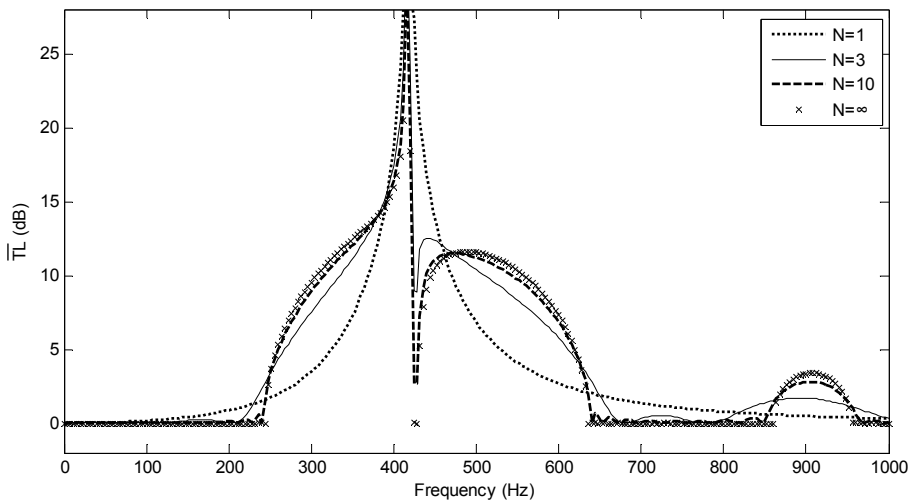

Figure 3-8. Using the averaged transmission loss $\overline{TL}$ to estimate the attenuation constant μ_r in terms of $20\log_{10}(e^{\mu_r})$.

3.3 Numerical Simulation Based on the Finite Element Method

A three-dimensional finite element method (FEM) was used to verify the theoretical analysis of the finite-length duct with periodic resonators; investigate the influence of number of Helmholtz resonator on noise reduction characteristic, and compare with the experimental results in next section. The detailed description of this method

for time-harmonic acoustics in this thesis, which are governed by the Helmholtz equation, can be found in numerous sources.[61] The commercial software COMSOL Multiphysics® version 2009 is used in the thesis as a validation tool, which also offers an extensive interface to MATLAB and its toolboxes for a large variety of programming and postprocessing works. The numerical model consisted of a duct with different number of identical side-branch resonators and an excitation from an oscillating sound pressure at fixed magnitude $P_0 = 1$. The end termination was set to be anechoic (i.e. $\partial P / \partial x + jkP = 0$).[62] To ensure accuracy, a fine mesh spacing of less than 5 cm was maintained for the models (compared to the wavelength of the upper frequency, i.e. 1000 Hz, considered in this chapter). For example, when considering the case used in Figs. 3-2 and 3-8 with *N*=5, the mesh divided the duct-resonator structure into more than 8,000 triangular elements; and the maximum element was observed in the duct with a side length of 4.8 cm; the minimum element was observed in the neck-duct interface with a side length of 1.7 mm.

Fig. 3-9 shows the noise attenuation effect formed by the wave coupling in the periodic duct instead of the resonance of a single resonator ($f_0 = 415$ Hz), sound field distribution (pressure magnitude) on the sliced plane along the duct were examined at 500 Hz. In Fig. 3-9, the geometries of the duct-resonator system are the same as those used in Fig. 3-8, i.e. r_1=1.7 cm, l_1=4.55 cm r_2=4.7 cm, l_2=4 cm,

S_d=13.2 cm^2, D=40 cm, $L_{begin} = 30$ cm, $L_{end} = 30$ cm, $P_0 = 1$ Pa and $\alpha = 0$. It can be seen from Fig. 3-9 that sound pressure dropped noticeably at a rate of around 10 dB per cell, which agrees well with the theoretical analysis shown in Fig. 3-8 at 500 Hz.

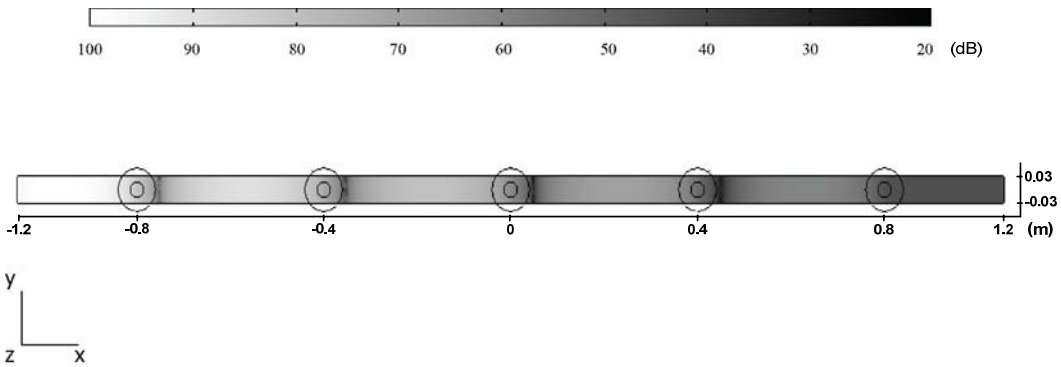

Figure 3-9. Sound field (pressure magnitude) of the finite periodic structure.

Secondly, FEM is used to investigate the influence of number of resonators in the periodic duct-resonator system, which results in an evolution of the noise attenuation from a single peak to the three different stop-band types; and the FEM simulation is compared with the theoretical analysis of the stop-band width developed in Section 3.1.4, as shown in Figs. 3-10 and 3-11. The geometries of the duct-resonator system in Fig. 3-10/3-11 is the same as those used in Fig. 3-5(a)/(b) respectively, i.e. $r_1 = 2$ cm, $l_1 = 2.1$ cm, $V_2 = 136.75\pi$ cm^3, $S_d = 12$ cm^2, $D = 45$ cm for Fig. 3-10; $D = 34.4$ cm with others unchanged for Fig. 3-11.

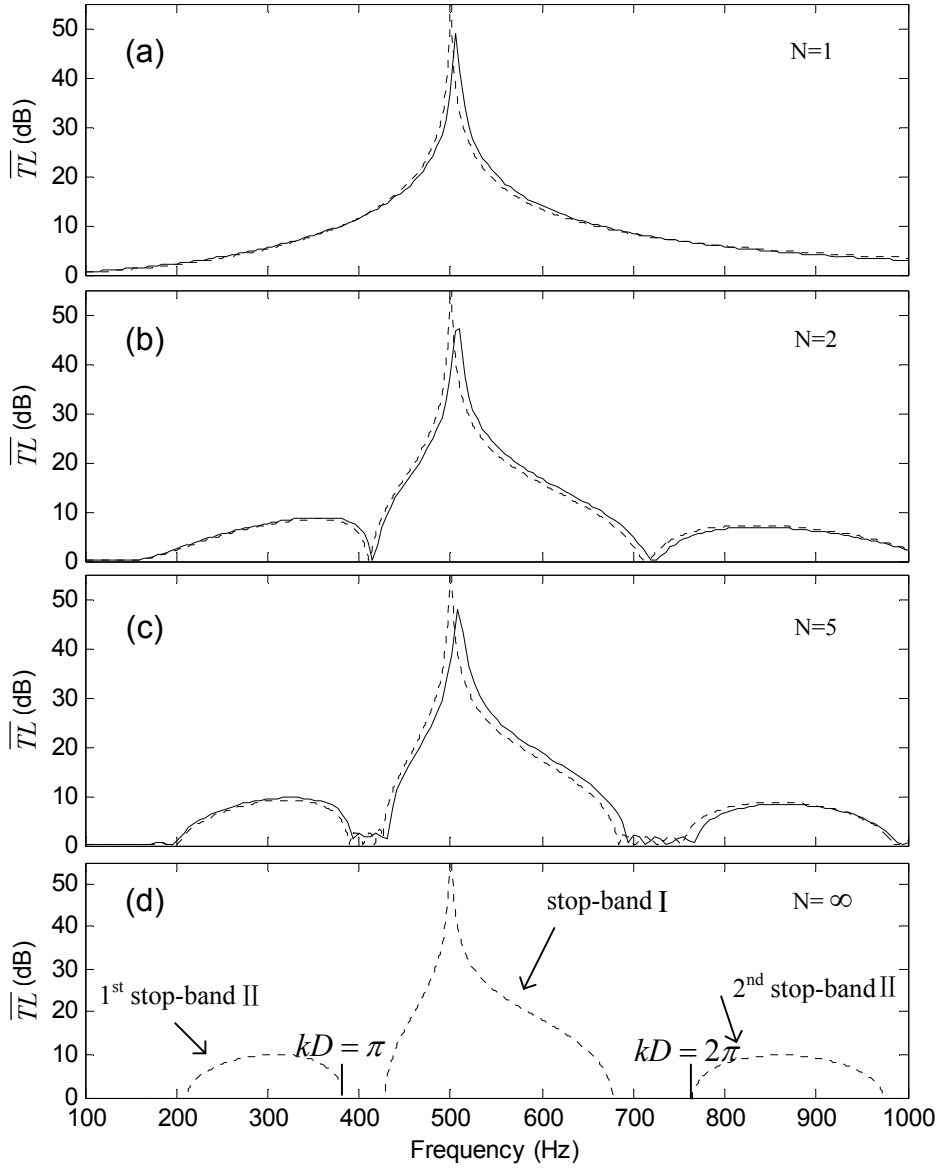

Figure 3-10. The averaged transmission loss $\overline{TL}$ of the duct with *N* resonators (the solid lines represent the FEM simulation and the dotted lines represent the theoretical prediction).

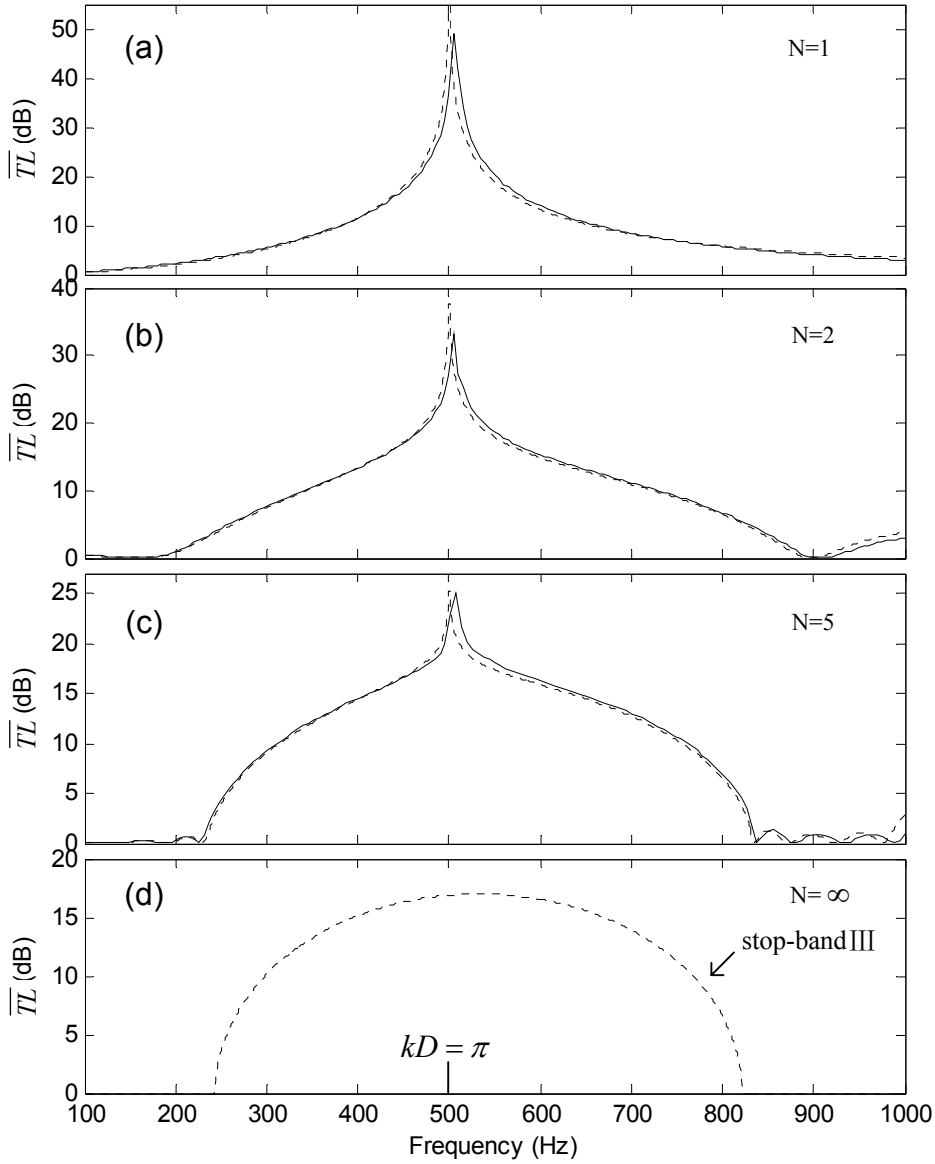

Figure 3-11. The averaged transmission loss $\overline{TL}$ of the duct with *N* resonators (the solid lines represent the FEM simulation and the dotted lines represent the theoretical prediction).

Compared to the geometries of the duct, the resonators used in Figs. 3-10 and 3-11 are large. To ensure the validity of the lumped model, the interested frequency range is kept well below the cut-on frequency of the duct and neck. The deviation between

the theoretical prediction and the FEM simulation can be observed in Fig. 3-10(a) and Fig. 3-11(a), which is very similar to that observed in Fig. 2-2. However, although the distributed models will give a better prediction (as shown in Fig. 2-2), the lumped one helps in the discussion on the band types with the geometries of resonators. Moreover, the theoretical predictions in Fig. 3-10 and 3-11(a) diverge at the resonance frequency in this lossless case ($\overline{TL} \to \infty$); and there is a truncation on the peak in these figures (dotted lines). Truncated the peaks can show clearly the main attenuation bands in thesis figures without considering the peaks that are unrealistic in practice. Due to the calculation error in the FEM simulation, sound pressure in the downstream duct can not accurately equal to zero at the resonance frequency, the resonance peak of solid lines will not diverge. In Fig. 3-11(b), (c) and (d), the peaks of both dotted and solid lines are suppressed due to structural periodicity in the case $\omega_m = \omega_0$.

In Figs. 3-10 and 3-11, when the cases *N*=1 are compared to other cases, there is a clear impression of the difference caused by structural periodicity. The cases *N*=2, shown in both Fig. 3-10(b) and Fig. 3-11(b), illustrate the rudiments of the frequency attenuation caused by structural periodicity; the original pattern of frequency attenuation begins to break down under the influence of the emerging structural periodicity. In the cases *N*=5, shown in Figs. 3-10(c) and 3-11(c), the width of the

stop-bands decreases and a ripple pattern is observed beside them. That pattern disappears when $N=\infty$, as can be seen in both Fig. 3-10(d) and Fig. 3-11(d).

As the case shown in Fig. 3-11(c), beside the peak resulted from the resonance of a single resonator, the duct with five identical resonators provides an averaged transmission loss with a broadband around 240-820 Hz at the level of around 3-15 dB; the overall transmission loss of this system is quintupling, providing around 15-75 dB in this wide frequency range.

3.4 Experiment

Fig. 3-12 shows the experimental setup for the measurement of the sound pressure in a duct with an array of resonators. Similar to the numerical model shown in Fig. 3-9, the experimental apparatus consisted of a duct with five identical side-branch resonators and a loudspeaker mounted at the beginning. In the experiment, two replaceable end terminations were used. One is rigid end termination and one is a termination with absorptive materials. The transfer matrix method was used.[63-64] This method including the two-microphone technique[63] is used to separate incident and reflected waves for calculation of the transmission loss by placing one pair of microphones before and another pair after the resonators array, and the two-load

method[63] to yield strict anechoic end termination. A detailed description of the transfer matrix method can be found in Ref. 63. The testing apparatus consisted of four B&K ¼" type 4935 microphones, a B&K PULSE analyzer with four input channels and two output channels, and a B&K type 2706 power amplifier. The matching of the four microphones was carefully calibrated following Ref. 63. The calculated transmission loss is then divided by the number of resonators (N=5) as averaged transmission loss $\overline{TL}$, that can be regarded as an approximation of the attenuation constant μ_r in terms of $20\log_{10}(e^{\mu_r})$, as discussed in Section IV. The dimensions of duct, resonators are the same as those used in Fig. 3-8, except now $l_1 = 5$ cm and $D = 47$ cm (i.e. r_1=1.7 cm, l_1=5 cm r_2=4.7 cm, l_2=4 cm, S_d=13.2 cm^2, D=47 cm, $L_{begin} = 30$ cm, $L_{end} = 30$ cm, $P_0 = 1$ Pa and $\alpha = 0$). Furthermore, these dimensions of the duct and resonators are similar to that in Ref. 10, which are selected to investigate nonplanar waves excited in the resonators neck-cavity interface and to ensure planar wave propagation in the duct and neck with higher-mode waves decay quickly.

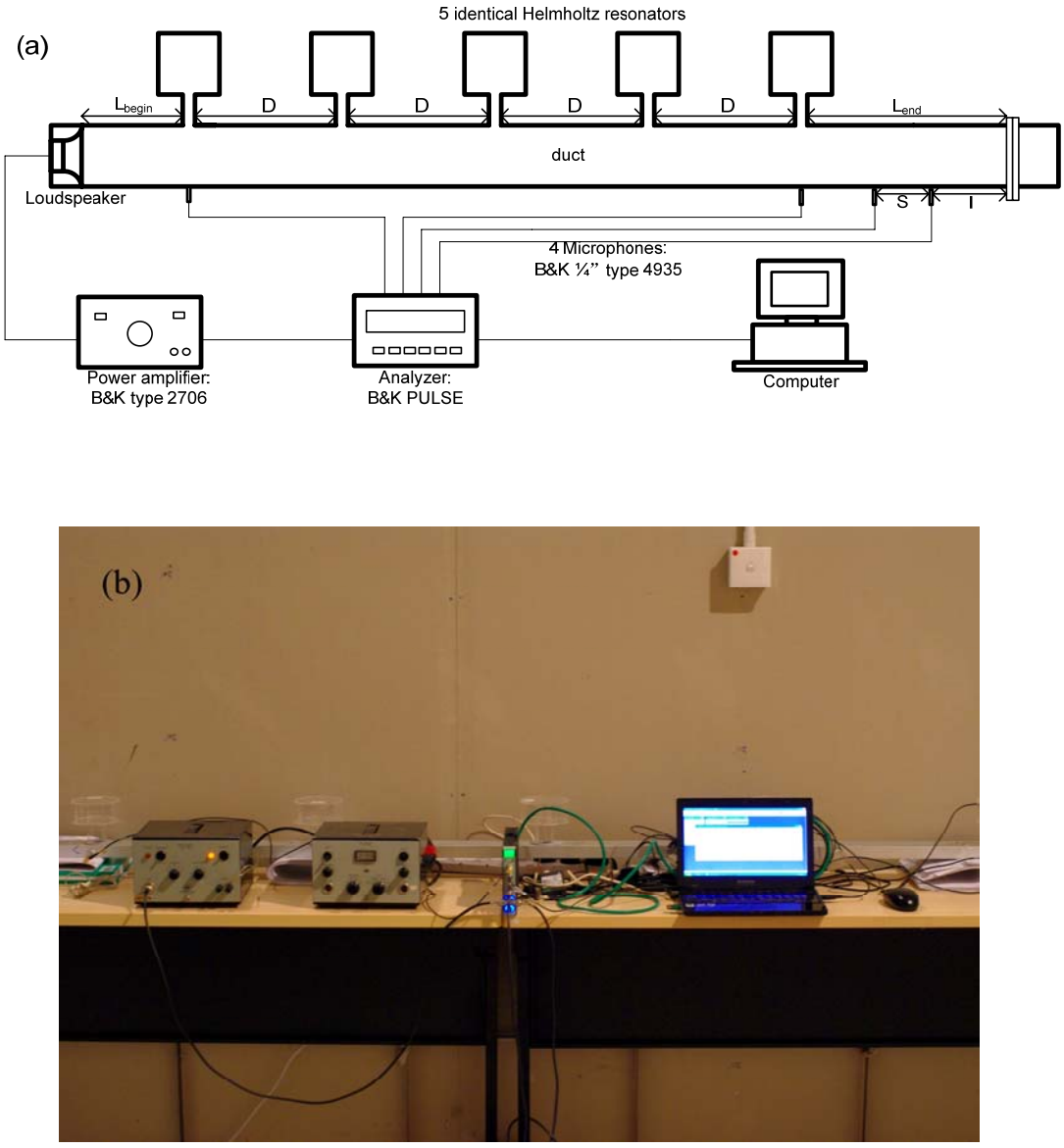

Figure 3-12. The experiment setup for measurement. (a) schematic, (b) installment.

3.5 Results and Discussion

Fig. 3-13 shows the comparison of the average transmission loss $\overline{TL}$ between the experiment, the theory using the distributed-parameter model, and the FEM

simulation for a duct with 5 identical side-branch resonators. It can be seen from Fig. 3-13 that the changes in the geometry of the structure result in the difference of the range of the main stop-band, the position of the gap, and the peak of the main stop-band compared to Fig. 3-8. As shown in Fig. 3-13, the FEM simulation fits better with the experimental data than the theoretical predictions both in the stop-bands and in the ripple of the pass-bands. The deviation of the experiment data from other two methods at the sharp peak is probably due to the sensitivity of the microphones, which is similar to that observed in Ref. 32. However, instead of the sharp peak resulted from the resonance of a single resonator, the broad noise attenuation band from 210 to 570 Hz is a more important feature for this periodic structure because it can provide considerable noise attenuation in both magnitude and bandwidth. It can be seen from Fig. 3-13 that the averaged transmission loss $\overline{TL}$ in the main stop-band is about 3-15 dB, except the narrow gap at around 380 Hz and the sharp peak at around 400 Hz. In this finite-length duct with five identical resonators (i.e. N=5), the overall transmission loss TL is about 15-75 dB (i.e. 5 × 3-15 dB) in the stop-band except the gap and the peak.

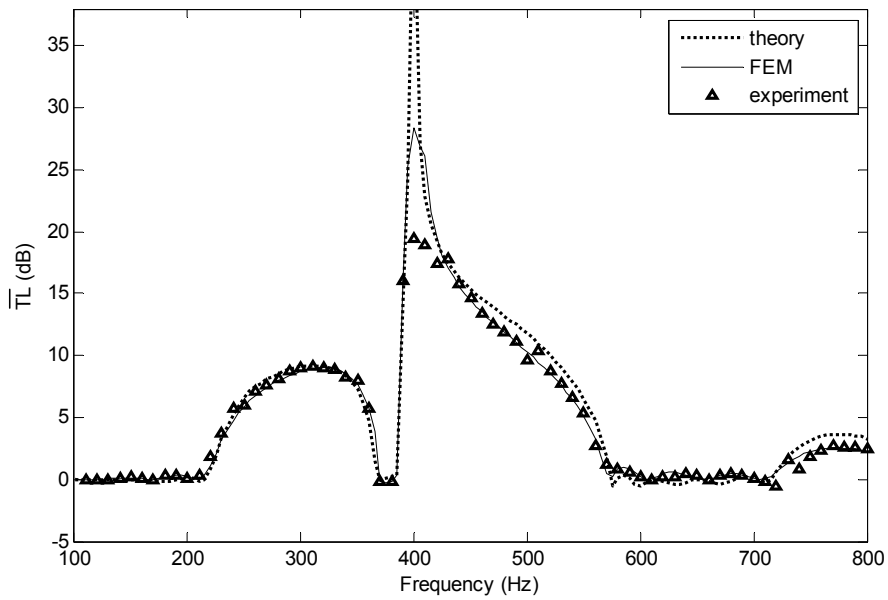

Figure 3-13. A comparison of $\overline{TL}$ between experiment, the theory using distributed-parameter model and the FEM simulation for a duct loaded periodically with 5 identical resonators.

3.6 Conclusion

This chapter has presented a theoretical study of a periodic resonators array based on the distributed-parameter resonator model. When waves travel through each resonator, they produce reflected and transmitted waves. Those reflected and transmitted waves are then reflected and transmitted again by the previous and next resonators. This process is physically repeated in the periodic structure. In this situation, instead of dividing the sound pressure field in the duct simply into positive- and negative-going planar waves, it is more appropriate to decompose it

into positive- and negative-going characteristic wave types. Three types of stop-bands of the characteristic wave types have been discussed, and their bandwidths have been predicted theoretically.

After introducing the characteristic wave type to describe the wave coupling in the periodic structure, both the semi-infinite duct with infinite periodic resonators and the finite-length duct with *N* periodic resonators have been discussed. The influence of the number of resonators has also been investigated. The predicted results using this theory fit well with the FEM simulation and the experimental results.

As the case shown in Fig. 3-11(c), beside the peak resulted from the resonance of a single resonator, the duct with five identical resonators provides an averaged transmission loss with a broadband around 240-820 Hz at the level of around 3-15 dB; the overall transmission loss of this system is quintupling, providing around 15-75 dB in this wide frequency range. This study indicates that compared to a single resonator, the use of periodic resonators may provide a much broader sound attenuation band under carefully designed.

In this chapter, the eigenvalue analysis on the periodic structure is the existing theory. However, as the original contribution, the duct with periodic resonators is found to

be an effective tool for broadband noise control. In particular, such as the influence of the number of resonators in the finite-length duct-resonator system and the modified bandwidth prediction are original works, so does the detailed analysis on the physical meanings of the characteristic wave types.

Chapter 4

Disorder in a Periodic Helmholtz Resonators Array

4.1 Theoretical Analysis

As shown in Fig. 4-1, a "periodic" cell comprises a duct segment with a resonator attached to its left side. When considering the irregularity of the periodic distance between any two nearby resonators and the geometries of Helmholtz resonators, the system can no longer be represented by a single transmission matrix **T** and a single periodic distance D as it is in the pure-periodic case discussed in Chapter 3. Rather, we should specify each transmission matrix and "periodic" distance, noted as $\mathbf{T}_n$ and D_n for $n = 1, 2, ..., N$.

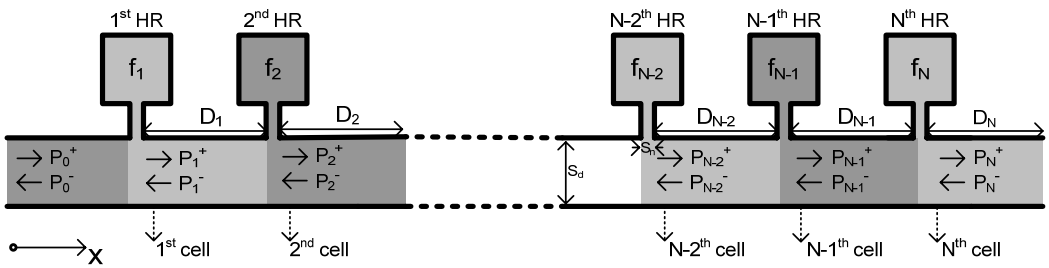

Figure 4-1. A duct with *N* Helmholtz resonators.

Similar to the pure-periodic case, the diameter of the resonator neck is assumed to be

negligible compared to the length of the duct segment between two nearby resonators, D_n. The frequency range considered is well below the cut-on frequency of the duct. In the duct segment of the nth cell, the sound traveling in positive- and negative-x directions can be described with sound pressure $P_n^+(x) = C_n^+ e^{-jk(x_n - D_n)}$ and $P_n^-(x) = C_n^- e^{jk(x_n - D_n)}$ for $0 \le x_n \le D_n$, where C_n^+ and C_n^- are complex constants and k is the wave number. If $\mathbf{c}_n = \begin{bmatrix} C_n^+ & C_n^- \end{bmatrix}^T$ and $\mathbf{c}_{n+1} = \begin{bmatrix} C_{n+1}^+ & C_{n+1}^- \end{bmatrix}^T$ represent the wave component in the duct segment of the nth and n^{th}+1 element of the "periodic" system, then it can be related through a wave transfer matrix $\mathbf{T}_{n+1}$ as follows:

$$\mathbf{c}_{n+1} = \mathbf{T}_{n+1}\mathbf{c}_n \tag{4.1}$$

As discussed in Chapter 3, the transfer matrix can be expressed as

$$\mathbf{T}_n = \begin{bmatrix} e^{-jkD_n} & 0 \\ 0 & e^{jkD_n} \end{bmatrix} \begin{bmatrix} 1-\xi_n & -\xi_n \\ \xi_n & 1+\xi_n \end{bmatrix} \tag{4.2}$$

where $\xi_n = Z_d / 2Z_n$, where Z_d / Z_n is the acoustic impedance of the duct/n^{th} resonator respectively. Furthermore, the transfer matrix $\mathbf{T}_n$ can be rewritten in terms of the transmission and reflection coefficients, t_n and r_n, as[65]

$$\mathbf{T}_n = \begin{bmatrix} e^{-jkD_n} & 0 \\ 0 & e^{jkD_n} \end{bmatrix} \begin{bmatrix} 1/t_n^* & -\left(r_n/t_n\right)^* \\ -r_n/t_n & 1/t_n \end{bmatrix} \tag{4.3}$$

where the superscript * means conjugation. It follows immediately that

$$\mathbf{c}_{n+1}\mathbf{c}_{n+1}^{T*} = \mathbf{T}_{n+1}(\mathbf{c}_n\mathbf{c}_n^{T*})\mathbf{T}_{n+1}^{T*} \tag{4.4}$$

where the superscript T means transposition; equation (4.4) can be rewritten in vector form as

$$\mathbf{e}_{n+1} = \mathbf{A}_{n+1}\mathbf{e}_n \tag{4.5}$$

where $\mathbf{e}_n = \left[C_n^+ C_n^{+*} \quad C_n^+ C_n^{-*} \quad C_n^- C_n^{+*} \quad C_n^- C_n^{-*} \right]^T$; and the entries of the 4×4 matrix $\mathbf{A}_n$ can be expressed in terms of the entries of $\mathbf{T}_n$. It should be noted that the final diagonal entry of the matrix $\mathbf{A}_n$ has the value $\mathbf{A}_n(4,4) = 1/|t_n|^2$,[40] and thus knowledge of $\mathbf{A}_{n+1}$ leads immediately to the modulus squared transmission coefficient between the nth and $n^{\text{th}}+1$ "periodic" elements. Furthermore, for the whole system, there is

$$\mathbf{e}_N = \left(\prod_{n=1}^{N} \mathbf{A}_{N+1-n} \right) \mathbf{e}_0 = \mathbf{\Lambda}\mathbf{e}_0 \tag{4.6}$$

where $\mathbf{A}_n$ is the matrix derived from $\mathbf{T}_n$ and $\mathbf{\Lambda}$ is the corresponding matrix of the whole system.

4.1.1 Random Disorder

If the periodic system subject to random disorder and the random variations in the properties of each "periodic" element are statistically independent, then Eq. (4.6) can be described by the ensemble average behavior of the system as[40]

$$E[\mathbf{\Lambda}] = \prod_{n=1}^{N} E[\mathbf{A}_{N+1-n}] \tag{4.7}$$

Here, $E[\ ]$ represents the ensemble average. If the random variations in the system

properties are homogeneous, so that the various "periodic" elements have the same probability distribution, then Eq. (4.7) can be reduced to

$$E[\mathbf{A}] = E[\mathbf{A}]^N \tag{4.8}$$

If the duct-resonator system is initially periodic, with periodic distance D and the transmission and reflection coefficients of a side-branched Helmholtz resonator t and r, the matrices $\mathbf{A}_n$ are all the same with the omission of the subscript n and take the form

$$\mathbf{A} = \begin{bmatrix} 1/|t|^2 & -r/|t|^2 & -r^*/|t|^2 & |r|^2/|t|^2 \\ -r^*\delta/t^{*2} & \delta/t^{*2} & r^{*2}\delta/t^{*2} & -r^*\delta/t^{*2} \\ -r/\delta t^2 & r^2/\delta t^2 & 1/\delta t^2 & -r/\delta t^2 \\ |r|^2/|t|^2 & -r/|t|^2 & -r^*/|t|^2 & 1/|t|^2 \end{bmatrix} \tag{4.9}$$

where $\delta = \exp(-2jkD)$. The expected value of $\mathbf{A}$ may be computed if the statistical properties of the system are known. For example, it is assumed that the Helmholtz resonators are identical while the periodic distance D is allowed to vary in a random fashion with a probability density function $p(D)$. In this case, the expected value of $\mathbf{A}$ is given by Eq. (4.9), with the parameters δ interpreted as average values, as

$$\delta = \int_{-\infty}^{\infty} e^{-2jkD} p(D) dD = M(-2k) \tag{4.10}$$

Here, $M(\theta)$ is the characteristic function of the random "periodic" distance. For a Gaussian distribution, $M(\theta)$ would be $\exp(jD_0\theta - \sigma^2\theta^2/2)$, where D_0 is the mean "periodic" distance and σ is the standard deviation.

Eq. (4.8) can also be expressed in the form

$$E[\mathbf{\Lambda}] = \mathbf{P}\mathbf{\Gamma}^N\mathbf{P}^{-1} \tag{4.11}$$

where $\mathbf{\Gamma}$ is a diagonal matrix containing the eigenvalues of $E[\mathbf{A}]$ and $\mathbf{P}$ is a matrix whose columns are the corresponding eigenvectors. If N is allowed to tend to infinity and $E[\mathbf{\Lambda}]$ has at least one real eigenvalue greater than unity, there is

$$\lim_{N\to\infty}\{E[1/|t_N|^2]\} = N\ln\lambda_{\max} \tag{4.12}$$

4.1.2 Man-made Disorder

However, sometimes the disorder is not an imperfection but a man-made disorder to achieve a modified filter characteristic of the "periodic" system, which means the disorder in periodicity is no longer weak but significant. Furthermore, in practice, the duct-resonator system does not contain a large number of resonators that are suitable to be described by a statistical method, as discussed above. This case is considered in this section. As discussed above, the duct-resonator system can no longer be represented by the mean transmission matrix **T** and the mean periodic distance D. In other words, each transmission matrix and "periodic" distance should be specified as $\mathbf{T}_n$ and D_n for $n = 1, 2, ..., N$. As considered in this section, the finite "periodic" system only contains five side-branched Helmholtz resonators (i.e. N=5). Two cases are considered: (1) disorder in the periodic distance with the geometries of the resonators unchanged and (2) disorder in the geometries of the resonators with

the periodic distance remaining unchanged. So, the whole system can be described as

$$\begin{bmatrix} C_5^+ \\ C_5^- \end{bmatrix} = \mathbf{T}_5\mathbf{T}_4\mathbf{T}_3\mathbf{T}_2\mathbf{T}_1 \begin{bmatrix} C_0^+ \\ C_0^- \end{bmatrix} \tag{4.13}$$

By introducing Eq. (4.4), there is

$$\mathbf{e}_5 = \left(\prod_{j=1}^{5} \mathbf{A}_{6-j} \right) \mathbf{e}_0 = \mathbf{\Lambda}\mathbf{e}_0 \tag{4.14}$$

It has been discussed that in the matrix $\mathbf{\Lambda}$, the entry of $\mathbf{\Lambda}(4,4)$ equals the modulus squared transmission coefficient of the whole system t_{total}, that is $\mathbf{\Lambda}(4,4) = 1/|t_{total}|^2$. So, the average transmission loss of the whole system can be described as

$$\overline{TL} = {}^{10}\!/_{N} \log_{10}(\mathbf{\Lambda}(4,4)), \qquad N=5 \tag{4.15}$$

4.2 Results and Discussion

It is found that a periodic Helmholtz resonators array may provide a considerable broad noise attenuation band. To compare this with the case of disorder in periodicity, some results derived from the pure-periodicity case in Chapter 3 are discussed here. The average transmission loss for a duct mounted periodically by five identical Helmholtz resonators with the geometries $S_1 = 4\pi$ cm^2, $l_1 = 2.1$ cm, $V_2 = 136.75\pi$ cm^3, $S_d = 12$ cm^2, and $D = 34.3$ cm is shown in Fig. 4-2(a). The detailed description of such pure-periodic duct-resonator system is presented in

Chapter 3. The theoretical prediction is compare with the FEM simulation using the commercial software COMSOL Multiphysics® version 2009, which offers an extensive interface to MATLAB and its toolboxes for a large variety of programming and postprocessing works.

4.2.1 Disorder in Periodic Distance

In this section, the disorder in the distance between two nearby resonators is considered, while the geometries of the Helmholtz resonator remain unchanged. The five distances between two nearby resonators are expressed as D_k, $k = 1, 2, ..., 5$.

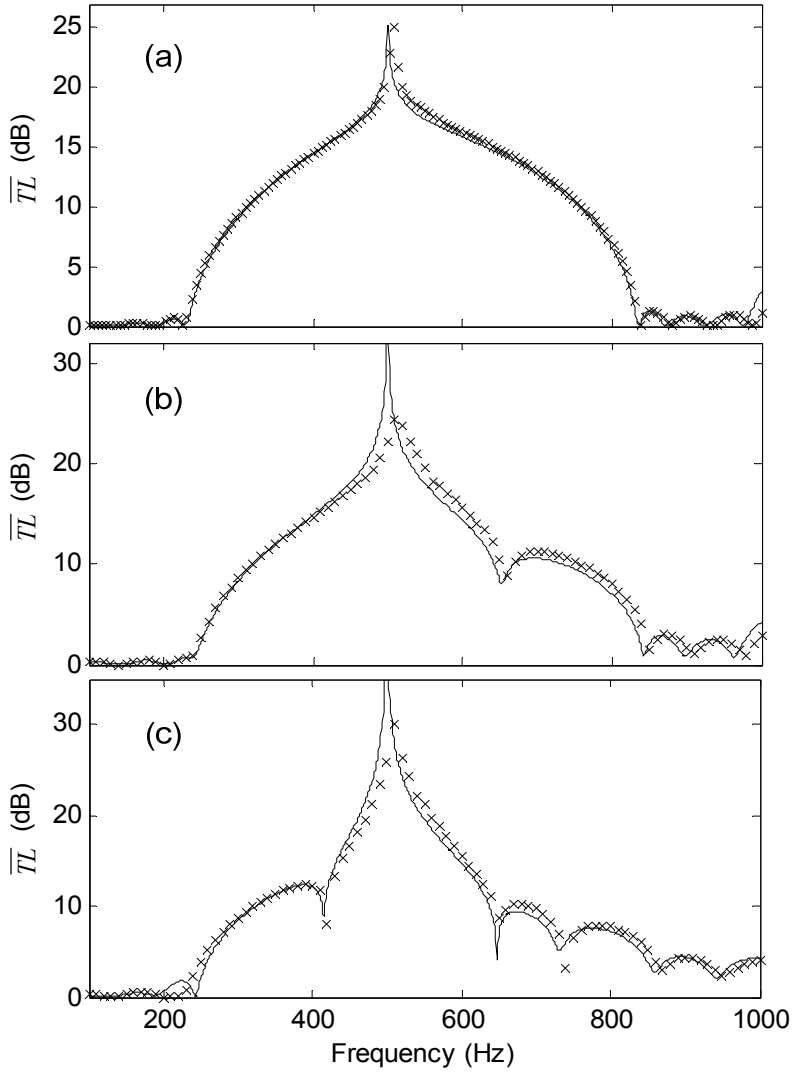

Figure 4-2. Disorder in periodic distance ("x" represents the FEM simulation and the solid lines represent the theoretical prediction).

Fig. 4-2(a) shows the case in which the periodic distance between two nearby resonators is perfectly maintained in the whole system as D=34.3 cm; this case is the same as that discussed in Chapter 3. Fig. 4-2(b) shows the simple case in which one distance is changed (D_1=24.3 cm) while the other periodic distances are kept unchanged. In this case, the "defect" is adiabatic, which means that the "defect" does

not affect the other periodic elements. It can be seen that due to the single "defect," the pattern of the whole main noise attenuation band changes significantly. First, the attenuation peak at the frequency of 500 Hz is more obvious than it is in the perfect periodic system shown in Fig. 4-2(a). Owing to the single "defect" in periodic distance, the resonance peak at the frequency of 500 Hz in the system seems to be not as strongly suppressed as it is in the original perfectly periodic system. The suppression in this region is due to structural periodicity in the case in which the periodic distance D matches the condition $kD = m\pi$, $m = 1, 2, ..., \infty$, as discussed in Chapter 3. Second, an obvious reduction in the main attenuation band can be seen at around 630 Hz. As discussed before, the introduction of defects into the perfect periodicity may lead to narrow frequency transmission bands (i.e. defect states) within the stop-band gaps.[35] Fig. 4-2(c) shows the case in which there are two defects in periodic distance, D_1=24.3 cm and D_2=44.3 cm, while the other periodic distances are kept unchanged. Compared to the previous case shown in Fig. 4-2(b), the defects in this case are no longer adiabatic; the variation of D_1 also affects the nearby distance D_2, which can be interpreted as moving the second Helmholtz resonator (Fig. 4-1) to the left of the system by 10 cm. As shown in Fig. 4-2(c), the affect introduced by these two "defects" is more obvious, and due to the structural periodicity, the original pattern of the noise attenuation band begins to break down under the influence of these two "defects." It can be seen that the suppression due to

the periodicity at 500 Hz is no longer strong as the attenuation peak is much stronger than those in Fig. 4-2(a) and (b). It can be seen that the main noise attenuation band seems difficult to define, especially the upper frequency boundary. In general, the periodic system seems to be very "sensitive" to the defects in the periodic distance, and such "defects" should be carefully avoided in manufacturing such periodic systems.

4.2.2 Disorder in the Geometries of Helmholtz Resonators

In this section, the disorder in the geometries of Helmholtz resonators is considered, with the periodic distance between each of the two nearby resonators being kept unchanged. Owing to the disorder in their geometries, the five resonators may have different resonance frequencies, noted as f_n, $n = 1, 2, ..., 5$.

Fig. 4-3(a) shows the case in which the periodicity is perfect, with all of the resonators resonating at 500 Hz, which is the same case as that discussed in Chapter 3, with the geometries $S_n = 4\pi$ cm^2, $l_n = 2.1$ cm and $V_c = 136.75\pi$ cm^3. Fig. 4-3(b) shows the case in which there are two resonators in disorder, with resonance frequencies of 400 Hz and 600 Hz, with the geometries $S_n = 4\pi$ cm^2, $l_n = 2.1$ cm, $V_c = 213.67\pi$ cm^3 and $S_n = 4\pi$ cm^2, $l_n = 2.1$ cm, $V_c = 95\pi$ cm^3 respectively, while the other three resonators resonate at 500 Hz. It can be seen that in this case,

the main broad noise attenuation band is well maintained, with the bandwidth being kept unchanged at around 240-820 Hz. However, when compared to the perfectly periodic case shown in Fig. 4-3(a), the pattern of the main attenuation band is significantly different in its frequency range. Two new attenuation peaks are found at the frequencies of around 400 Hz and 600 Hz. Furthermore, although three resonators resonate at the frequency of 500 Hz, the average transmission loss $\overline{TL}$ in the vicinity of 500 Hz seems to be suppressed significantly; a similar phenomenon can also be found in Fig. 4-3(c). The suppression in this region is due to structural periodicity in the case in which the periodic distance D matches the condition $kD = m\pi$, $m = 1, 2, ..., \infty$, as discussed in Chapter 3. Fig. 4-3(c) shows the case in which there are two resonators in disorder, with resonance frequencies of 250 Hz and 800 Hz, with the geometries $S_n = 4\pi$ cm^2, $l_n = 2.1$ cm, $V_c = 547\pi$ cm^3 and $S_n = 4\pi$ cm^2, $l_n = 2.1$ cm, $V_c = 53.42\pi$ cm^3 respectively, which are close to the lower and upper boundary of the main attenuation band, while the other three resonators resonate at 500 Hz. In general, Fig. 4-3(c) shows that as long as the variation of the resonance frequencies of the disordered Helmholtz resonators is kept within the frequency range of the main attenuation band, the band will be well maintained, with the bandwidth being kept unchanged. This is a useful way for the design of such a system to achieve a relatively wide noise attenuation band and to track some narrow noise peaks within it. It is especially effective for the kind of

noise that is low frequency and broad band and has some peaks.

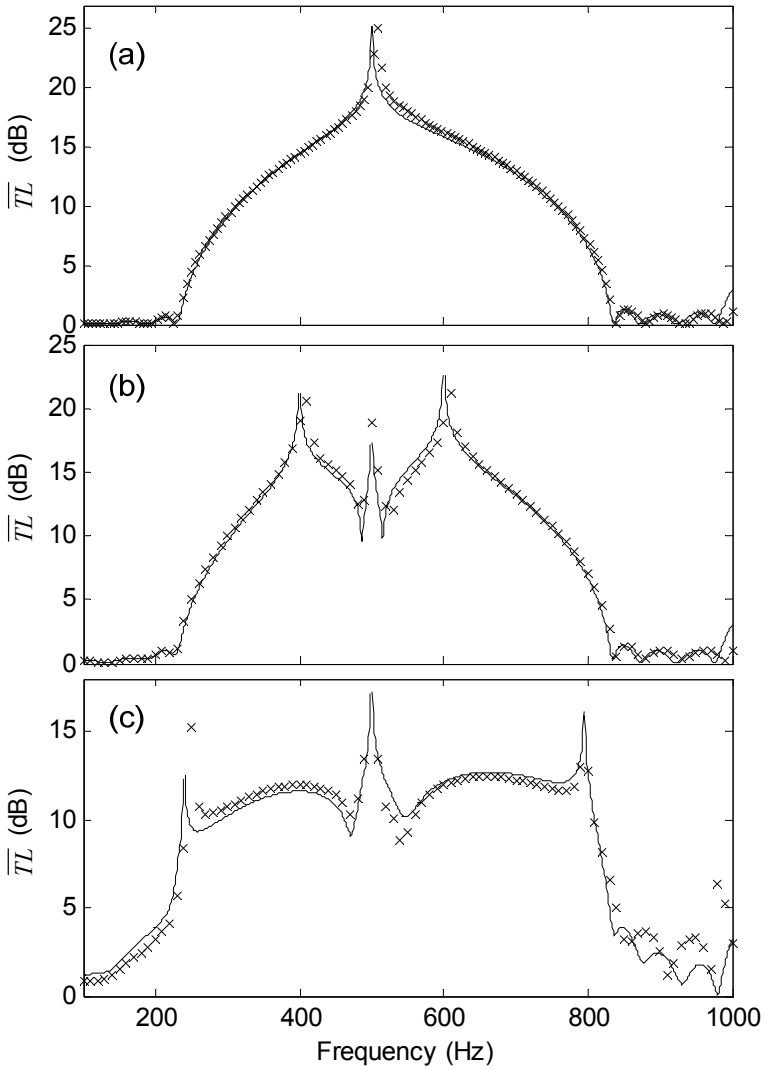

Figure 4-3. Disorder in the geometries of Helmholtz resonators ("x" represents the FEM simulation and the solid lines represent the theoretical prediction).

4.2.3 Comparison of Differently Tuned Helmholtz Resonators with and without Periodic Mounts

It can be seen from the previous section that the main noise attenuation band (240-820 Hz) results mainly from the appropriated design of the periodic distance *D*. In engineering, combining differently tuned resonators is usually one possible way of obtaining a broader noise attenuation band, and this has been investigated by some researchers.[66,67] This section investigates the noise reduction effect of an array of differently tuned resonators with and without periodic mounts.

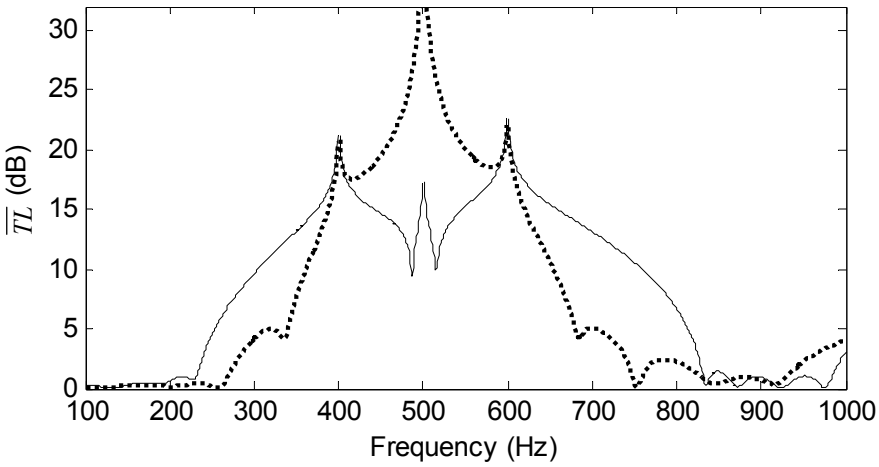

Figure 4-4. Noise attenuation of an array of differently tuned resonators (the solid/dotted lines represent the theoretical prediction for resonators with/without periodic mounts, respectively).

Fig. 4-4 shows the comparison of differently tuned resonators with and without periodic mounts. The case of differently tuned resonators with periodic mounts is the

same as that shown in Fig. 4-3(b). The geometries of the resonators in these two cases are the same, with resonance frequencies of f_1=400 Hz, f_2=600 Hz, and f_3=f_4=f_5=500 Hz. In the case without periodic mounts, the distance between the two nearby resonators is random, with D_1= 15 cm, D_2=20 cm, D_3=17 cm, D_4=18.5 cm, and D_5=16.5 cm. In the other case, the distance between the two nearby resonators is the same: D=34.3 cm. It can be seen that the averaged transmission loss $\overline{TL}$ in the case without periodic mounts has a significant peak at around 500 Hz, which is the advantage of the uncoupled resonators array, compared to the other case; the relatively poor performance at around 500 Hz in the latter case is the result of the strong suppression due to structural periodicity in the case where the periodic distance D matches the condition $kD = m\pi$, $m = 1, 2, ..., \infty$, as discussed in Chapter 3. However, the coupled resonators (the solid lines in Fig. 4-3) provide a much broader noise attenuation bandwidth than the uncoupled ones, and this is the advantage of the coupled resonators. Hence, there are trade-offs between both cases, and one can choose the resonators array that is suitable according to the properties of the noise type encountered in engineering.

4.4 Conclusion

This chapter has investigated the influence of disorder in the periodic duct-resonator

system. Disorder in periodicity includes the disorder in periodic distance and the disorder in the geometries of Helmholtz resonators. With regard to the disorder in periodic distance, the periodic system seems to be very “sensitive” to both the defects in the periodic distance and the original pattern of the noise attenuation band due to the fact that the structural periodicity begins to break down under the influence of these “defects.” Such “defects” should be carefully avoided in manufacturing such periodic systems. However, in the case of the disorder in the geometries of Helmholtz resonators, the main attenuation band will be well maintained, with the bandwidth being kept unchanged, as long as the variation of the resonance frequencies of the Helmholtz resonators are kept within its frequency range. This is a useful way for the design of such systems to achieve a relatively wide noise attenuation band and to track some of the narrow noise peaks within it. Comparing the latter case to the traditional case of a differently tuned resonators array taking no account of periodic mounting, the latter case provides a much broader attenuation band and the traditional way gives a much higher resonance peak. In general, the disorder in the geometries of Helmholtz resonators in the duct-resonator periodic system may provide an optional way to reduce the noise, especially the kind of noise that is low frequency and broad band and has some noise peaks. As an extension of pure-periodic case discussed in Chapter 3, this chapter is also an original work.

Chapter 5

Ventilation Performance of Helmholtz Resonators

5.1 A Fluid Dynamic Model of a Single Opening Enclosure

As shown in Fig. 5-1, in fluid dynamics, the phenomenon of turbulent wind induced ventilation of a room with a single opening has been reported by several researchers.[52-54] A room with a single opening can be considered as a big Helmholtz resonator. From now on, for the sake of consistence, in most part of the chapter, either a room with a single opening or a Helmholtz resonator will be called single-opening enclosure, with the room or the cavity of the resonator called enclosure, the opening or the neck of the resonator called opening. The fluid dynamic modeling of a single-opening enclosure will lead to a non-linear oscillator equation. Interested readers can find a detailed discussion of the non-linear oscillator equation in many papers, such as Refs. 53 and 54. However, for the sake of completeness, the derivation of the nonlinear oscillator equation is discussed here.

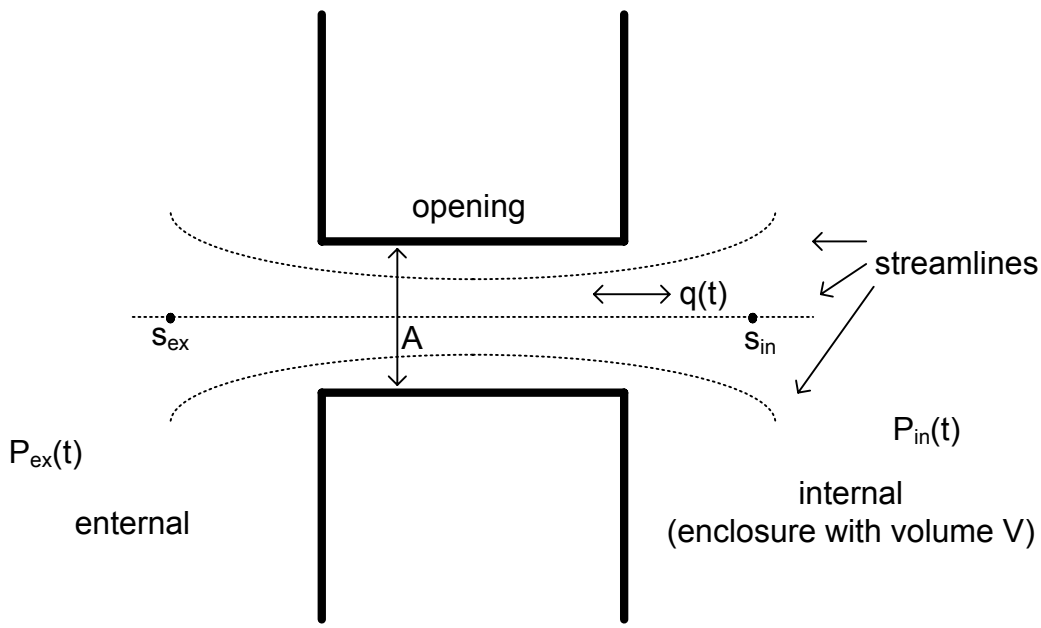

Figure 5-1. Airflow through a single opening.

When considering the ventilation of a single opening enclosure, the wavelength of the external pressure oscillation is assumed to be much larger the geometries of the enclosure and the mean air density and ambient pressure can be treated as uniform in the enclosure. The density of the internal air can be expressed as

$$\rho_{in}(t) = \overline{\rho_{in}} + \rho_{in}^{'}(t) \tag{5.1}$$

where $\rho_{in}^{'}(t) << \overline{\rho_{in}}$ where density changes are assumed to be very small compared to the mean value. Applying a compressible form of the continuity equation to the internal air gives

$$V\frac{d\rho_{in}}{dt} = \rho_0 q(t) \tag{5.2}$$

where ρ_0 denotes the mean density of the internal and external air, as $\overline{\rho_{in}} = \overline{\rho_{ex}} = \rho_0$, and V is the volume of the enclosure. And $q(t)$ is the airflow rate through the

opening (defined as the product of the area of the opening and the mean velocity of the airflow). The internal and external air pressure $P_{in}(t)$ and $P_{ex}(t)$ can be expressed as

$$P_{in}(t) = \overline{P_{in}} + p_{in}(t) \quad , \quad P_{ex}(t) = \overline{P_{ex}} + p_{ex}(t) \tag{5.3}$$

where $p_{in}(t) << \overline{P_{in}}$, $p_{ex}(t) << \overline{P_{ex}}$; and $\overline{P_{in}} = \overline{P_{ex}} = P_0$. The equation of state for the internal air is

$$\frac{P_{in}(t)}{\rho_{in}^{\gamma}(t)} = \frac{P_0}{\overline{\rho_{in}}^{\gamma}} \tag{5.4}$$

where γ is the isentropic index for assuming this is a isentropic process. Thus

$$\frac{\mathrm{d}\rho_{in}}{\mathrm{d}t} = \frac{\overline{\rho_{in}}}{\gamma P_{in}} \frac{\mathrm{d}P_{in}}{\mathrm{d}t} = \frac{\overline{\rho_0}}{\gamma P_0} \frac{\mathrm{d}p_{in}}{\mathrm{d}t} \tag{5.5}$$

and substituting in Eq. (5.2) gives

$$\frac{V}{\gamma} \frac{\mathrm{d}p_{in}}{\mathrm{d}t} = P_0 q(t) \tag{5.6}$$

By ignoring the viscous and the gravity effect of the air, the momentum equation can be expressed as (for 2-dimentional condition)

$$\frac{\partial v_x}{\partial t} + v_x \frac{\partial v_x}{\partial x} + v_y \frac{\partial v_x}{\partial y} + \frac{1}{\rho_0} \frac{\partial p}{\partial x} = 0 \quad \text{and} \quad \frac{\partial v_y}{\partial t} + v_x \frac{\partial v_y}{\partial x} + v_y \frac{\partial v_y}{\partial y} + \frac{1}{\rho_0} \frac{\partial p}{\partial y} = 0 \tag{5.7}$$

where flow velocity $\mathbf{v} = (v_x, v_y)$. Assuming that the flow through the opening can be regarded as irrotational flow with velocity potential ϕ with

$$v_s = -\frac{\partial \phi}{\partial s} \tag{5.8}$$

where v_s is the flow velocity along a streamline and s denotes the distance along a

streamline (a streamline is a line that is everywhere tangent to the velocity field of the flow).[50] The irrotational form of incompressible Bernoulli equation then can be given as

$$\frac{p(t)}{\rho_0}+\frac{v_s^{\,2}(t)}{2}-\frac{\partial\phi}{\partial t}=F(t) \tag{5.9}$$

Applying Eq. (5.9) to a point on the external side and to another point on the internal side, gives

$$\frac{p_{ex}(t)}{\rho_0}+\frac{v_{ex}^{\,2}(t)}{2}-\left.\frac{\partial\phi}{\partial t}\right|_{ex}=\frac{p_{in}(t)}{\rho_0}+\frac{v_{in}^{\,2}(t)}{2}-\left.\frac{\partial\phi}{\partial t}\right|_{in} \tag{5.10}$$

Since the instantaneous velocity and velocity potential can be expressed as a spatial-related term and a time-dependent term $T(t)$, Eq. (5.10) can be expressed as

$$\frac{p_{ex}(t)-p_{in}(t)}{\rho_0}=\frac{T^2(t)}{2}\left[v_{s,in}^{\;2}-v_{s,ex}^{\;2}\right]+(\phi_{s,ex}-\phi_{s,in})\frac{\partial T}{\partial t} \tag{5.11}$$

where $\phi_{s,ex}/\phi_{s,in}$ is the spatial term of ϕ_{ex}/ϕ_{in}. Since $T(t)=e^{j\omega t}$ and

$$\phi_{s,ex}-\phi_{s,in}=\int_{s_{ex}}^{s_{in}}v_s ds \tag{5.12}$$

Eq. (5.12) can be simplified by introducing the concept of an effective length l_e, which is the distance along the central streamline that follows the x-axis from the external point where the flow velocity can be ignored to the internal point at some distance from the outlet whose speed can be given by $q(t)/\beta A$, where A is the cross sectional area of the opening and β is the contraction ratio (describes the contraction of the flow in sharp-edged opening, as A_{jet}/A shown in Fig. 5-5) as[49]

$$\Delta p(t) = p_{ex}(t) - p_{in}(t) = \rho_0 \frac{T^2(t) q_s^{\ 2}}{2\beta^2 A^2} + \rho_0 \frac{dT}{dt} \int_{s_{ex}}^{s_{in}} v_s ds \tag{5.13}$$

where $q(t) = q_s T(t)$. An effective length l_e can be defined by

$$\frac{q_s}{A} l_e = \int_{s_{ex}}^{s_{in}} v_s ds \tag{5.14}$$

So that Eq. (5.13) becomes

$$p_{ex}(t) = p_{in}(t) - \rho_0 \frac{T^2(t) q_s^{\ 2}}{2\beta^2 A^2} - l_e \frac{q_s}{A} \frac{dT}{dt} \tag{5.15}$$

Combining Eqs. (5.6) and (5.15) gives

$$\rho_0 \frac{l_e}{A} \frac{dq}{dt} + \frac{\gamma P_0}{2\beta^2 A^2} q^2(t) + \rho_0 \frac{c_0^{\ 2}}{V} \int q dt = p_{ex}(t) \tag{5.16}$$

where $c_0^{\ 2} = \gamma P_0 / \rho_0$ is the sound speed. Eq. (5.16) describes the ventilation of a room with a single opening by the relation of the instantaneous airflow rate *q(t)* with the external pressure fluctuation $p_{ex}(t)$. And the result of Eq. (5.16) is somehow similar to the modeling of a Helmholtz resonator in acoustics way, which is to find the relation of the instantaneous particle velocity *v*(*t*) in the neck with the external pressure $p_{ex}(t)$, as

$$\rho_0 l_e \frac{dv}{dt} + \rho_0 c \frac{K^2 A}{2\pi} v(t) + \rho_0 c^2 \frac{A}{V} \int v dt = p_{ex}(t) \tag{5.17}$$

where K is the damping force coefficient, which is defined as *F*/*v* (*F* is the damping force of air piston in the neck and *v* is the mean velocity of the air piston). Note that the flow rate $q(t) = Av(t)$, which equals to the concept of sound volume velocity in acoustics. It can be seen that Eq. (5.16) and Eq. (5.17) only differs in the

second term on the left-hand side. The acoustic solution is identical to that for a mechanical oscillator with linear damping. A damping force of this type can be associated with a low Reynolds number (a dimensionless number that describes the ratio of inertial forces to viscous forces for a given flow condition) flow through a narrow opening where the surface shear stress is proportional to the flow rate q. The difference of the second term on the left-hand side of Eq. (5.16) makes the fluid dynamic solution of the resonator a non-linear oscillator equation and there are several works on the linearization process of this non-linear oscillator equation.[68,69] It can be imagined that when the applied sound pressure continues to grow, the behavior of the Helmholtz resonator at the resonance frequency can no longer be described by the linearised oscillator equation, Eq. (5.17), but the non-linear oscillator equation, Eq. (5.16).

However, both the fluid dynamic modeling in Eq. (5.16), and the acoustic modeling in Eq. (5.17), does not provide any information about the ventilation performance of the single-opening enclosure since that either the flow rate $q(t)$ or the particle velocity $v(t)$ may only describe the backward-forward motion of the "air piston" in the opening. The actual ventilation performance, if any, can be described by the air exchange between the external and the internal air of the enclosure. In detail, this process may contain three parts in a fluctuation period: the air exchange between the

internal space (enclosure) and the opening, the air mixing in the opening and the air exchange between the external space (may refers to duct in mechanical ventilation) and the opening. To investigate the air exchange between the enclosure and the duct is the main object in the following part of this chapter.

5.2 Fluid Dynamic Modeling of Inlet and Outlet Airflow

To investigate the air exchange performance of a single opening enclosure, it is necessary to know the characteristics (such as airflow velocity distribution) of both the external and internal flow near the opening. In flow dynamics, the flow sucked into the opening is distinct from the flow pumped out from the opening, and this can be described by the sink-jet model. For the sake of simplicity, this chapter considers only the two-dimensional flow in the x-y plane, which can be approximated by assuming the enclosure, slot-typed opening and external duct has the same width W in z-direction, and the width W is relatively large (as shown in Fig.5-2); so in the x-y plane of z=0, the flow can be regarded as two-dimensional. This is the common approach used by many researchers to simplify the complexity of the fluid dynamic problem.[70,71]

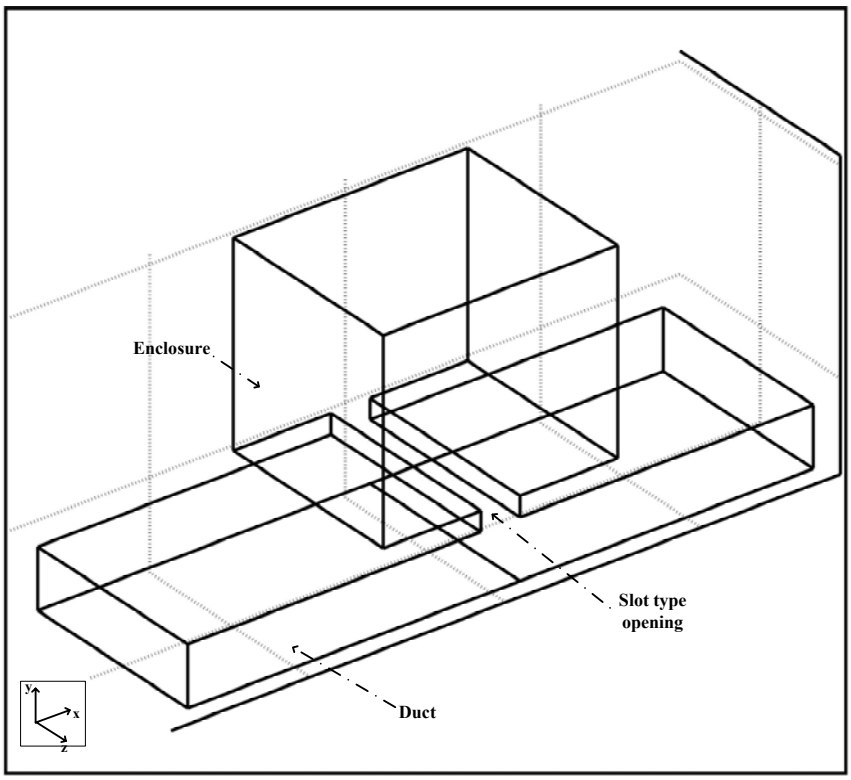

Figure 5-2. A duct with single opening enclosure.

5.2.1 Inlet Airflow

The flow sucked into the opening (or called inlet flow) from either internal or external space can be described by a sink. A point sink is the point that into which fluid submerges in a uniform manner, as shown in Fig. 5-3. This can be used to represent the flow field induced by sucking through a pipe or a hole in an infinite plane wall.[72] For two-dimensional flow considered in this chapter, a line sink perpendicular to the *x*-*y* plane with length *W* exists, as shown in Fig. 5-4, into which

fluid passed at a flow rate per unit length denoted by Q'.

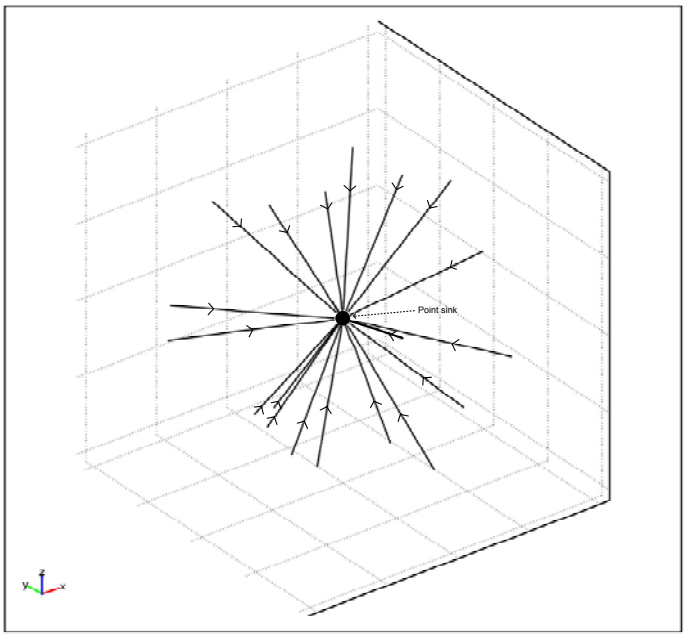

Figure 5-3. Point sink.

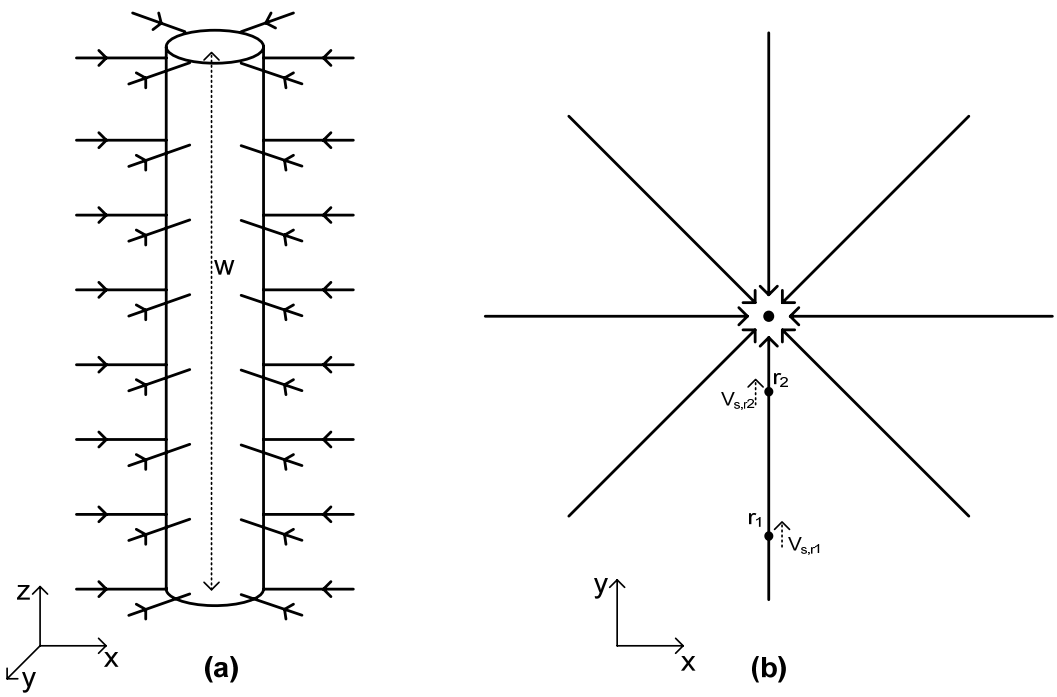

Figure 5-4. Line sink. (a) line sink, (b) view on top of a line sink.

It is apparent that in this situation, the streamlines in x-y plane are radial lines and the equipotential lines are concentric spheres center at the origin.[50] If the inlet flow rate per unit length into the opening in Fig. 5-2 is Q/W, the corresponding flow into the sink is $2Q/W$. The velocity along the streamline is

$$v_s = \frac{Q}{\pi W r} \tag{5.18}$$

In spite of the instantaneous quantities of the flow are varying with time as a perturbation, when the majority of flow is steady, the relationship between the pressures at two points, at r_1 and r_2 (along the streamline) can be expressed as

$$p_{r_1} - p_{r_2} = \rho Q^2 \left(\frac{1}{r_2^{\,2}} - \frac{1}{r_1^{\,2}}\right) \Big/ 4\pi^2 W^2 \tag{5.19}$$

Given that the mean velocity through the opening is

$$v_0 = \frac{Q}{WD} \tag{5.20}$$

and this speed will occur at a distance $r = D/\pi$, where D is the width of the opening in x-direction in Fig. 5-2. The corresponding pressure will be taken to be the inlet pressure p_{in}. So the pressure difference at two points is given by

$$p_{r_1} - p_{in} = \rho Q^2 \left(1 - \frac{D^2}{\pi r_1^{\,2}}\right) \Big/ 2WD^2 \tag{5.21}$$

Thus it can be seen for $\pi r_1/D > 10$, the pressure difference is essentially unaffected by the presence of the opening, furthermore at the point of three or four widths away from the opening for the effect of the flow induced by the sucking flow can be

negligible.

As considered in this chapter, due to fluctuation, the inlet flow varies with time in the sucking stage (half of the fluctuation period), this can be generated by varying the strength of the sink with time, as $Q = q_0 e^{j\omega t}$ with $q_0 < 0, \quad t = (2k, 2k+1)\pi/\omega, \quad k = [0, \infty)$. However, as the fluctuation frequency increases, the spatial acceleration terms decreases and can be ignored compared to the temporal acceleration terms in the momentum equation, Eq. (5.7). This is the assumption in acoustics that leads to the linearised wave equation. In this situation, the motion of the airflow close to the opening can be approximately regard as one-dimensional with the direction perpendicular to opening surface.

5.2.2 Outlet Airflow

The flow pumped out from the opening (or called outlet flow) can be described by a jet. An isothermal jet is characterized by its initial flow rate, Q_{jet}. Steady jets can be either laminar or turbulent. However, most of jets are somehow turbulent since the onset of transition from laminar to turbulent jet is found to occur at Reynolds numbers as low as 30.[73] The width of the jet increase as it traveled forward. For laminar jet, this is the result of molecular diffusion; for turbulent jet, this is due to the entrainment (a process whereby less turbulent fluid is incorporated into the

turbulent region of the entraining fluid).[49]

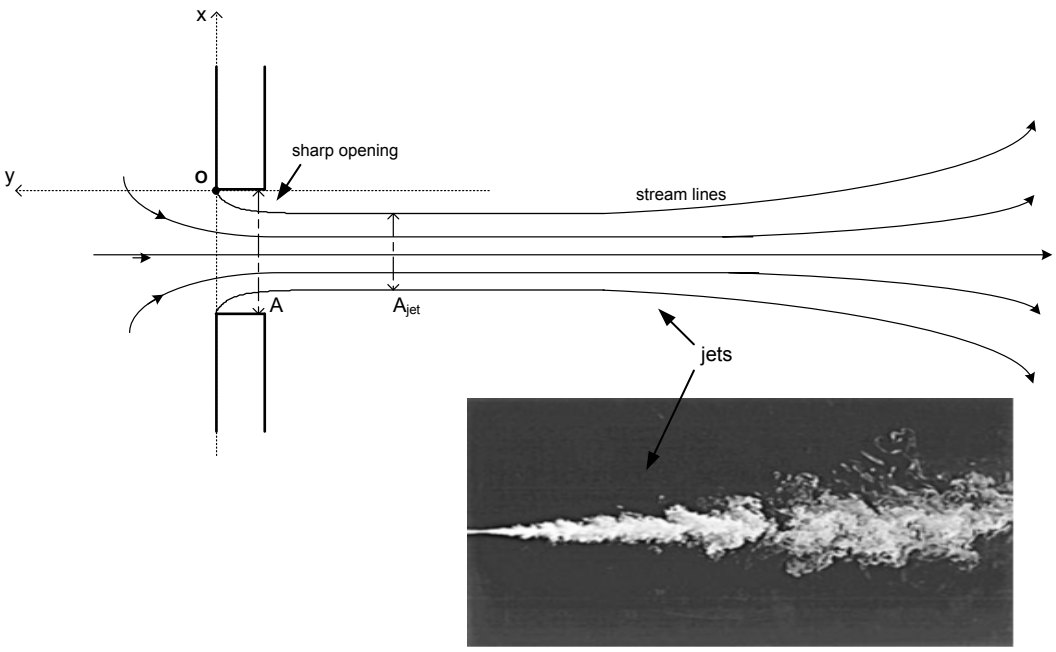

Figure 5-5. Jets.

In sharp-edged opening there is a contraction of the flow. As shown in Fig. 5-5. The diameter of the jet will be less than the diameter of the opening. This phenomenon is called the vena contracta effect. It is a result of the inability of the fluid to turn the sharp 90 degree corner since it would take an infinite pressure gradient across the streamline to cause the fluid to turn a sharp corner.[50] As shown in Fig. 5-5, the contraction coefficient is defined by the ratio of area at vena contract and the opening area, $\mu = A_{jet} / A$. The mathematical expression of the vena contract effect of flow through sharp opening is given by Kirchhoff.[74] Considering a

two-dimensional flow through a sharp opening from $(-\pi-2,0)$ to $(0,0)$, the jet is bounded by two equation sets:

$$x = e^{-\phi} - 1, \qquad y = \sqrt{1-e^{-2\phi}} - \ln\left(e^{\phi} + \sqrt{e^{2\phi}-1}\right) \qquad \left(\phi > 0, \psi = 0\right) \tag{5.22}$$

$$x = -\pi - 2 + 1 - e^{-\phi}, \qquad y = \sqrt{1-e^{-2\phi}} - \ln\left(e^{\phi} + \sqrt{e^{2\phi}-1}\right) \qquad \left(\phi > 0, \psi = \pi\right) \tag{5.23}$$

where ϕ is the velocity potential and ψ is the streamline function.[77] It can be seen that the contraction coefficient for a shaped-edged opening, $\mu = \pi/(\pi+2) = 0.611$.[75]

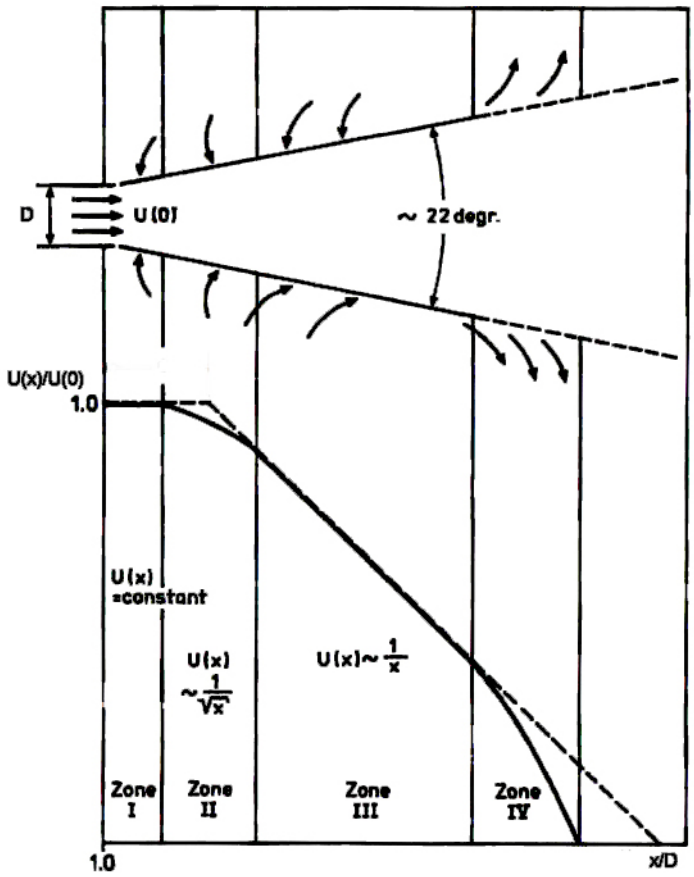

Figure 5-6. Four zones in isothermal jet expansion.

In practice the jets from real supply device are complicated. As shown in Fig. 5-6, four major zones can be distinguished in the development of a three-dimensional jet issuing from an opening.[76] Zone 1: A short zone extending about 4 diameters from the outlet surface, in which the centerline velocity remains practically unchanged, $U(x) = \text{constant}$, and the velocity profile close to the opening exhibits a top hat profile. Zone 2: A transition zone extending to about 8 diameters, most of which the centerline velocities vary inversely as the square root of the distance from the outlet, $U(x) \sim 1/\sqrt{x}$. Zone 3: A long zone of major engineering importance in which the centerline velocity varies inversely with the distance from the outlet, $U(x) \sim 1/x$, which extends to about 25~100 diameters long depending on the shape of opening. For an ideal isothermal jets, the centerline velocity in the zone 3 can be expressed as

$$\frac{U(x)}{U(0)} = C\frac{1}{x/\sqrt{A_{jet}}} \tag{5.24}$$

where $U(0)$ is the mean velocity of the jet at the outlet surface of the opening and A_{jet} is the corresponding cross section area of the jet, and there is $U(0) = Q_{jet}/A_{jet}$. The value of *C* is commonly used to characterize terminal performance and is know as "throw constant" or "C-value". In sharp-edged opening, C-value can be given as[49]

$$C = \frac{1}{2\alpha}\frac{1}{\sqrt{\mu}}\sqrt{\frac{2}{\pi}\frac{1}{1+\gamma_t}} \tag{5.25}$$

where α is the entrainment coefficient equals to 0.0535 ± 0.0025 for an axisysmetric jet,[77] and γ_t is a fraction of the momentum flux due to the mean

velocity, lies around 15%.[78] Zone 4: A terminal zone in which the centerline velocity decreases at an increasing rate. In zone 4 the jet becomes indistinguishable.

When a jet is approaching an opposite wall, it is decelerated by the adverse pressure gradient and is then deflected by the wall to turn into a radial wall jet.[79] And the effect of the wall is felt when x/L is greater then 0.84, where L is the distance between the opening and the opposite wall.

As considered in this chapter, due to fluctuation, the jet is characterized by its initial flow rate with its amplitude varying with time, as $Q_{jet} = q_0 e^{j\omega t}$ with $q_0 > 0, \quad t = (2k, 2k+1)\pi/\omega, \quad k = [0, \infty]$. As the unsteady jet travels downstream, vortex on the boundary of the jet shed, and moves downstream with the flow. This vortex makes the unsteady jet spreads much faster than both the steady laminar and turbulent flow. However, as the fluctuation frequency increases, the spatial acceleration terms eventually become small enough to be ignored when compared to the temporal acceleration term in the momentum equation, Eq. (5.7). In this situation, the motion of the outlet flow is complicated. Fortunately, this is the frequency range that acoustics engineer interested, and the outlet flow in this frequency range usually travels only a very small distance along the y-direction (as shown in Fig. 5-2) from the opening in a pumping stage (half of the fluctuation

period). The outlet flow can be approximately described as a top hat "short" jet with no flow contraction, which is similar to the characteristics of the inlet flow in relatively high frequency.[72]

5.3 Air Exchange Mechanism of a Single Opening Enclosure

As shown in the Fig. 5-7 (the *x*-*y* plane of Fig. 5-2), the case considered in this chapter is a duct connected with an enclosure through a single small opening. The flow velocity in the duct can be described as a combination of a mean velocity and a fluctuating velocity, i.e. $V(t) = \overline{V} + V^{'}(t)$, where $V^{'}(t) = V_0^{'} e^{j\omega t}$. The mean flow is provided by a mechanical ventilation fan, and the perturbation can be given by a loudspeaker with the sound pressure $p(t) = p_0 e^{j\omega t}$, where the amplitude $p_0 = \rho_0 c_0 V_0^{'}$ for assuming only plane wave exists (interested sound frequency below the cut-on frequency of the duct).

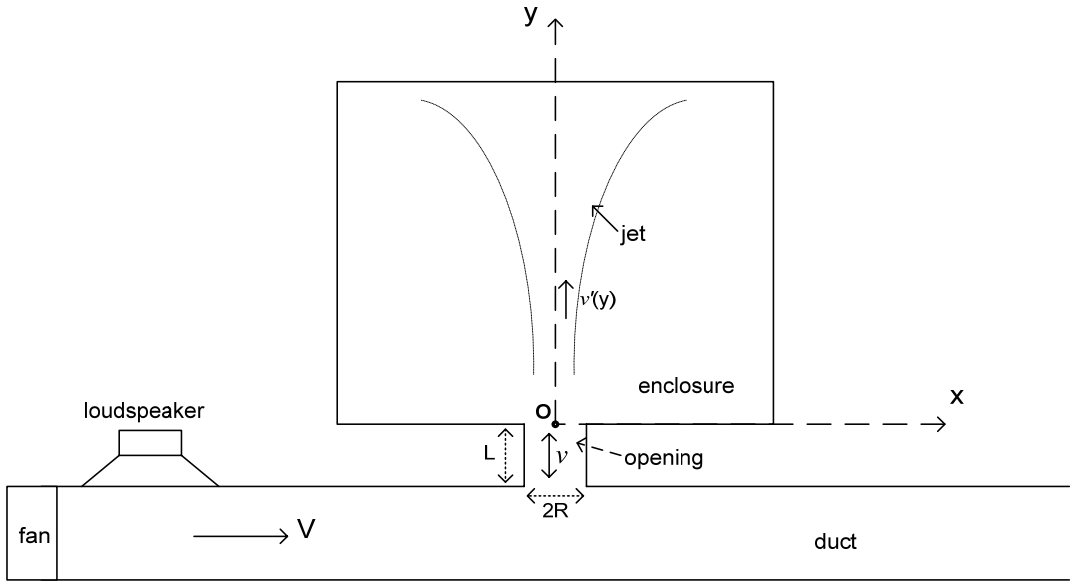

Figure 5-7. View on x-y plane of a duct with single opening enclosure.

5.3.1 The Air Exchange between the Duct and the Opening

Without lose of generality, we assume that a fluctuation period begins with the flow pumping out of the opening into the duct, so the first half period can be considered as a pumping stage and the second half period can be regarded as a sucking stage. Due to the presence of the mean flow in the duct, the air exchange mechanism between the opening and the duct region can be greatly simplified by ignoring the complexity of the inlet and outlet flow behaviors. The air exchange can be interpreted as in each fluctuation periodic, the mean flow "sweeps off" the air volume pumping out from the opening in the pumping stage and providing the "fresh" air into the opening in the sucking stage when the mean flow velocity in duct

is high enough. The quantitative analysis on the mean flow velocity required by the "sweep off" effect is now being investigated.

5.3.2 Air Mixing in the Opening

The mechanism of the air mixing in the opening is relatively least well understood and is currently being investigated. For the single opening enclosure designed to investigate the air exchange between duct and enclosure, the opening usually should be have a relatively short length *L*. It seems that in the short-length opening the turbulent diffusion plays an important role in mixing the air, which is the transportation of contaminants by turbulent fluctuations that occurs much more rapidly than molecular diffusion and provides rapid mixing during processing.[80] Further work needs to analyze the air mixing quantitatively in this part.

5.3.3 The Air Exchange between the Enclosure and the Opening

It is the mechanism of the air exchange between the enclosure and the opening attracted the major attention in this chapter. And it is found that this part plays an important role in the whole air exchange system. Without lose of generality, we still assume that a fluctuation period begins with the flow pumping out of the opening

into the enclosure, so the first half of the period can be considered as a pumping stage and the second half can be regarded as a sucking stage.

As discussed in previous section, when the frequency is relatively low that the spatial and temporal acceleration terms both play important roles in the fluid momentum equation, Eq. (5.7), the behavior of the flow pumping out from and sucking into the opening in the enclosure can be described by the sink-jet model, as shown in Fig 5-8.

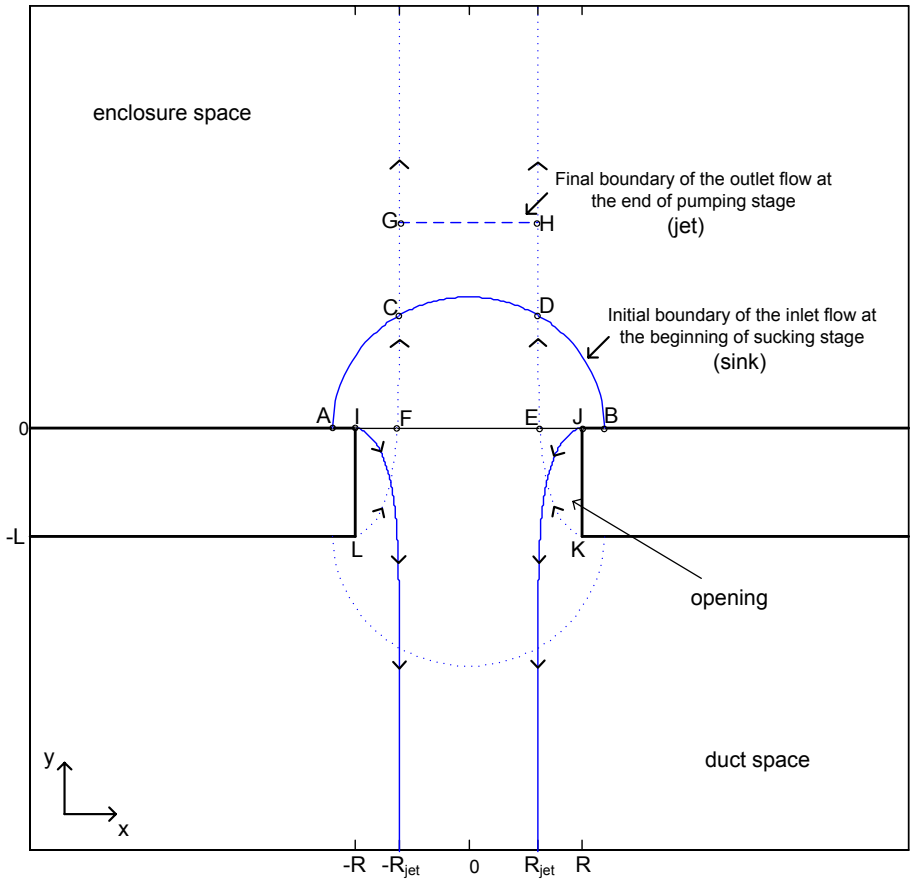

Figure 5-8. The sink-jet model.

(The dotted line represents the pumping flow in the first half period, and the solid line represents the sucking flow in the second half period.)

The line FE is the boundary of the fluid initially on the opening surface at the beginning of the pumping stage; at the end of the pumping stage, the surface (line FE) moves to the line GH. So the strip EFGH is the air jet formed in the fist half period (pumping stage). Similarly, the arc line ACDB is the initial fluid boundary at the beginning of the sucking stage, which is also the time of the end of the pumping stage; at the end of the sucking stage the boundary (arc line ACDB) moves to the line IJ. So the semicircle ACDB is the air sucked into the opening during the second half period (sucking stage). For the conservation of mass, there must be a relation of the area of the semicircle ACDB equals to the area of the strip EFGH. It can be seen that there is an overlap of the strip EFGH with the semicircle ACDB, the composite CDEF can be considered as the part of the air jet that "hauled back" into the opening in the sucking stage, with the other part (composite GHDC) "escaped" from the pumping-sucking cycling of the flow near the opening. From now on, the "escaped" air is irrelevant to the air motion in the opening.

It is the "escaped" air jet (composite GHDC) that results from the difference behavior of the inlet and outlet flow causes the air exchange between the opening and the enclosure. In each fluctuation period there is a fraction of the air jet

“escaped” and moved freely downstream with its original velocity directed into the enclosure. Along in the centerline of the enclosure, as shown in Fig. 5-7, at some distance from the opening, there is a jet path composing many moving air masses that are escaped in each fluctuating period. In this jet path, at a certain point on the centerline, the velocity is pulsating with time (non-zero mean), with pulsating peak proportional to the flow velocity through the opening $v_0^{'}(y) \sim v_0$ and the pulsating frequency equals to that of the supplying sound waves in the duct. If the frequency is very low, the pulsating peak is sparse in the time spectrum, and the peak means there is an escaped air mass passing through. If the air flow in the opening is oscillating in a relative high frequency, for example oscillating at the frequency of 100 Hz for a Helmholtz resonator, the peak of pulsating velocity is very dense and can be regarded as one combined with another in the time spectrum. This means the air jet form by the “escaped” air masses can be regards as a quasi-steady jet with small perturbation. In this situation, the flow in the whole jet path can be regarded as a quasi-steady jet characterized by mean part of the centerline velocity $\overline{v'}(y)$ and a fluctuating part with amplitude $\upsilon(y,t)$, as $v'(y,t) = \overline{v'}(y) + \upsilon(y,t)$. Both the mean velocity and the fluctuating amplitude will decrease as y increases.

As discussed in the previous section, at the beginning the jet speed in the centerline vary inversely as the square root of the distance from the outlet to about 8 width of

the opening, then the jet speed in the centerline varies inversely with the distance from the outlet to about 25~100 widths long, finally the centerline velocity decreases at an increasing rate and the jet becomes indistinguishable. Usually before the jet becomes indistinguishable, it will be affected by the opposite wall and decelerated by the adverse pressure gradient, then deflected by the wall to turn into a radial wall jet. It can be simply approximated as that the "escaped" air masses will evenly spread on the surface of the opposite wall as a thin boundary, and this thin boundary contains "fresh" air from the opening will be hauled down slightly when the air in the bottom is sucked into the opening in the sucking stage. It should be noted that due to its fluctuation, this jet will cause more significant vortex at the interface of the jet boundary and the still air in the enclosure. So this jet will spread more quickly with the flow slowdown a little quicker with the distance from the outlet of the opening than the steady turbulent jet discussed in previous section.

When the sound frequency is high enough, the spatial acceleration term can be ignored when compared with the temporal acceleration term in the momentum equation, Eq. (5.7), and this leads to the linearised wave equation of acoustics. Furthermore, for the special case of the Helmholtz resonator this leads to the linearised differential equation, Eq. (5.17). As discussed in previous section, the fluid behavior in the opening-enclosure interface is almost the same as a one-dimensional

motion in both the sucking and pumping stage in a fluctuation period. In this situation that no air masses can escape from the opening in the pumping-sucking cycling and no air exchange between the opening and the enclosure occurs. So compared to the jet-sink model, the air motion in the opening at high frequency is more appropriate to be regarded as an air piston.

However, Helmholtz resonator usually designed to control the noise by resonating at a relatively low frequency. At low enough resonance frequency, the spatial acceleration term in momentum equation, Eq. (5.7), is no longer appropriate to be ignored. It can be imagined that when such kind of Helmholtz resonator is resonating, the flow behavior in the opening-enclosure interface is in some extent similar to a sink-jet model. In this situation, the air jet formed by the "escaped" air masses can be found. Fig. 5-9 shows the air jet path in a preliminary experiment of an axisysmetric Helmholtz resonator with the opening radius 5.5 mm, opening length 6 mm, enclosure radius 67 mm and enclosure length 110 mm under supplying sound pressure level 100 dB. The resonance frequency is 112.5 Hz. It can be seen when the resonator is driven at the resonance frequency, the air jet is form. When there is no velocity perturbation induced by sound or the driven frequency is high (500Hz), no air jet can be found.

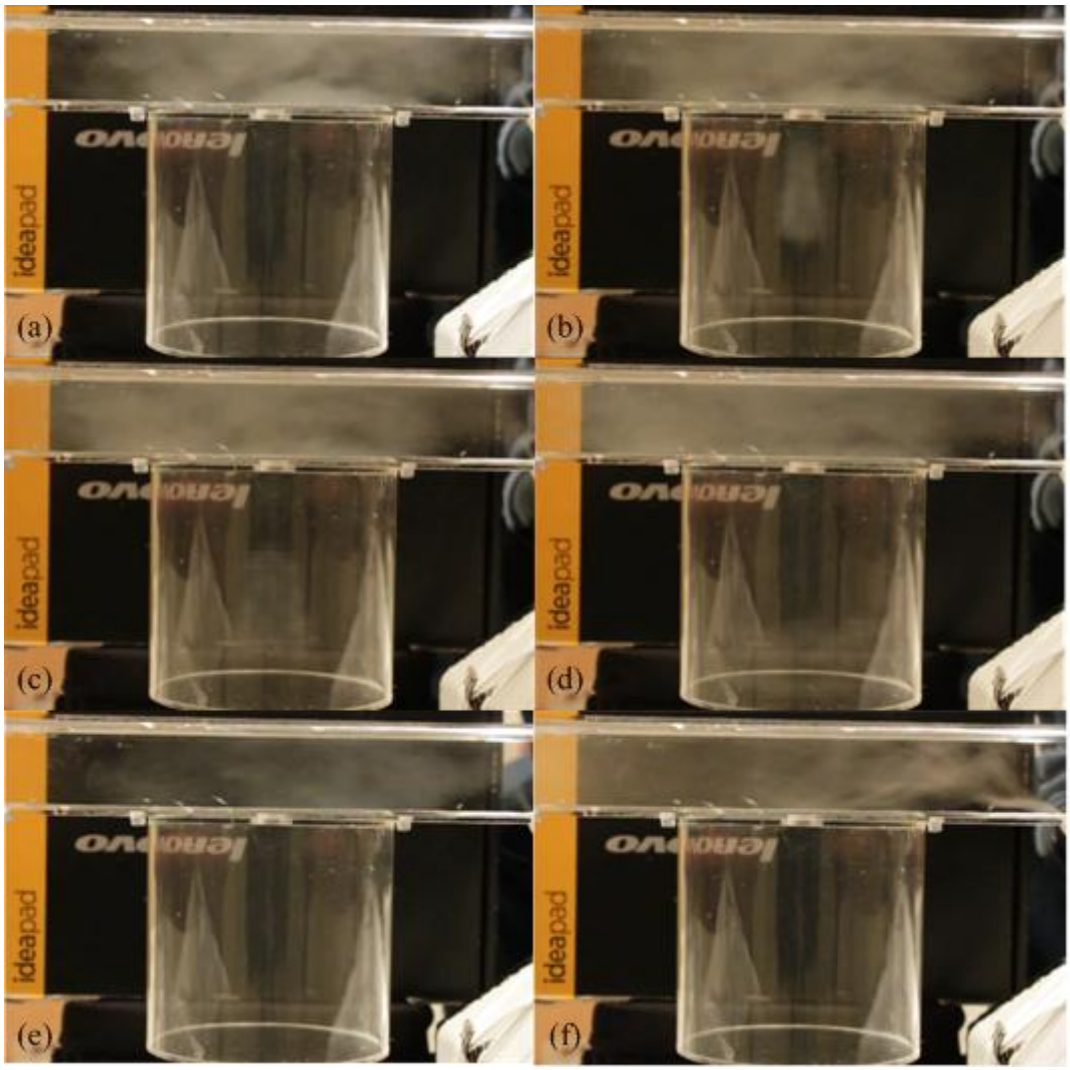

Figure 5-9. Air jet in the resonator.
(a) *f*=112.5 Hz, *t*=0 s; (b) *f*=112.5 Hz *t*=1/30 s; (c) *f*=112.5 Hz, *t*=2/30 s; (d) *f*=112.5 Hz, *t*=3/30 s; (e) *f*=500 Hz; and (f) no sound supplied.

5.4 Conclusion

This chapter investigates the mechanical ventilation of an enclosure connect to a ventilation duct through a single opening. The ventilation is caused by sound

induced velocity fluctuation. Especially at the resonance frequency of the enclosure-opening structure (Helmholtz resonator), the motion of the airflow in the opening may results in an air jet formed in the enclosure that provides the fresh air from the ventilation duct. This air jet is composed of the “escaped” air masses, and the “escaped” air masses results from the behavior of the airflow in the region of opening-enclosure interface that can be described by the sink-jet model in each fluctuation period.

In Chapter 5, the linearised oscillator equation and the non-linear oscillator equation are directly from the existing literature, so are the jet model and the sink model. However, the sink-jet model and the observation of air jet in the Hemholtz resonator are original works.

However, at the present only the qualitatively analysis is provided; lack of the quantitatively analysis, the numerical simulation and experimental verification, this part of work is far from enough. Actually, this is just a beginning that focuses on finding the air jet in cavities by using various kinds of resonators and trying to explain the air jet the observed. This work will be extended, which includes the quantitative analysis on the variation of the air exchange rate with frequency and amplitude of supplying sound, as well as the corresponding experiment on

measuring the mean and fluctuating velocity of the air jet in the enclosure.

Compared to the traditional mechanical ventilation that uses mechanical fans for supplying and/or extracting air, the ventilation method discussed in this chapter can be considered as “AC” ventilation with the electrical analogy, which indicates the backward-forward motion of the airflow in the opening may result in an air jet formed in the enclosure that provides the fresh air from the ventilation duct. Similarly the traditional mechanical ventilation can be regarded as “DC” ventilation. Although we called it “AC” ventilation, the air jet in the enclosure can be regarded as a “DC” flow with the flow velocity fluctuating at the same frequency as that of the supplying sound waves. To the author’s knowledge, the “AC” ventilation is a relatively innovative ventilation method that attracts little attention and is far less understood than the traditional ventilation method.

Chapter 6

Conclusion and Suggestions for Future Work

6.1 Conclusion

Both the broadband noise control and ventilation effects of Helmholtz resonators have been investigated in this thesis. Experiments have been carried out at The Hong Kong Polytechnic University to validate some of the theoretical analysis. The experimental data agreed well with the FEM simulation and the theoretical predictions.

First of all, a single Helmholtz resonator has been discussed. This part mainly comes from the existing literature. For the lumped-parameter model of a Helmholtz resonator, the air in the neck acts as mass and the air inside its cavity acts as a spring. For the distributed-parameter model, the multi-dimensional wave propagation inside both the neck and cavity has been considered. It has been shown that the distributed-parameter model has a more accurate description of the frequency characteristic of a Helmholtz resonator.

Secondly, a theoretical study of sound propagation in a one-dimensional duct with

identical side-branch resonators mounted periodically has been reported in this thesis. This is the main chapter in the thesis. The characteristic wave type has been introduced to describe the wave coupling in this periodic system. Three types of stop-bands that result from either the resonance of the resonators or the Bragg reflection, or from both, have been discussed and their bandwidths have been predicted theoretically. Both the semi-infinite duct with infinite number of side-branched resonators and the finite duct with N side-branched resonators have been discussed, and the influence of the number of resonators has also been investigated. The predicted results using this theory fit well with the FEM simulation and the experimental result. The long-term significance is that the use of periodic resonators may lead to a more effective noise control method for duct-borne sound transmission by broadening the attenuation bandwidth and increasing the magnitude of sound attenuation. This broadband of sound attenuation is related to two basic parameters in the periodic resonators: the resonance frequency of a single resonator and the periodic distance. In this chapter, the eigenvalue analysis on the periodic structure is the existing theory. However, as the original contribution, the duct with periodic resonators is found to be an effective tool for broadband noise control. In particular, such as the influence of the number of resonators in the finite-length duct-resonator system and the modified bandwidth prediction are original works, so does the detailed analysis on the physical meanings of the characteristic wave types.

Furthermore, the influence of the disorder in the periodic duct-resonator system has been investigated. The disorder in periodicity included two cases: the disorder in periodic distance, the distance between any two nearby resonators, and the disorder in the geometries of Helmholtz resonators. For the first case, the periodic system seemed to be very “sensitive” to the defects in the periodic distance and the original pattern of noise attenuation band due to the structural periodicity began to break down under the influence of these “defects”. Such “defects” should be carefully avoided in manufacturing such periodic systems. However, for the latter case, the main attenuation band was well maintained with the bandwidth kept unchanged as long as the variation of the resonance frequencies of Helmholtz resonators kept within its frequency range. This is a useful way for the design of such a system to achieve a relatively wide noise attenuation band and to track some narrow noise peaks within it. In general, the disorder in the geometries of Helmholtz resonators in the duct-resonator periodic system may provide an optional way to reduce the noise, especially for the kind of noise that is low-frequency broadband and with some noise peaks. As an extension of pure-periodic case discussed in Chapter 3, this chapter is also an original work. However, this chapter only investigated the disorders in periodic distance and geometries of resonators with some specific cases; as well as the validation by FEM simulation. Further systematic analysis is need.

Last but not least, the mechanical ventilation effect of the Helmholtz resonator, which can be regarded as an enclosure connected to a ventilation duct through a single opening, has been investigated. Especially at the resonance frequency of the enclosure-opening structure (Helmholtz resonator), the motion of the airflow in the opening may result in an air jet formed in the enclosure that provides the fresh air from the ventilation duct. This air jet was composed of the "escaped" air masses, and the "escaped" air masses resulted from the behavior of the airflow in the region of opening-enclosure interface that can be described by the sink-jet model in each fluctuation period. Compared to the traditional mechanical ventilation that uses mechanical fans for supplying and/or extracting air, the ventilation method discussed in this chapter can be considered as "AC" ventilation with the electrical analogy. To the author's knowledge, the "AC" ventilation is a relatively innovative ventilation method that attracts little attention and is far less understood than the traditional ventilation method. As a new type of mechanical ventilation, "AC" ventilation has many potential applications. For example, "AC" ventilation can be used in relative small space that is not suitable for a traditional ventilation method. Furthermore, "AC" ventilation can also be used as a supplementary method to deal with the dead-zones of the traditional ventilation. However, in "AC" ventilation, the noise induced by the sound radiation from the opening is annoying. This means the AC

ventilation may not be a ventilation method for improving the human comfort but a special way to remove harmful gas in some particular occasions, such as decreasing the methane concentration in mine. In Chapter 5, the linearised oscillator equation and the non-linear oscillator equation are directly from the existing literature, so are the jet model and the sink model. On the other hand, the sink-jet model and the observation of air jet in the Helmholtz resonator are original works. However, Chapter 5 only contains qualitative analysis; much more works are need for it to become useful.

It is hoped that the present study can provide a stepping stone for investigation of both the acoustic and ventilation performance of Helmholtz resonators, and seeking their potential application in passive noise control and mechanical ventilation.

6.2 Suggestions for Future Work

The work conducted in this thesis systematically investigates the acoustic performance of sound propagation in a one-dimensional duct with identical side-branch resonators mounted periodically in both perfect and imperfect conditions, based on both lumped- and distributed-parameter model of the Helmholtz resonator. However, the investigation of the disorder in a periodic Helmholtz resonators array

and the “AC” ventilation performance of Helmholtz resonators are still far from enough. On the basis of the present work, future works are recommended as follows:

1. The chapter on the defects in periodic arrays could do with a systematic sensitivity analysis to determine the trend of performance variations with each of the important system parameters, i.e. periodic distance and geometries of resonators. In extreme case, this could also be related to other important types of non-periodic arrays, such as those with linear or number sequence variations.

2. This thesis only proposes a qualitative investigation on the ventilation mechanism of the Helmholtz resonator. In order to achieve a deeper understanding of its ventilation effect, the quantitative analysis based on the sink-jet model is need. The ventilation effect can be described by the variation of the air exchange rate with frequency and amplitude of supplying sound. This is the major work being conducted.

3. To verify the proposed AC ventilation effect of the Helmholtz resonator, experimental work is required. This experimental work aims at measuring the mean and fluctuating velocity of the air jet in the enclosure. This is the further work to be done.

4. A subsequence experiment measuring the variation of the concentration of the contaminants in the resonator with time at its resonance frequency is necessary.

Appendix

A.1 MATLAB Codes of Distributed-parameter Model of Single Helmholtz Resonator

Part of the MATLAB Codes for solving the distributed-parameter model of Helmholtz resonator

%==========An example for solving the distributed-parameter model ==========

```
%CIRCULAR CONCENTRIC HELMHOLTZ RESONATOR
%SOUND DISTRIBUTION
clear
c0=344;ro=1.21;
p0=1;Pi=1;a1=0.017;a2=0.047;b1=0.0455;b2=0.04;
Sd=3*0.0601*0.022;
Sn=pi*(a1)^2;
%-------------------------------------
%FIND ROOTS OF 1ST ORDER BESSEL
x=0:0.05:50;
y=besselj(1,x);
LD0=[];
for k=1:1000,
    if y(k)*y(k+1)<0
        h=interp1(y(k:k+1),x(k:k+1),0);
        LD0=[LD0,h];
    end
end
x20=LD0./a2;
x10=LD0./a1;
%-------------------------------------
%initial marix
frequency=0:4:1000;
for jf=1:length(frequency),
    f0=frequency(jf);
    w0=2*pi*f0;k0=w0/c0;
```

```
   N1=[1:5]; LN1=5;
   N2=[1:5]; LN2=5;
   LD=[LD0(N2)];
   x2=[x20(N2)];
   v2=(k0^2-x2.^2).^0.5;
   x1=[x10(N1)];
   v1=-(k0^2-x1.^2).^0.5;
   C=[];
   C(1,:)=[Sd+0.5*Sn Sd-0.5*Sn zeros(1,LN1) 0 zeros(1,LN2)];
   C(2,:)=[a1^2*exp(-j*k0*b1) -a1^2*exp(j*k0*b1) zeros(1,LN1)
-a2^2*(exp(j*k0*b2)-exp(-j*k0*b2)) zeros(1,LN2)];
   C(3,:)=[0.5*a1^2*exp(-j*k0*b1) 0.5*a1^2*exp(j*k0*b1) zeros(1,LN1)
-0.5*a1^2*(exp(j*k0*b2)+exp(-j*k0*b2))
-a1*a2./LD.*besselj(1,a1/a2*LD).*(exp(-j*v2*b2)+exp(j*v2*b2))];
   for k1=0:LN1,
      if k1~=0
         C(k1+3,:)=[0 0 zeros(1,LN1) 0
-a1./(x2.^2-x1(k1)^2).*x2.*besselj(0,LD(k1)).*besselj(1,a1/a2.*LD).*
(exp(-j*v2*b2)+exp(j*v2*b2))];
         C(k1+3,k1+2)=0.5*a1^2*besselj(0,LD(k1))^2*exp(j*v1(k1)*b1);
      end
   end
   for k2=0:LN2,
      if k2~=0

C(k2+LN1+3,:)=[k0*exp(-j*k0*b1)*a1*a2/LD(k2)*besselj(1,a1*LD(k2)/a2)
-k0*exp(j*k0*b1)*a1*a2/LD(k2)*besselj(1,a1*LD(k2)/a2)
-v1.*exp(j*v1*b1).*a1./((x2(k2)^2)-x1.^2).*x2(k2).*besselj(0,x1*a1).
*besselj(1,a1/a2*LD(k2)) 0 zeros(1,LN2)];

C(k2+LN1+3,k2+LN1+3)=-(exp(j*v2(k2)*b2)-exp(-j*v2(k2)*b2))*v2(k2)*0.
5*a2^2*(besselj(0,LD(k2)))^2;
      end
   end
%-------------------------------------
%made the adjective matrix C
   while (abs(det(C))>1)&(imag(v2(length(v2)))<10)
      LN2=LN2+1;
      N2=[1:LN2];
      LD=[LD0(N2)];
      x2=[x20(N2)];
```

```
        v2=(k0^2-x2.^2).^0.5;
        while (imag(v1(length(v1)))<10)&(LN1<LN2)
            LN1=LN1+1;
            N1=[1:LN1];
            x1=[x10(N1)];
            v1=-(k0^2-x1.^2).^0.5;

%X=[Pbi Pbo C0 ...Cn(LN1)  D0...Dn(LN2)] Y C
            C=[];
            C(1,:)=[Sd+0.5*Sn Sd-0.5*Sn zeros(1,LN1) 0 zeros(1,LN2)];
            C(2,:)=[a1^2*exp(-j*k0*b1) -a1^2*exp(j*k0*b1) zeros(1,LN1)
-a2^2*(exp(j*k0*b2)-exp(-j*k0*b2)) zeros(1,LN2)];
            C(3,:)=[0.5*a1^2*exp(-j*k0*b1) 0.5*a1^2*exp(j*k0*b1)
zeros(1,LN1) -0.5*a1^2*(exp(j*k0*b2)+exp(-j*k0*b2))
-a1*a2./LD.*besselj(1,a1/a2*LD).*(exp(-j*v2*b2)+exp(j*v2*b2))];
            for k1=0:LN1,
                if k1~=0
                  C(k1+3,:)=[0 0 zeros(1,LN1) 0
-a1./(x2.^2-x1(k1)^2).*x2.*besselj(0,LD(k1)).*besselj(1,a1/a2.*LD).*
(exp(-j*v2*b2)+exp(j*v2*b2))];

C(k1+3,k1+2)=0.5*a1^2*besselj(0,LD(k1))^2*exp(j*v1(k1)*b1);
                end
            end
            for k2=0:LN2,
                if k2~=0

C(k2+LN1+3,:)=[k0*exp(-j*k0*b1)*a1*a2/LD(k2)*besselj(1,a1*LD(k2)/a2)
-k0*exp(j*k0*b1)*a1*a2/LD(k2)*besselj(1,a1*LD(k2)/a2)
-v1.*exp(j*v1*b1).*a1./((x2(k2)^2)-x1.^2).*x2(k2).*besselj(0,x1*a1).
*besselj(1,a1/a2*LD(k2)) 0 zeros(1,LN2)];

C(k2+LN1+3,k2+LN1+3)=-(exp(j*v2(k2)*b2)-exp(-j*v2(k2)*b2))*v2(k2)*0.
5*a2^2*(besselj(0,LD(k2)))^2;
                end
            end
        end
    end

    Y=[];
    Y(1,1)=Sd*Pi;
```

```
    Y(2,1)=0;
    Y(3,1)=0;
    for k30=0:LN1,
        if k30~=0
          Y(k30+3,1)=0;
        end
    end
    for k3=0:LN2,
        if k3~=0

%Y(k3+LN1+3,1)=-k0*p0*exp(-j*k0*b1)*a1*a2/LD(k3)*besselj(1,a1/a2*LD(
k3));
          Y(k3+LN1+3,1)=0;
        end
    end
%-------------------------------------------------------------
    X=C\Y;
%-----------------------------------------------
    Pbi=X(1);Pbo=X(2);
    Po=Pbi*(-0.5*Sn/Sd)+Pbo*(0.5*Sn/Sd);
    pressure(jf)=20*log10(1./abs(Pbi+Pbo));
    Zb(jf)=(Pbi+Pbo)/(Pbi-Pbo)*ro*c0;
    %pressure(jf)=abs(Pbi+Pbo);
    %reflection(jf)=20*log10(abs(Po));
    reflection(jf)=abs(Po);
end
plot(frequency,reflection);
%plot(frequency,pressure);
%plot(frequency,abs(Zb));
clc


%==============================================================
```

A.2 MATLAB Codes of Finite Periodic Duct-resonator System Base on the Distributed -parameter Model

Part of the MATLAB Codes for solving the finite periodic duct-resonator system based on the distributed-parameter model

%========An example for solving the finite periodic duct-resonator system ========

```
%FINITE PERIODIC SYSTEM
%DISTRIBUTED-PARAMTER MODEL
clear
c0=344;ro=1.21;
p0=1;Pi=1;a1=0.0175;a2=0.047;b1=0.052;b2=0.04;D=0.47;
Sn=pi*(a1)^2;
Sd=0.0601*0.022;
%p0=1;Pi=1;a1=0.017;a2=0.047;b1=0.0455;b2=0.04;D=0.4;
%Sd=0.022*0.0601;
%Sn=pi*a1^2;
reflect=0;
Lbegin=0.3;
Lend=0.3;
n=5; %periodic number-1
%-------------------------------------
%FIND ROOTS OF 1ST ORDER BESSEL
x=0:0.05:50;
y=besselj(1,x);
LD0=[];
for k=1:1000,
    if y(k)*y(k+1)<0
        h=interp1(y(k:k+1),x(k:k+1),0);
        LD0=[LD0,h];
    end
end
x20=LD0./a2;
x10=LD0./a1;
```

```
%-------------------------------------
%initial marix
frequency=0:5:1000;
%frequency=150;
for jf=1:length(frequency),
    f0=frequency(jf);
    w0=2*pi*f0;k0=w0/c0;
    N1=[1:5]; LN1=5;
    N2=[1:5]; LN2=5;
    LD=[LD0(N2)];
    x2=[x20(N2)];
    v2=(k0^2-x2.^2).^0.5;
    x1=[x10(N1)];
    v1=-(k0^2-x1.^2).^0.5;
    C=[];
    C(1,:)=[Sd+0.5*Sn Sd-0.5*Sn zeros(1,LN1) 0 zeros(1,LN2)];
    C(2,:)=[a1^2*exp(-j*k0*b1) -a1^2*exp(j*k0*b1) zeros(1,LN1)
-a2^2*(exp(j*k0*b2)-exp(-j*k0*b2)) zeros(1,LN2)];
    C(3,:)=[0.5*a1^2*exp(-j*k0*b1) 0.5*a1^2*exp(j*k0*b1) zeros(1,LN1)
-0.5*a1^2*(exp(j*k0*b2)+exp(-j*k0*b2))
-a1*a2./LD.*besselj(1,a1/a2*LD).*(exp(-j*v2*b2)+exp(j*v2*b2))];
    for k1=0:LN1,
        if k1~=0
           C(k1+3,:)=[0 0 zeros(1,LN1) 0
-a1./(x2.^2-x1(k1)^2).*x2.*besselj(0,LD(k1)).*besselj(1,a1/a2.*LD).*
(exp(-j*v2*b2)+exp(j*v2*b2))];
           C(k1+3,k1+2)=0.5*a1^2*besselj(0,LD(k1))^2*exp(j*v1(k1)*b1);
        end
    end
    for k2=0:LN2,
        if k2~=0

C(k2+LN1+3,:)=[k0*exp(-j*k0*b1)*a1*a2/LD(k2)*besselj(1,a1*LD(k2)/a2)
-k0*exp(j*k0*b1)*a1*a2/LD(k2)*besselj(1,a1*LD(k2)/a2)
-v1.*exp(j*v1*b1).*a1./((x2(k2)^2)-x1.^2).*x2(k2).*besselj(0,x1*a1).
*besselj(1,a1/a2*LD(k2)) 0 zeros(1,LN2)];

C(k2+LN1+3,k2+LN1+3)=-(exp(j*v2(k2)*b2)-exp(-j*v2(k2)*b2))*v2(k2)*0.
5*a2^2*(besselj(0,LD(k2)))^2;
        end
    end
```

```
%-------------------------------------
%made the adjective matrix C
   while (abs(det(C))>1)&(imag(v2(length(v2)))<10)
      LN2=LN2+1;
      N2=[1:LN2];
      LD=[LD0(N2)];
      x2=[x20(N2)];
      v2=(k0^2-x2.^2).^0.5;
      while (imag(v1(length(v1)))<10)&(LN1<LN2)
         LN1=LN1+1;
         N1=[1:LN1];
         x1=[x10(N1)];
         v1=-(k0^2-x1.^2).^0.5;

%X=[Pbi Pbo C0 ...Cn(LN1)  D0...Dn(LN2)] Y C
         C=[];
         C(1,:)=[Sd+0.5*Sn Sd-0.5*Sn zeros(1,LN1) 0 zeros(1,LN2)];
         C(2,:)=[a1^2*exp(-j*k0*b1) -a1^2*exp(j*k0*b1) zeros(1,LN1)
-a2^2*(exp(j*k0*b2)-exp(-j*k0*b2)) zeros(1,LN2)];
         C(3,:)=[0.5*a1^2*exp(-j*k0*b1) 0.5*a1^2*exp(j*k0*b1)
zeros(1,LN1) -0.5*a1^2*(exp(j*k0*b2)+exp(-j*k0*b2))
-a1*a2./LD.*besselj(1,a1/a2*LD).*(exp(-j*v2*b2)+exp(j*v2*b2))];
         for k1=0:LN1,
            if k1~=0
              C(k1+3,:)=[0 0 zeros(1,LN1) 0
-a1./(x2.^2-x1(k1)^2).*x2.*besselj(0,LD(k1)).*besselj(1,a1/a2.*LD).*
(exp(-j*v2*b2)+exp(j*v2*b2))];

C(k1+3,k1+2)=0.5*a1^2*besselj(0,LD(k1))^2*exp(j*v1(k1)*b1);
            end
         end
         for k2=0:LN2,
            if k2~=0

C(k2+LN1+3,:)=[k0*exp(-j*k0*b1)*a1*a2/LD(k2)*besselj(1,a1*LD(k2)/a2)
-k0*exp(j*k0*b1)*a1*a2/LD(k2)*besselj(1,a1*LD(k2)/a2)
-v1.*exp(j*v1*b1).*a1./((x2(k2)^2)-x1.^2).*x2(k2).*besselj(0,x1*a1).
*besselj(1,a1/a2*LD(k2)) 0 zeros(1,LN2)];

C(k2+LN1+3,k2+LN1+3)=-(exp(j*v2(k2)*b2)-exp(-j*v2(k2)*b2))*v2(k2)*0.
5*a2^2*(besselj(0,LD(k2)))^2;
```

```
            end
        end
    end
end

Y=[];
Y(1,1)=Sd*Pi;
Y(2,1)=0;
Y(3,1)=0;
for k30=0:LN1,
    if k30~=0
      Y(k30+3,1)=0;
    end
end
for k3=0:LN2,
    if k3~=0

%Y(k3+LN1+3,1)=-k0*p0*exp(-j*k0*b1)*a1*a2/LD(k3)*besselj(1,a1/a2*LD(
k3));
      Y(k3+LN1+3,1)=0;
    end
end
%-------------------------------------------------------------
X=C\Y;
%-----------------------------------------------
Pbi=X(1);Pbo=X(2);
pressure(jf)=20*log10(1./abs(Pbi+Pbo));
%pressure(jf)=abs(Pbi+Pbo);
Zb(jf)=(Pbi+Pbo)/(Pbi-Pbo)*ro*c0;
k=2*pi*frequency/c0;

%u(i)=acos(0.5*0.5*((2-ro*c0*s./Zb(i)).*exp(-j*k(i)*D)+(2+ro*c0*s./Z
b(i)).*exp(j*k(i)*D)));
A=0.5*[(2-Sn/Sd*ro*c0/Zb(jf))*exp(-j*k(jf)*D)
-Sn/Sd*ro*c0/Zb(jf)*exp(j*k(jf)*D);
Sn/Sd*ro*c0/Zb(jf)*exp(-j*k(jf)*D)
(2+Sn/Sd*ro*c0/Zb(jf))*exp(j*k(jf)*D)];

%u(jf)=acos(0.5*0.5*((2-Sn/Sd*ro*c0./Zb(jf)).*exp(-j*k(jf)*D)+(2+Sn/
Sd*ro*c0./Zb(jf)).*exp(j*k(jf)*D)));
%ui(jf)=abs(real(u(jf)));
```

```
    %ur(jf)=abs(imag(u(jf)));
    [V,B]=eig(A);
    r11=B(1,1);r22=B(2,2);  %eignvalue
    ev11=V(:,1);ev22=V(:,2);  %eignvector
    if abs(abs(r11)-1)<0.002
        if abs(ev11(2)/ev11(1))<1
            r1=r11;r2=r22;ev1=ev11;ev2=ev22;
        else
            r1=r22;r2=r11;ev1=ev22;ev2=ev11;
        end
    else
        if abs(r11)<1
            r1=r11;r2=r22;ev1=ev11;ev2=ev22;
        else
            r1=r22;r2=r11;ev1=ev22;ev2=ev11;
        end
    end
    %----------------
    % anechonic termination
    an=[ev1(1)*exp(j*k(jf)*Lbegin) ev2(1)*exp(j*k(jf)*Lbegin);
r1^n*ev1(2) r2^n*ev2(2)]\[Pi;0];
    %----------------
    % rigid wall termination
    %an=[ev1(1)*exp(j*k(jf)*Lbegin) ev2(1)*exp(j*k(jf)*Lbegin);
r1^n*ev1(1)*exp(-j*k(jf)*Lend)-r1^n*ev1(2)*exp(j*k(jf)*Lend)
r2^n*ev2(1)*exp(-j*k(jf)*Lend)-r2^n*ev2(2)*exp(j*k(jf)*Lend)]\[Pi;0]
;
    a=an(1);b=an(2);

ans(jf)=-20/(n-1)*log10(abs((a*r1^(n-1)*(ev1(1)+ev1(2))+b*r2^(n-1)*(
ev2(1)+ev2(2)))/(a*(ev1(1)+ev1(2))+b*(ev2(1)+ev2(2)))));
    %pressure difference
    %ans(jf)=abs(b/a);
    %ratio wave type2/wave type1
end

plot(frequency,ans)
clc
%==============================================================
```

References

[1] L. F. Hermann and M. D. Helmholtz, *On the sensations of tone as a physiological basis for the theory of music*, Second English Edition (London: Longmans, Green, and Co., 1895)

[2] J. W. S. Rayleigh, *The Theory of Sound, Volume II* (Dover, New York, 1945).

[3] J. W. S. Rayleigh, Scientific Papers, Dover, New York (1964).

[4] U. Ingard, "On the radiation of sound into a circular tube, with an application to resonators," *J. Acoust. Soc. Am.* **20**, 665-682(1948).

[5] U. Ingard, "On the theory and design of acoustic resonators," *J. Acoust. Soc. Am.* **25**, 1037-1061(1953).

[6] P. K. Tang and W. A. Sirignano, "Theory of a generalized Helmholtz resonator," *J. Sound Vib.* **26,** 247-262 (1973).

[7] R. L. Panton and J. M. Miller, "Resonant frequencies of cylindrical Helmholtz resonators," *J. Sound Vib.* **178**, 337-348(1994).

[8] P. A. Monkewitz and N. M. Nguyen-Vo, "The response of Helmholtz resonators to external excitation. Part 1. Single resonators," *J. Fluid Mech.* **151,** 477-497 (1985).

[9] A. Selamet and N. S. Dickey, "Theoretical, computational and experimental investigation of Helmholtz resonators with fixed volume: lumped versus distributed analysis," *J. Sound Vib.* **187(2),** 358-367 (1995).

[10] A. Selamet, P. M. Radavich, N.S. Dickey and J.M. Novak, "Circular concentric Helmholtz resonator," *J. Acoust. Soc. Am.* **101,** 41-51 (1997).

[11] R. C. Chanaud, "Effects of geometry on the resonance frequency of Helmholtz resonators," *J. Sound Vib.* **178**, 337-348(1994).

[12] R. C. Chanaud, "Effects of geometry on the resonance frequency of Helmholtz resonators, part II," *J. Sound Vib.* **204**, 829-834(1997).

[13] A. Trochidis, "Sound transmission in a duct with an array of lined resonators," *J. Vib. Acoust.* **113**, 245-249 (1991).

[14] K. T. Chen, Y. H. Chen, K. Y. Lin and C. C. Weng, "The improvement of the transmission loss of a duct by adding Helmholtz resonators," *Appl. Acoust.* **57**, 71-82 (1998).

[15] S. H. Seo and Y. H. Kim, "Silencer design by using array resonators for low-frequency band noise reduction," *J. Acoust. Soc. Am.* **118(4),** 2332-2338 (2005).

[16] J. F. Groeneweg, "Current understanding of Helmholtz resonator arrays as duct boundary conditions," *a conference held at NASA Headquarters*, July 14-15, 1969, Washington, D.C., pp. 357-368, (1969), edited by I. R. SCHWARTZ NASA, Washington, D.C., (1969).

[17] B. S. Cazzolato, C. Q. Howard, and C. H. Hansen, "Finite element analysis of an industrial reactive silencer," *The Fifth International Congress of Sound and Vibration*, University of Adelaide, Adelaide, Australia, Vol. 3, pp. 1659-1667 (1997).

[18] D. J. Mead, "A general theory of harmonic wave propagation in linear periodic system with multiple coupling," *J. Sound Vib.* **27(2),** 235-260 (1973).

[19] C. E. Bradley, "Acoustic Bloch wave propagation in a periodic waveguide," Technical Report of Applied Research Laboratories, **ARL-TR-91-19 (July)**, The University of Texas at Austin (1991).

[20] J. W. S. Rayleigh, "On the maintenance of vibrations by forces of double frequency, and on the propagation of waves through a medium endowed with a periodic structure," *Philosophical Magazine* **XXIV,** 145-159 (1887).

[21] M. Heckl, "Investigations on the vibrations of grillages and other simple beam structures," *J. Acoust. Soc. Am.* **36,** 1335-1343 (1964).

[22] D. J. Mead, "Free wave propagation in periodically supported infinite beams," *J. Sound Vib.* **11,** 181-197 (1970).

[23] G. S. Gupta, "Natural flexural waves and the normal modes of periodically supported beams and plates," *J. Sound Vib.* **13,** 89-101 (1970).

[24] B. R. Mace, "Periodically stiffened fluid loaded plates II: response to line and point forces," *J. Sound Vib.* **73,** 487-504 (1980).

[25] D. J. Mead and N. S. Bardell, "Free vibration of a thin cylindrical shell with discrete axial stiffeners," *J. Sound Vib.* **111,** 229-250 (1986).

[26] D. J. Mead and N. S. Bardell, "Free vibration of a thin cylindrical shell with periodic circumferential stiffeners," *J. Sound Vib.* **115,** 499-520 (1987).

[27] Y. Yun and C. M. Mak, "A study of coupled flexural-longitudinal wave motion in a periodic dual-beam structure with transverse connection," *J. Acoust. Soc. Am.* **126(1),** 114-121 (2009).

[28] C. Kittel, *Introduction to Solid State Physics*, **6**th edition (John Wiley and Sons, Inc., New York, 1986).

[29] Z. Y. Tao, W. Y. He and X. L. Wang, "Resonance-induced band gaps in a periodic waveguide," *J. Sound Vib.* **313**, 830-840 (2008).

[30] Y. T. Duan, W. Koch, C. M. Linton and M. Mciver, "Complex resonances and trapped modes in ducted domains," *J. Fluid Mech.* **571**, 119-147 (2007).

[31] N. Sugimoto and T. Horioka, "Dispersion characteristics of sound waves in a tunnel with an array of Helmholtz resonators," *J. Acoust. Soc. Am.* **97(3),** 1446-1459 (1995).

[32] N. Fang, D. J. Xi, J. Y. Xu, M. Ambati, W. Srituravanich, C. Sun, and X. Zhang, "Ultrasonic metamaterials with negative modulus," *Nature Mater.* **5**, 452-456 (2006).

[33] D. J. Mead and A. S. Bansal, "Mono-coupled periodic systems with a single disorder: Free wave propagation," *J. Sound Vib.* **61**, 481-496(1978).

[34] B. Djafari-Rouhani, J. O. Vasseur, A. Akjouj, L. Dobryznski, M. S. Kushwaha, P. A. Deymer, and J. Zemmouri, ''Giant stop bands and defect modes in one-dimensional waveguide with dangling side branches,'' *Prog. Surf. Sci.* **59**, 255–264 (1998).

[35] J. N. Munday, C. B. Bennett and W. M. Robertson, "Band gaps and defect modes in periodically structured waveguides," *J. Acoust. Soc. Am.* **112**(4), 1353-1358(2002).

[36] L. Schächter, *Beam-Wave Interaction in Periodic and Quasi-Periodic Structures* (Springer, Berlin, 1997).

[37] P. W. Anderson, "Absence of diffusion in certain random lattices," *Phys. Rev.* **109**, 1492-1505 (1958).

[38] C. H. Hodges, "Confinement of vibration by structural irregularity," *J. Sound Vib.* **82**, 411–424 (1982).

[39] C. H. Hodges and J. Woodhouse, "Vibration isolation from irregularity in a nearly periodic structure: Theory and measurements," *J. Acoust. Soc. Am.* 74(3), 894-905(1983).

[40] R. S. Langley, "Wave transmission through one-dimensional near periodic structures: Optimum and random disorder," *J. Sound Vib* **188**, 717-743(1995).

[41] C. Pierre, "Weak and strong vibration localization in disordered structures: A statistical investigation," *J. Sound Vib.* **139**, 111-132(1990).

[42] T. R. Lin, "A study of modal characteristics and the control mechanism of finite periodic and irregular ribbed plates," *J. Acoust. Soc. Am.* **123**, 729-737(2008).

[43] D. S. Shechtman, I. Blech, D. Gratias, and J. W. Cahn, "Metallic phase with long-range orientation order and no translational symmetry," *Phys. Rev. Lett.* **53**, 1951-1953(1984).

[44] J. P. Lu and J. L. Birman, "Electronic structure of a quasiperiodic system," *Phys. Rev. B* **36**, 4471-4474(1987).

[45] J. P. Lu and J. L. Birman, "Acoustic-wave propagation in quasiperiodic, incommensurate, and random systems," *Phys. Rev. B* **38**, 8067-8074(1988).

[46] H. B. Awbi, *Ventilation of Buildings*, 1st Ed. (Chapman & Hall , New York, 1991).

[47] Ventilation and Infiltration chapter, Fundamentals volume of the ASHRAE Handbook, ASHRAE, Inc., Atlanta, GA, (2005).

[48] E. David, *Natural Ventilation of Buildings: Theory, Measurement and Design*

(Wiley, West Sussex, 2012).

[49] E. David and S. Mats, *Building Ventilation Theory and Measurement* (John Wiley and Sons, Inc., England, 1996).

[50] B. R. Munson, D. F. Young, T. H. Okiishi and W. W. Huebsch, *Fundamentals of Fluid Mechanics*, 6th Ed. (Wiley, New York, 2009).

[51] BSI, Code of practice for ventilation principles and designing for natural ventilation, British Standard BS5925, (1991).

[52] H. Liu and K.H. Rhee, "Helmholtz oscillation in building models," *J. Wind Eng. Ind. Aerodyn.* **24**, 95-115(1986).

[53] B.J. Vickery and C. Bloxham, "Internal pressure dynamics with a dominant opening," *J. Wind Eng. Ind. Aerodyn.* **41**, 193-204(1992).

[54] G. C. Chaplin, J. R. Randall and C. J. Baker, "The turbulent ventilation of a single opening enclosure," *J. Wind Eng. Ind. Aerodyn.* **85**, 145-161(2000).

[55] M. L. Munjal, *Acoustics of Ducts and Mufflers* (Wiley, New York, 1987).

[56] B. G. Korenev, *Bessel Functions and their Applications* (Taylor and Francis, London, 2002).

[57] J. Miles, "The reflection of sound due to a change in cross section of a circular tube," *J. Acoust. Soc. Am.* **16**, 14-19 (1944).

[58] D. C. Lay, *Linear Algebra and its Applications* (Addison Wesley, New York, 1994).

[59] L. Friis and M. Ohlrich, "Coupling of flexural and longitudinal wave motion in a periodic structure with asymmetrically arranged transverse beams," *J. Acoust. Soc. Am.* **118(5),** 3010-3020 (2005).

[60] F. Shengjin, "A new extracting formula and a new distinguishing means on the one variable cubic equation," *Journal of Hainan Normal University* (Natural Science), **2(2)**, 91-98(1989) (in Chinese)

[61] L. L. Thompson, "A review of finite-element methods for time-harmonic

acoustics," *J. Acoust. Soc. Am.* **119(3),** 1315-1330 (2006).

[62] C. Q. Wang and L. X. Huang, "Analysis of absorption and reflection mechanisms in a three-dimensional plate silencer," *J. Sound Vib.* **313,** 510-524 (2008).

[63] ASTM E 2611-09 Standard Test Method for Measurement of Normal Incidence Sound Transmission of Acoustical Materials Based on the Transfer Matrix Method (American Society for Testing and Materials, Philadelphia, 2009).

[64] Y. S. Choy, *Sound Induced Vibration and Duct Noise Control* (Ph.D. dissertation, The Hong Kong Polytechnic University, Hong Kong, 2003).

[65] B. R. Mace, "Reciprocity, conservation of energy and some properties of reflection and transmission coefficients," *J. Sound Vib*. **155**, 375-381 (1992).

[66] A. Trochidis, "Sound transmission in a duct with an array of lined resonators," *J. Vib. Acoust.* **113**, 245-249 (1991).

[67] S. H. Seo and Y. H. Kim, "Silencer design by using array resonators for low-frequency band nose reduction," *J. Acoust. Soc. Am*. **118**(4), 2332-2338 (2005).

[68] B. J. Vickery and C. Bloxham, "Internal pressure dynamics with a dominant opening," *J. Wind Eng. Ind. Aerodyn.* **41**, 193-204 (1992).

[69] G. C. Chaplin, J. R. Randall and C. J. Baker, "The turbulent ventilation of a single opening enclosure," *J. Wind Eng. Ind. Aerodyn.* **85**, 145-161 (2000).

[70] M. S. Howe, "On the theory of unsteady shearing flow over a slot," *Phil. Trans. R. Soc. Lond. A* **303**, 151-180 (1981).

[71] P. A. Nelson, N. A. Halliwell and P. E. Doak, "Fluid dynamics of a flow excited resonance, part 1: experiment," *J. Sound Vib.* **78,** 15-38 (1981).

[72] G. K. Batchelor, *An Introduction to Fluid Dynamics* (Cambridge University Press, Cambridge, 1967).

[73] H. Schlichting, *Boundary-Layer Theory* (McGraw-Hill, New York, 1979).

[74] G. Kirchhoff, "Zur Theorie frier Flüssigkeitsstrahlen," *J. Math.* **70**, 37-69 (1869).

[75] H. Lamb, *Hydrodynamics*, 6th Ed. (Cambridge University Press, Cambridge, 1932).

[76] H. Straub, "Principles of room air distribution," Heating, Piping and Air Conditioning, April, 122-128 (1969).

[77] H. B. Fischer, J. E. List, R. C. Y. Koh, I. Imberger and N. H. Brooks, *Mixing in Inland and Coastal Waters* (Academic Press, New York, 1979).

[78] J. Hussein, S. P. Capp and W. K. Gworge, "Velocity measurements in a high-Reynolds-number, momentum-conserving, axisymmetric, turbulent jet," *J. Fluid Mech.* **258**, 31-75 (1994).

[79] T. Karimipanah and M. Sandberg, "Decay of momentum and velocity in an axisymmetric impinging jet." *Proceedings Roomvent '94*, Cracow, Poland, 15-17 (1994).

[80] A. J. Majda and P. R. Kramer, "Simplified models for turbulent diffusion: Theory, numerical modeling, and physical phenomena," *Physics Reports* **314**, 237-574 (1999).